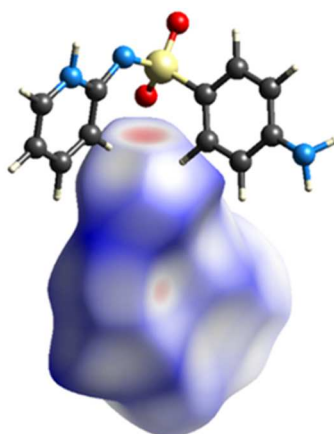# Multicomponent crystals of sulfapyridine and sulfadiazine

by

KELLY NZWANAI SHUNJE

Thesis submitted in fulfilment of the requirements for the degree
Master of Applied Science: Chemistry
in the Faculty of Applied Sciences at the

CAPE PENINSULA UNIVERSITY OF TECHNOLOGY

Supervisor: Professor Nikoletta B. Báthori
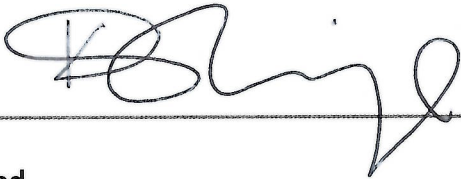**Co-supervisor: Dr Elise de Vries**

Cape Town
December 2017

Declaration

I, Kelly Nzwanai Shunje, declare that the contents of this dissertation/thesis represent my own unaided work, and that the dissertation/thesis has not previously been submitted for academic examination towards any qualification. Furthermore, it represents my own opinions and not necessarily those of the Cape Peninsula University of Technology.

Signed

14/03/2018

Date

Abstract

Crystal engineering principles were used to cocrystallize sulfa drugs, sulfapyridine (SFP) and sulfadiazine (SFD) with aromatic acids and an amine via solution crystallization. Sulfapyridine formed cocrystals with 3-nitrobenzoic acid (SFP·3NBA), 5-bromosalicylic acid (SFP·5BSA), 4-dimethylaminopyridine (SFP·4DMAP) and salts with 4-nitrobenzoic acid [SFP$^+$][4NBA$^-$], 3,5-dinitrosalicylic acid [SFP$^+$][DNSA$^-$] and 3,5-dibromosalicylic acid [SFP$^+$][DBSA$^-$], while sulfadiazine formed a salt with 3,5-dinitrosalicylic acid [SFD$^+$][DNSA$^-$]. The newly formed complexes were analyzed by differential scanning calorimetry (DSC), thermogravimetric analysis (TGA), fourier transform infrared spectroscopy (FTIR), single crystal X-ray diffraction (SCXRD), powder X-ray diffraction (PXRD) and nuclear magnetic resonance spectroscopy (^{1}H and ^{13}C NMR).

The hydrogen bonding and crystal packing of the new solid forms were analyzed with the aid of Mercury and CrystalExplorer. The SFP and SFD compounds exhibit tautomerism. In this work it was investigated how the introduction of coformers with varying acidity provides the possibility to form a variety of synthons, and therefore disrupt the common preferred interactions within the sulfonamides. Using selected acids as coformers, the effect on crystal packing of the coformer's substituent position was examined by using the isomers 3NBA and 4NBA. 5BSA and DBSA were employed to analyse the effect of the number of substituents on hydrogen bond formation and crystal packing. In addition, it was investigated how small structural changes in the pharmaceutical compound influences the crystal packing by cocrystallising structurally similar SFP and SFD with the same coformer. Evaluation of the change in coformer acidity was studied by using a pyridine coformer, 4DMAP, and its crystal packing was analyzed and compared to structures formed with carboxylic acid coformers.

Finally, we examined how inter-conversion of tautomers promotes crystal formation by conforming to the geometric demands of the different coformers.

Acknowledgements

First and foremost, I want to express my gratitude towards my supervisor, Professor Nikoletta Báthori whose immense support helped me to accomplish my MSc. I am grateful for the countless hours and effort you dedicated to making me a better individual both in and outside the lab. Thank you.

I would like to thank my co-supervisor Dr Elise de Vries for her valuable input. I wish to thank Dr Edith Antunes for the NMR data collection and her aid with the interpretation.

I am also indebted to Dr Merrill Wicht and Dr Meredith Hearshaw for their support since undergraduate level. Thank you for your encouragement and affection. I also want to thank Professor Luigi Nassimbeni for his help with crystallographic studies and counsel about life.

I also want to thank Kudzanai Nyamayaro, for all his assistance and willingness to help always. To the group members, I will always cherish the moments we shared.

Finally, I want to thank my family and friends. My mom, sister and brother for their love and constant support. To Marcy and Betsi, I want to say thank you for taking care of mom while I'm away from home.

Dedication

To Mom

"…….Some Gave All"

Conferences

"**Cocrystals of pyrazinamide with unusual stoichiometry, Z' and Z'' values**", Poster presentation at the 23rd International Conference on the Chemistry of the Organic Solid State (ICCOSS XXIII), Stellenbosch, South Africa (2-7 April 2017). Kelly Nzwanai Shunje and Nikoletta B. Báthori

"**Hydrogen bonding in selected crystals of sulfapyridine and sulfadiazine**", Poster presented at the South African Chemical Institute (SACI) Inorganic Conference, Arabella Hotel & Spa, Hermanus, Western Cape, South Africa (25–29 June 2017). Kelly Nzwanai Shunje, Elise de Vries and Nikoletta B. Báthori

Table of Contents

List of Figures

List of Tables

Glossary of Terms

Abbreviation/Acronyms/Terms	Name
API	Active Pharmaceutical Ingredients
GRAS	Generally Regarded As Safe
FDA	Federal Drug Administration
DNA	Deoxyribonucleic acid
CSD	Cambridge Structural Database
DSC	Differential Scanning Calorimetry
TGA	Thermogravimetric Analysis
SCXRD	Single Crystal X-ray Diffraction
PXRD	Powder X-ray Diffraction
FTIR	Fourier Transform Infrared Spectroscopy
^{1}H NMR	Proton Nuclear Magnetic Resonance Spectroscopy
^{13}C NMR	Carbon Nuclear Magnetic Resonance Spectroscopy
SFP	Sulfapyridine
SFD	Sulfadiazine
3NBA	3-nitrobenzoic acid
4NBA	4-nitrobenzoic acid
DNSA	3,5-dinitrosalicylic acid
5BSA	5-bromosalicylic acid
DBSA	3,5-dibromosalicylic acid
4DMAP	4-dimethylaminopyridine
SD	Sulfa Drug

Atom colour code

Bromine

Carbon
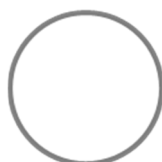
Hydrogen

Nitrogen
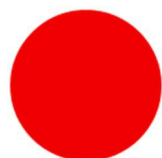
Oxygen

Sulphur

Chapter 1

Introduction

1.1 Supramolecular chemistry

In 1978, Jean-Marie Lehn coined the term 'supramolecular chemistry' which he concisely defined as the chemistry beyond the molecule.[1] In other terms, he described supramolecular chemistry as *"…the chemistry of the intermolecular bond, covering the structures and functions of the entities formed by association of two or more chemical species…".[2]* The genesis of supramolecular chemistry can be traced back to the 1800s when Sir Humphry Davy discovered the inclusion compound chlorine hydrate.[3] Although supramolecular chemistry was already in existence, it did not gain attention in chemical research until the discovery of crown ethers by Cram and Pedersen.[4]

Supramolecular chemistry is divided into two classes, i.e. host-guest chemistry and self-assembly. The latter involves non-covalent joining of two or more species, which are of the same relative size; whereas in the former, although species associate via non-covalent interactions, there is a significant difference in the size and shape of the host and guest species. Typically, the host molecule is larger and can wrap around the smaller molecule, the guest, which becomes enclosed.[3] The main goal in supramolecular chemistry is to design functional chemical systems based on molecular components held together by non-covalent intermolecular forces,[5] such as $\pi - \pi$ stacking interactions,[6] dipole-dipole interactions,[7] hydrogen bonds (H-bonds),[8] halogen bonds,[9] C-H$\cdots\pi$ interactions[10] and van der Waals interactions.[11]

Molecular recognition and self-assembly are the centrepiece of supramolecular chemistry. In molecular recognition, molecules interact with complementary functional groups using non-covalent intermolecular interactions in an orderly manner. Complementarity is well demonstrated by the 'lock and key' principle.[12] Most biological systems in nature are directed by molecular recognition and self-assembly. Another example of self-assembly is the deoxyribonucleic acid (DNA) molecule (Figure 1.1). The DNA molecule consists of purine and pyrimidine bases: adenine (A), guanine (G), thymine (T) and cytosine (C). Complementary base pairs A=T and G≡C interact via strong hydrogen bonding to form the double helix. Additionally, the double helix is stabilized by $\pi - \pi$ stacking.

Adenine-Thymine base pair

Guanine-Cytosine base pair
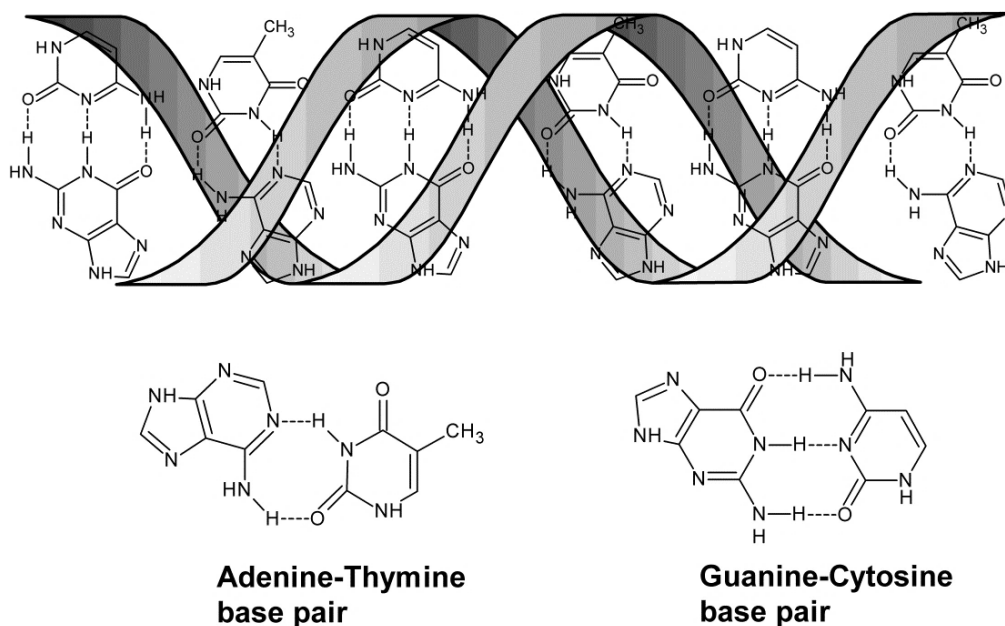
Figure 1.1 Self-assembly of nucleobases generating DNA, (Figure was reproduced[3]).

1.2 Crystal engineering

Crystal engineering focuses on design and synthesis of crystalline materials based on studies and knowledge of known structures of the building blocks. In order to predict the structural features of the newly designed crystals, crystal engineering examines landscapes, such as steric factors and the recurring intermolecular interactions (synthons) between functional groups.[13] Literature shows that the term 'crystal engineering' was first introduced by Pepinsky in 1955.[14] This was not implemented until 1971, when the work done by Schmidt on the solid state photodimerization reactivity of trans-cinnamic acids and alkenes laid the foundation of the subject.[15] From then, the crystal engineering field started to receive more attention from scientists including Thomas and co-workers[16] who described the topochemical phenomenon in organic solid state chemistry. Great progress has been made over the past years and the field now encompasses various areas of interest, including: physical chemistry, inorganic chemistry, organic chemistry and materials science.

1.3   Intermolecular interactions

The most popular design method for crystalline materials is using hydrogen bonding (H-bonding) to formulate the required solid form.[17] In this approach, complimentary hydrogen bond donor and hydrogen bond acceptor sites are required to be present on the molecular building blocks.

1.3.1   Hydrogen bonding

The hydrogen bond is an *"….attractive interaction between a proton donor and a proton acceptor in the same or different molecules…".[18]* The donor atom (D) is covalently bonded to the hydrogen atom (H) and also it has a high affinity for electrons. Due to this behaviour, the electrons, which the donor shares with the hydrogen, are unequally shared and this causes the hydrogen to take a slight positive charge. On the other hand, the acceptor atom (A), e.g. (N, O, F) has a pair of unshared electrons, which gives the atom a slight negative charge. H-bonds are electrostatic and directional, i.e. the D-H⋯A angles lean towards linearity. Through electrostatic attractions the donor atom shares its hydrogen atom with the acceptor atom forming the H-bond. Hydrogen bond can either be very strong [F-H-F]⁻, strong (N-H⋯N, N-H⋯O, O-H⋯N and O-H⋯O) or weak (C-H⋯π and C-H⋯O) depending on the electro-negativities of the interacting atoms.[19]

Very strong hydrogen bonds typically have D⋯A distances ranging from 2.2-2.5 Å and angles of 175-180° and are usually associated with strong acids such as [F-H-F⁻]. Additionally, they have binding energies of about 160 kJ mol⁻¹. Strong hydrogen bonds are the most prevalent in nature e.g. in the protein structures. They are characterized by D⋯A distances ranging between 2.5-3.1 Å, with bond angles of 130-180°. Weak hydrogen bonds include poor proton donors like C-H bonds and poor acceptors such as π electron density and halogen atoms (Br, Cl, I) and S. For weak hydrogen bonds bond lengths and bond angles lie in the range of 3.0-4.0 Å and 110-150° respectively. Weak hydrogen bonds have binding energies of less than 15 kJ mol⁻¹, while strong hydrogen bonds have energies of 60-120 kJ mol⁻¹.[19]It is important however, to note that these ranges are not absolute and may they may be some drift in the bond lengths and angles.

Graph Set Notation[20] is a tool used to explain H-bonding patterns in crystals. This was designed by Etter and co-workers[20-21] who did a comprehensive Cambridge Structural Database (CSD) analysis on the preference for singular functional groups and their arrangements in solids. Subsequently they developed a general formula to describe the observed patterns, given as $G_d^a r$, where G is the graphical descriptor of the motif (S-intramolecular, C-chain, R-ring, D-discrete bonds), 'a' is the number of acceptor atoms, 'd' is the number of donor atoms and 'r' is the number of atoms involved in the motif.

The cocrystal of nicotinamide formed with 2,4-dihydroxybenzoic acid[22] (24DHBA) is an example whereby the three types of graph set descriptors are illustrated. The hydrogen bonded acid-amide dimer forms a ring described by the $R_2^2(8)$ graph set. Additionally, the nicotinamide N-atom connects with 24DHBA through a discrete O-H⋯N bond, designated as $D_1^1(2)$ graph set and 24DHBA forms an intramolecular hydrogen bond given by $S_1^1(6)$ descriptor (Figure 1.2). Graph Set Notation was used to describe the observed H-bond networks in detail in this thesis.
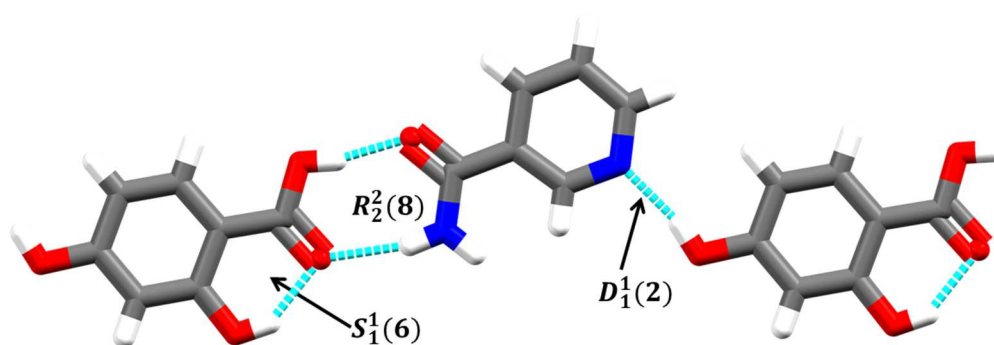
Figure 1.2 Graph set descriptors in a cocrystal of nicotinamide with 2,4-dihydroxybenzoic acid

1.3.2 $\pi - \pi$ interactions

These interactions are formed through attraction between the π electron cloud of one molecule and the positively charged part of an adjacent molecule.[23] π-π interactions are controlled by electrostatics and their occurrence is contingent upon the orientation of the two interacting molecules.[24] The π interactions are classified into three types: (i) face-to-face (direct), (ii) face-to-face (displaced), where the association is between the electron cloud of one of the parallel ring and the hydrogens of the other parallel ring, and (iii) edge-

to-face, where the hydrogen atom from one perpendicular ring interacts with the electron cloud of a neighbouring ring (Figure 1.3).[3] The edge-to-face interaction is also classified as a weak hydrogen bond. The strength of these interactions ranges from about 5-40 kJ mol^{-1}. Additionally, the direct face to face and displaced face to face interactions have aromatic ring centroid-to-centroid distances of up to 3.8 Å, while for the edge to face interaction the hydrogen atom to centroid distance can go up to 5.0 Å.[19]
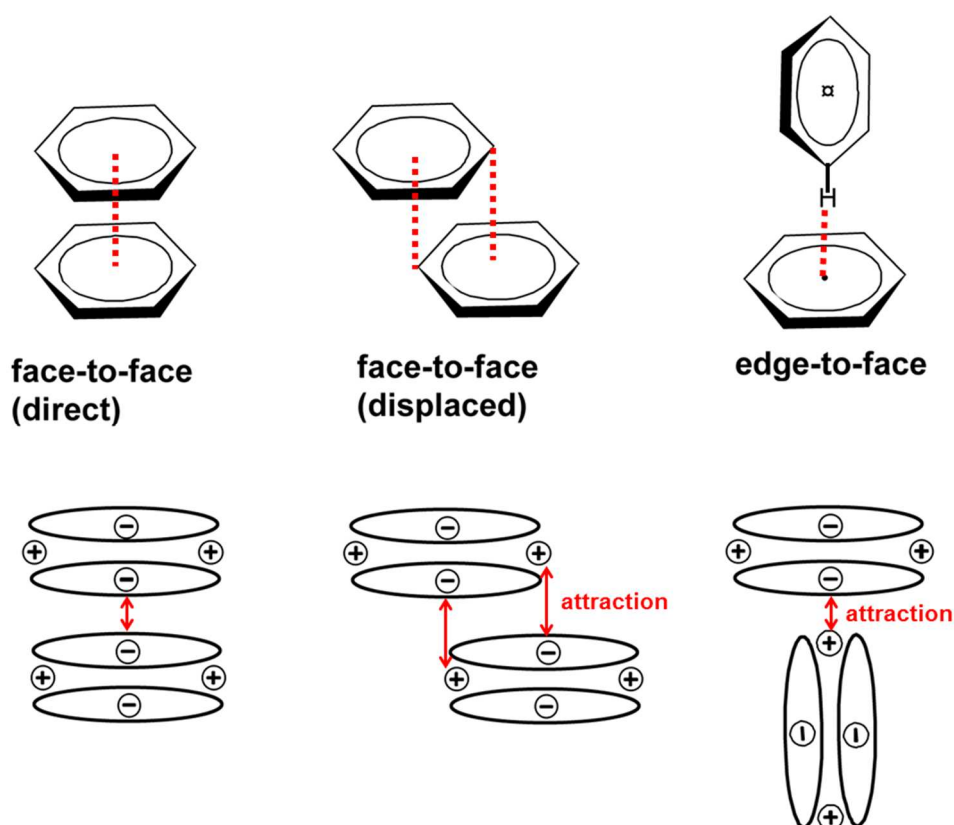
Figure 1.3 Types of π-π interactions: face-to-face (direct), face-to-face (displaced) and edge-to-face interaction.

1.3.3 Halogen bonds

The halogen bond has recently gained attention in supramolecular chemistry due to its strong and directional nature.[25] It occurs *"when there is a net attractive interaction between an electrophilic region associated with a halogen atom in a molecular entity and a nucleophilic region in another, or the same, molecular entity".[26]* The most crucial part to the halogen interaction is the presence of the electron-poor tip of the halogen atom (σ hole)

which interacts with the nucleophilic region of the neighbouring molecule.[27] The strength of the interaction is known to increase from chlorine to iodine.[28] Figure 1.4 shows a halogen bond formed between iodine and nitrogen.
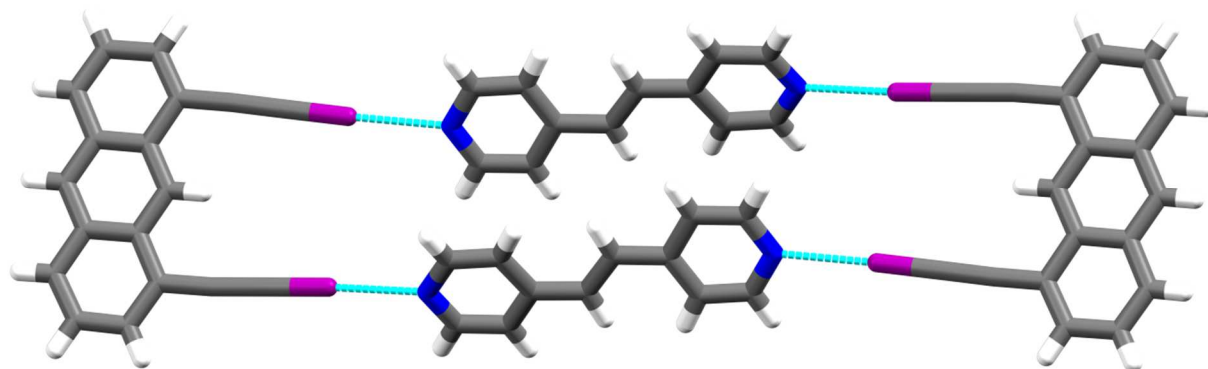
Figure 1.4 Halogen bond formed between the iodine of TW-10-15 1,8-di (iodoethynyl)anthracene, and the pyridine nitrogen of 1,2-bis(4-pyridyl)ethylene.[29]

1.4   Supramolecular synthons

Supramolecular synthons were defined by Desiraju as *"structural units within supermolecules that can be formed and/or assembled by known or conceivable synthetic processes involving intermolecular interactions".[30]* Supramolecular synthons are classified into two types; homosynthon and heterosynthon. Supramolecular homosynthons form between the same complimentary functional groups (e.g. amide dimers or carboxylic acid dimers), while supramolecular heterosynthons form between different but complementary functional groups (e.g. carboxylic acid-amide dimer).[31] Studies shows that heterosynthon formation (alcohol-amine,[32] acid-amide,[31a, 33] acid-aromatic nitrogen[34] and alcohol-aromatic nitrogen[35]) (Figure 1.5) is favoured where different functional groups are present in the molecular building blocks.
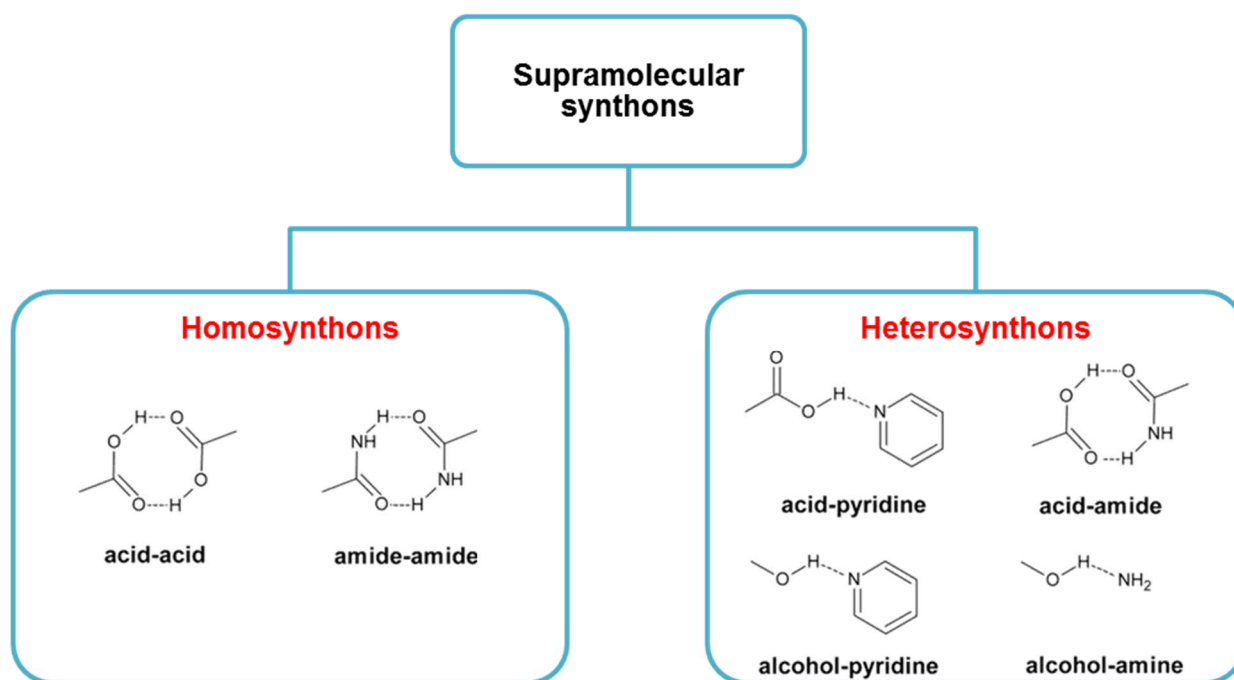
Figure 1.5 Examples of supramolecular synthons.

1.5 Multicomponent crystals

Multicomponent crystals can be categorized into five main types: cocrystals, salts, hydrates, solvates and polymorphs (Figure 1.6). A polymorph is a crystalline solid phase of a given compound resulting from the possibility of at least two crystalline arrangements of the molecules of a given compound in the solid state.[36] Solvates/hydrates can be defined as crystalline solids formed when a compound includes a solvent/water molecule into its structure either in stoichiometric or non-stoichiometric ratio. In 1844, Wöhler[37] synthesized the first multicomponent crystal, quinhydrone, a cocrystal of benzoquinone and hydroquinone. Later, other multicomponent crystals were reported but termed differently such as molecular complexes,[38] heteromolecular crystals,[39] organic molecular compounds[40] and addition compounds.[41]

| Cocrystal | Solvate/ Hydrate | Polymorph | Salt |

| pharmaceutical compound | coformer | counter-ion | solvent/ water |
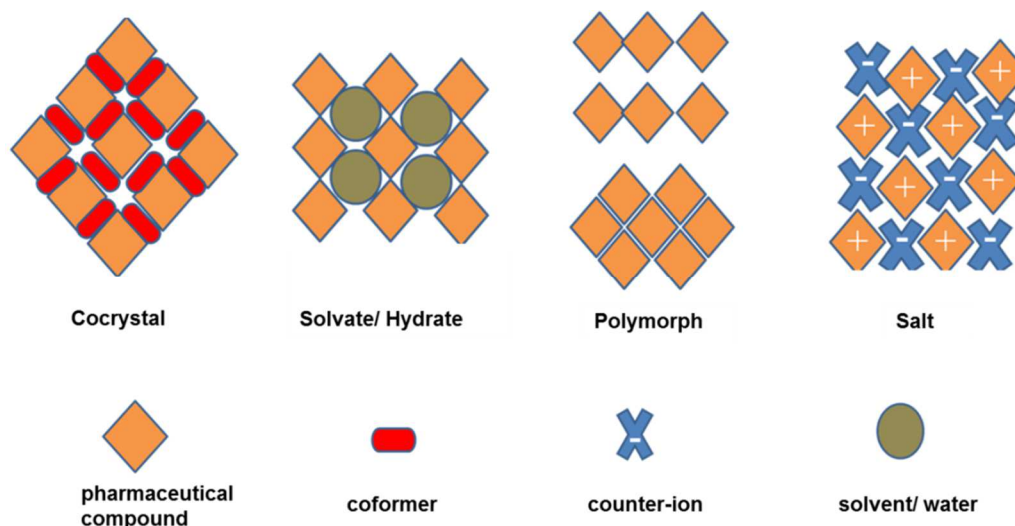
Figure 1.6 Possible multicomponent crystal forms: cocrystals, solvates/hydrates, polymorphs or salts.

1.5.1   Salts and Cocrystals

For ionisable compounds, preparation of salt forms, using acids and bases, is a common strategy to obtain multicomponent crystals. Salt formation occurs in solution, when an ionisable compound forms a strong ionic interaction with an oppositely charged counter ion. The formation of salts is highly dependent on the strength of the acid or base (pK_a), and the acidity and basicity constants of the compounds involved. In formulation development, preparation of salts is relatively simple, and about 50 % of marketed active pharmaceutical ingredients are administered as salts.[42] However, the limitation of salt formation is the small number of acceptable compounds, which possess ionisable sites.[43] As a result, the design and synthesis of cocrystals have become an important tool because of the ability to cocrystallize neutral and/or non-ionisable compounds.

A cocrystal can be defined as *"a solid crystalline single phase material which composed of two or more different neutral/ionic molecules in a stoichiometric ratio".[34a, 44]* Salt and cocrystal formation is governed by the quantitative 'pKa rule'. According to Cruz-Cabeza,[45] if the ΔpKa (ΔpK_a = pK_a [protonated base] − pKa [acid]) is less than -1, the appearance of a cocrystal is expected, and if the ΔpK_a is higher than 4, the formation of a salt is expected. In the range of -1 ≤ ΔpK_a ≤ 4, every increase in one ΔpK_a increases the probability of a salt formation by 17 %. The data was analyzed for aqueous pKa values and she highlighted that it is crucial to note that the pK_a values are solvent dependant. Also, it is stated that the ΔpK_a can be implemented in compounds with only one donor or acceptor site.

1.5.2 Pharmaceutical cocrystals

The beneficial activity of drugs is judged or determined on the basis of key factors like bioavailability, solubility, chemical stability, dissolution rate, hygroscopicity, etc. Drug synthesis was discovered as a result of traditional remedies, however with the emergence of new diseases and the development of drug-resistance in microbes, the demand for design and synthesis of new drug molecules has risen.[46]

Most drugs are generally preferred in the solid form because it is compatible and easy to handle. More importantly the thermodynamically most stable crystalline form of the compound is highly favourable. However, the stable crystal form of the parent compound may exhibit inadequate solubility or dissolution rate resulting in poor oral absorption, particularly for water-insoluble compounds as in the case of saquinavir and ganciclovir.[47] In such cases, alternative solid forms may be investigated such as co-crystals, polymorphs, salts, and amorphous solids of poorly soluble drugs.[48] Cocrystallization of APIs with GRAS compounds (Generally Regarded As Safe), non-toxic substances as defined by the Federal Drug Association (FDA), may yield pharmaceutical multicomponent crystals that can be considered for pharmaceutical purposes.

The pharmaceutical cocrystal approach employs the principles of crystal engineering and has the advantage that the number of harmless potential cocrystal formers is large. Through cocrystallization, (S,S)-moxifloxacin hydrochloride hemihydrate a fluoroquinolone based antibiotic formed a pharmaceutical cocrystal with 4-hydroxybenzoic acid (4HBA) which improved its solubility and dissolution significantly.[49] Additionally, multicomponent crystal formation was used as a tool for solubility enhancement in the case of meloxicam, a nonsteroidal anti-inflammatory drug, which formed a cocrystal with carboxylic acids (1-hydroxy-2-naphthoic acid, succinic acid and salicylic acid).[50] The cocrystals showed increased aqueous solubility compared to that of meloxicam. Mechanical properties of paracetamol were also engineered via cocrystallization with theophylline, and layered cocrystals with high tensile strength were obtained.[51] The tablets made from the cocrystal improved the poor mechanical properties of the pure paracetamol tablets.

1.6 Sulfa drugs

Sulfonamides were the first compounds to be administered as antibacterial drugs, however the development of bacterial resistance resulted in most being withdrawn from the market.[52] They have gained interest in crystal engineering because they contain multiple hydrogen bond donor and acceptor sites as shown in the different structures of sulfonamides (Figure 1.7), which enables the formation of varied synthons.[53]

Previous studies have shown that the synthon engineering approach provides a guide for coformer selection in order to achieve predetermined structures.[54,55,56] Because sulfa drugs have strong hydrogen bonding groups, such as NH_2, SO_2 and NH (sulfonamide), they are challenging compounds to study in the context of hydrogen bonding preference.[57] The introduction of coformers with competing acceptor and donor sites creates multiple synthons, and can possibly disrupt the preferred dimers within the sulfonamides.
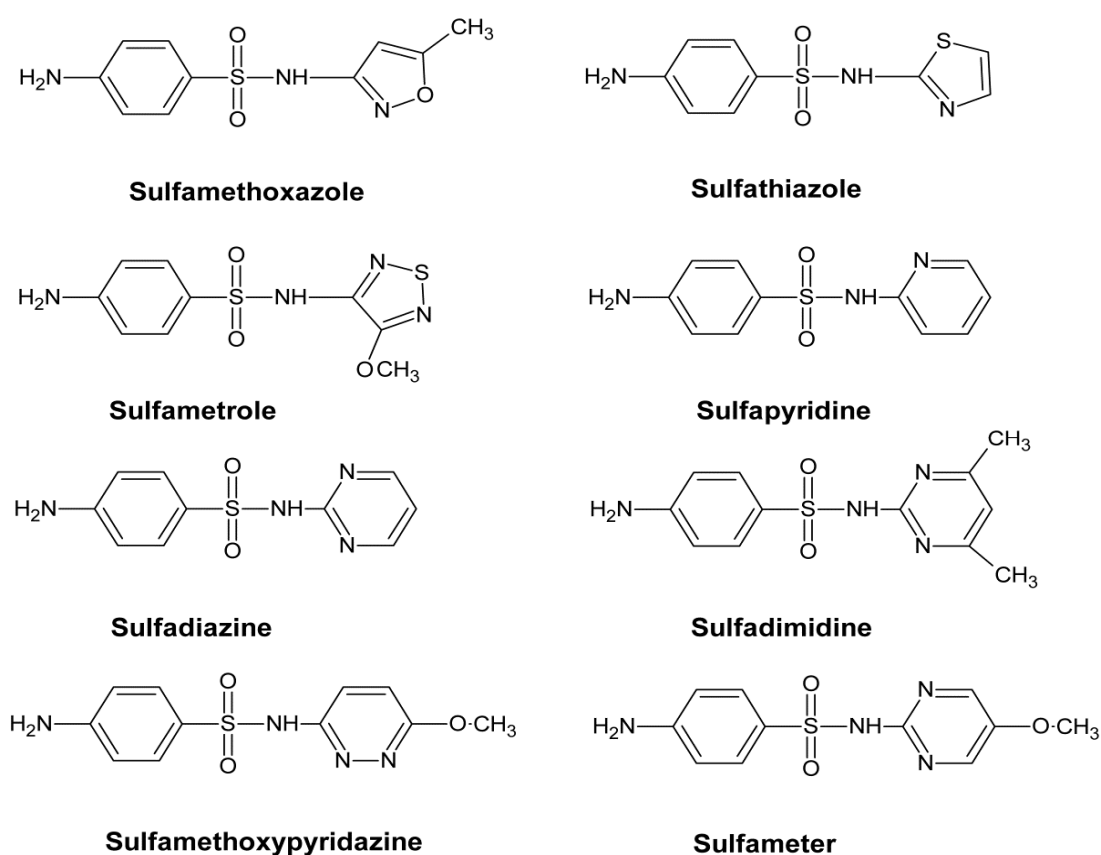
Figure 1.7 Chemical structures of common sulfonamide drugs.

In crystal packing of sulfonamides the $NH_2\cdots O$ (sulfoxide) is the most resilient interaction, which forms continuous $C_1^1(8)$ chains, as well as the (amidine) N—H$\cdots$N (pyrimidine) homodimer. It has been convincingly shown in previous studies that employing carboxylic acids, amines or amides has been a successful cocrystallization strategy to disrupt the common $R_2^2(8)$ homodimer (Figure 1.8a) and form new robust heterosynthons.[53-58] When Domingos and co-workers synthesized multicomponent crystals of sulfadimethoxine with amides, cyclic amines and carboxylic acids, characterization of their new solid forms showed disruption of the typical dimer formation(Figure 1.8b).[54] Also, Gosh and associates synthesized cocrystals of sulfamethazine, another antibacterial drug in veterinary and human medicines, with aromatic carboxylic acid and amide coformers(Figure 1.8c&d).[56,59] In all their crystal structures, the multicomponent crystals formed multiple heterosynthons and Figure 1.8 shows examples in different sulfonamide multicomponent crystals where the homodimer is formed and cases where it was disrupted.

(a) sulfapyridine dimer

(b) sulfamethoxine·isonicotinamide

(c) sulfamethazine·3-methylpyridine

(d) sulfamethazine·2,4-dihydroxybenzoic acid
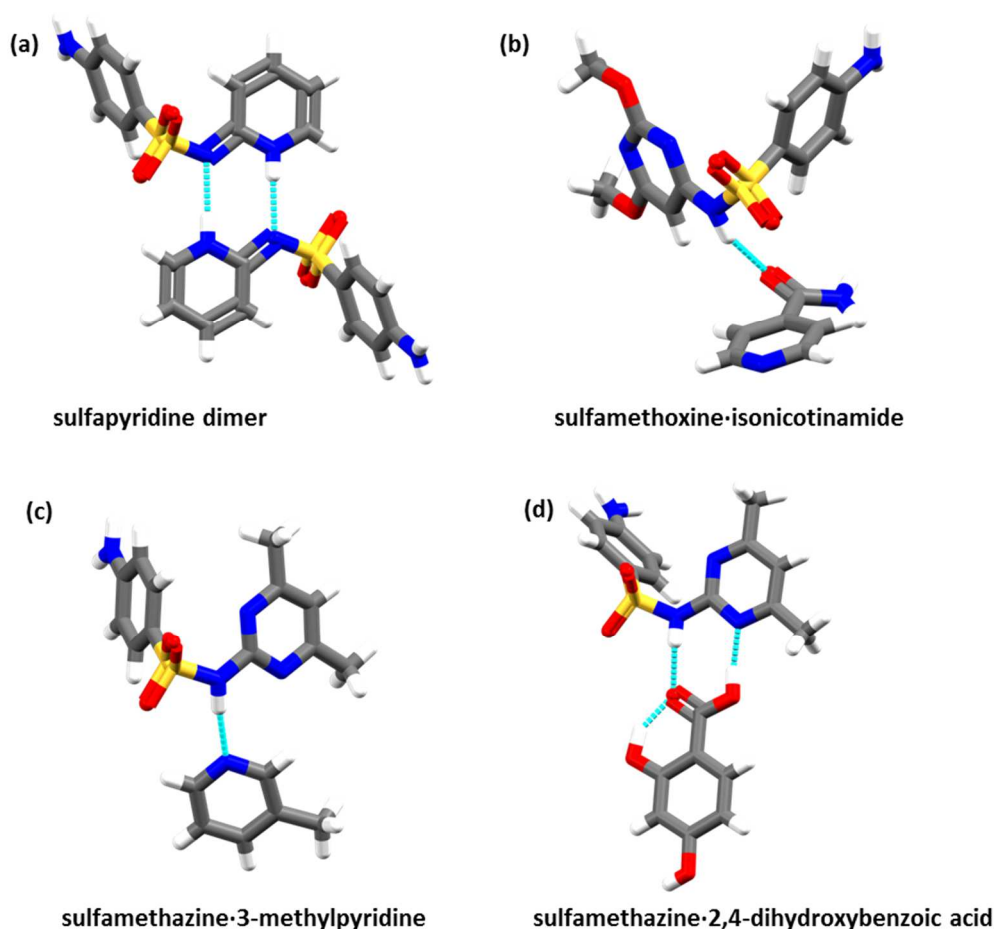
Figure 1.8 Examples from previous studies showing the sulfonamide dimer and cases where the sulfonamide dimers were disrupted.

Much attention is being given to sulfa compounds in the context of multicomponent crystals because of their ability to conform to the geometric demands of different coformers.[54, 56, 58b, 60] They exist in either amidine or imidine tautomeric forms (Figure 1.9), and when they are cocrystallized with coformers they form different hydrogen bonding motifs with different coformers, a phenomenon which is referred to as coformer assisted amidine-imidine tautomerism.[56] Among others, Elacqua and coworkers[58b] studied the role of tautomers and geometry of the anionic sulfa drug complexes and cocrystals. In their study, they measured the sulfonamide geometry parameter (S-N bond length) to effectively determine a cocrystal-salt continuum of their complexes. Their work successfully explored the structural relationship of tautomers and determined a distinct boundary between the salts and cocrystals.
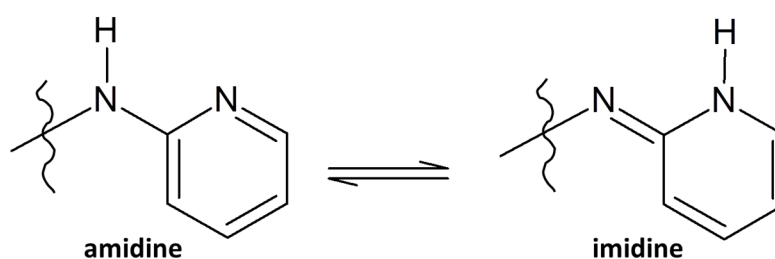
Figure 1.9 Scheme showing the positon of the H-atom in the amidine and imidine tautomer.

1.7   Scope of the dissertation

Two sulfa drugs, sulfapyridine (4-Amino-N-(2-pyridinyl) benzenesulfonamide, SFP) and sulfadiazine (4-Amino-N-(2-pyrimidinyl) benzenesulfonamide, SFD) were investigated in this study (Figure 1.10). These target pharmaceutical compounds contain multiple functional groups; three hydrogen bond acceptor sites: two S=O groups from (SO_2) and an imidine (–N) group, and two donor groups: the amine (-NH_2), and sulfonamide (–NH) atom. As such, they exhibit variable solid-state properties and the possibility to occur in multiple solid forms.[53, 57] In line with previous literature studies, SFP and SFD were analyzed to evaluate how they interact in the solid state with selected coformers. Our interest in SFP was ignited by the few structures of the drug reported in the Cambridge Structural Database (5 solvates and 10 polymorphs).[61]
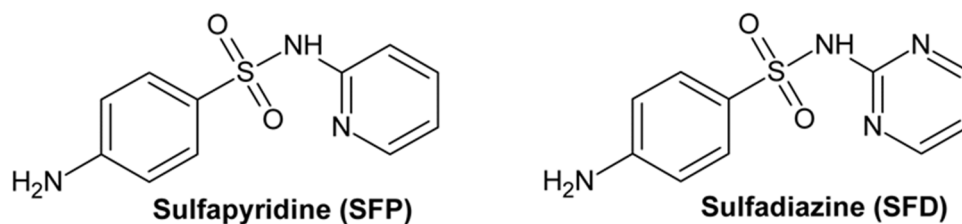
Figure 1.10 Sulfapyridine and sulfadiazine.

The SFD molecule was employed in this study for the purpose of investigating the effect of small structural changes. The new solid forms were constructed using carboxylic acids and a pyridine derivative: 3-nitrobenzoic acid (3NBA), 4-nitrobenzoic acid (4NBA), 3,5-dinitrosalicylic acid (DNSA), 5-bromosalicylic acid (5BSA), 3,5-dibromosalicylic acid (DBSA) and 4-dimethylamino pyridine (4DMAP). We expect our work to add to the ongoing study on the hydrogen bond competition of sulfa drugs in multicomponent crystals.

1.7.1 Objectives of the study

* To employ crystal engineering principles in the preparation of sulfapyridine and sulfadiazine multicomponent crystals.

* To examine the influence of pK$_a$'s of coformers on the type of hydrogen bonding motifs observed.

* To examine the physicochemical properties of newly synthesized solid forms.

* To limit the dimer formation in SFP and SFD by employing coformers with strong hydrogen bond donors and/or acceptors.

* To investigate the effect on crystal packing of the position of the substituent/s on the coformer,

* To investigate the effect on crystal packing of the number of substituent groups on the coformer,

* To investigate the influence of small structural changes on hydrogen bonding and crystal packing via cocrystallisation of structural similar compounds with the same coformer.

* To evaluate effect of acidity change in coformer by using a pyridine derivative coformer

* To perform conformational analysis and analyse how the interconversion of tautomers promotes crystal formation by conforming to the geometric demands of the different coformers.

1.8   References

1. Lehn, J. M., Supramolecular chemistry—scope and perspectives molecules, supermolecules, and molecular devices (Nobel Lecture). *Angewandte Chemie International Edition* **1988,** *27* (1), 89-112.
2. Lehn, J.-M., *Supramolecular chemistry*. 1995; Vol. 1.
3. Steed, J. W.; Turner, D. R.; Wallace, K., *Core concepts in supramolecular chemistry and nanochemistry*. John Wiley & Sons: **2007**.
4. Pedersen, C. J., Cyclic polyethers and their complexes with metal salts. *Journal of the American Chemical Society* **1967,** *89* (10), 2495-2496.
5. Lehn, J.-M., Supramolecular chemistry: Where from? Where to? *Chemical Society Reviews* **2017,** *46* (9), 2378-2379.
6. (a) Chang, Y.-C; Chen, Y.-D.; Chen, C.-H.; Wen, Y.-S.; Lin, J. T.; Chen, H.-Y.; Kuo, M.-Y.; Chao, I., Crystal Engineering for π–π Stacking via Interaction between Electron-Rich and Electron-Deficient Heteroaromatics. *The Journal of Organic Chemistry* **2008,** *73* (12), 4608-4614; (b) Hunter, C. A.; Sanders, J. K. M., The nature of pi-pi interactions. *Journal of the American Chemical Society* **1990,** *112* (14), 5525-5534.
7. Madura, I. D.; Czerwińska, K.; Jakubczyk, M.; Pawełko, A.; Adamczyk-Woźniak, A.; Sporzyński, A., Weak C–H⋯O and Dipole–Dipole Interactions as Driving Forces in Crystals of Fluorosubstituted Phenylboronic Catechol Esters. *Crystal Growth & Design* **2013,** *13* (12), 5344-5352.
8. (a) Aakeröy, C. B.; Schultheiss, N.; Rajbanshi, A.; Desper, J.; Moore, C., Supramolecular synthesis based on a combination of hydrogen- and halogen bonds. *Crystal Growth & Design* **2009,** *9* (1), 432-441; (b) George, A. J., *An Introduction to Hydrogen Bonding . Oxford University Press: Oxford.* **1997**; (c) Kollman, P. A.; Allen, L. C., Theory of the hydrogen bond. *Chemical Reviews* **1972,** *72* (3), 283-303.
9. (a) Farina, A.; Meille, S. V.; Messina, M. T.; Metrangolo, P.; Resnati, G.; Vecchio, G., Resolution of Racemic 1,2-Dibromohexafluoropropane through Halogen-Bonded Supramolecular Helices. *Angewandte Chemie International Edition* **1999,** *38* (16), 2433-2436; (b) Metrangolo, P.; Resnati, G., Halogen Versus Hydrogen. *Science* **2008,** *321* (5891), 918-919.
10. Desiraju, G. R., Crystal Engineering: A Holistic View. *Angewandte Chemie International Edition* **2007,** *46* (44), 8342-8356.
11. Bondi, A., van der Waals Volumes and Radii. *The Journal of Physical Chemistry* **1964,** *68* (3), 441-451.
12. Ball, P., The shapes of things to come. *Nature* **1994,** *371*, 202.
13. Braga, D.; Brammer, L.; Champness, N. R., New trends in crystal engineering. *CrystEngComm* **2005,** *7* (1), 1-19.
14. Datta, S.; Grant, D. J., Crystal structures of drugs: advances in determination, prediction and engineering. *Nature Reviews Drug Discovery* **2004,** *3* (1), 42-57.
15. Schmidt, G. M. J., Photodimerization in the solid state. In *Pure and Applied Chemistry*, **1971**; Vol. 27, p 647.
16. Thomas, J. M.; Morsi, S. E.; Desvergne, J. P., Topochemical Phenomena in Organic Solid-State Chemistry. In *Advances in Physical Organic Chemistry*, Gold, V.; Bethel, D., Eds. Academic Press: **1977**; Vol. 15, pp 63-151.
17. (a) Lehn, J.-M., Toward Self-Organization and Complex Matter. *Science* **2002,** *295* (5564), 2400; (b) Etter, M. C., Hydrogen bonds as design elements in organic chemistry. *The Journal of Physical Chemistry* **1991,** *95* (12), 4601-4610.
18. Bruton, E. A.; Brammer, L.; Christopher Pigge, F.; Aakeröy, C. B.; Leinen, D. S., Hydrogen bond patterns in aromatic and aliphatic dioximes. *New Journal of Chemistry* **2003,** *27* (7), 1084-1094.
19. Desiraju, G. R.; Vittal, J. J.; Ramanan, A., *Crystal engineering: a textbook*. World Scientific: 2011.
20. Etter, M. C.; MacDonald, J. C.; Bernstein, J., Graph-set analysis of hydrogen-bond patterns in organic crystals. *Acta Crystallographica Section B* **1990,** *46* (2), 256-262.
21. (a) Bernstein, J.; Davis, R. E., Graph Set Analysis of Hydrogen Bond Motifs. In *Implications of Molecular and Materials Structure for New Technologies*, Howard, J. A. K.; Allen, F. H.; Shields, G. P., Eds. Springer Netherlands: Dordrecht, **1999**; pp 275-290; (b) Etter, M. C., Encoding and decoding

hydrogen-bond patterns of organic compounds. *Accounts of Chemical Research* **1990,** *23* (4), 120-126.

22. Lemmerer, A.; Adsmond, D. A.; Esterhuysen, C.; Bernstein, J., Polymorphic Co-crystals from Polymorphic Co-crystal Formers: Competition between Carboxylic Acid⋯Pyridine and Phenol⋯Pyridine Hydrogen Bonds. *Crystal Growth & Design* **2013,** *13* (9), 3935-3952.

23. Steed, J. W.; Atwood, J. L., *Concepts in Supramolecular Chemistry*, John Wiley & Sons, Ltd: **2009;** pp 1-48.

24. Hunter, C. A.; Lawson, K. R.; Perkins, J.; Urch, C. J., Aromatic interactions. *Journal of the Chemical Society, Perkin Transactions 2* **2001,** (5), 651-669.

25. Cavallo, G.; Metrangolo, P.; Milani, R.; Pilati, T.; Priimagi, A.; Resnati, G.; Terraneo, G., The Halogen Bond. *Chemical Reviews* **2016,** *116* (4), 2478-2601.

26. Metrangolo, P.; Resnati, G., Type II halogen...halogen contacts are halogen bonds. *IUCrJ* **2014,** *1* (1), 5-7.

27. Metrangolo, P.; Neukirch, H.; Pilati, T.; Resnati, G., Halogen Bonding Based Recognition Processes: A World Parallel to Hydrogen Bonding. *Accounts of Chemical Research* **2005,** *38* (5), 386-395.

28. Zheng, Y.-Z.; Deng, G.; Zhou, Y.; Sun, H.-Y.; Yu, Z.-W., Comparative Study of Halogen- and Hydrogen-Bond Interactions between Benzene Derivatives and Dimethyl Sulfoxide. *ChemPhysChem* **2015,** *16* (12), 2594-2601.

29. Wijethunga, T. K.; Dakovic, M.; Desper, J.; Aakeröy, C. B., A new tecton with parallel halogen-bond donors: a path to supramolecular rectangles. *Acta Crystallographica Section B* **2017,** *73* (2), 163-167.

30. Desiraju, G. R., Supramolecular Synthons in Crystal Engineering—A New Organic Synthesis. *Angewandte Chemie International Edition in English* **1995,** *34* (21), 2311-2327.

31. (a) Walsh, R. D. B.; Bradner, M. W.; Fleischman, S.; Morales, L. A.; Moulton, B.; Rodriguez-Hornedo, N.; Zaworotko, M. J., Crystal engineering of the composition of pharmaceutical phases. *Chemical Communications* **2003,** (2), 186-187; (b) Almarsson, O.; Zaworotko, M. J., Crystal engineering of the composition of pharmaceutical phases. Do pharmaceutical co-crystals represent a new path to improved medicines? *Chemical Communications* **2004,** (17), 1889-1896.

32. (a) Hanessian, S.; Saladino, R.; Margarita, R.; Simard, M., Supramolecular Chirons Based on Enantiodifferentiating Self-Assembly between Amines and Alcohols (Supraminols). *Chemistry – A European Journal* **1999,** *5* (7), 2169-2183; (b) Dey, A.; Kirchner, M. T.; Vangala, V. R.; Desiraju, G. R.; Mondal, R.; Howard, J. A. K., Crystal Structure Prediction of Aminols: Advantages of a Supramolecular Synthon Approach with Experimental Structures. *Journal of the American Chemical Society* **2005,** *127* (30), 10545-10559; (c) Mondal, R.; Howard, J. A. K.; Banerjee, R.; Desiraju, G. R., Crystallographic Studies of Supramolecular Synthons in Amine Solvates of trans-1,5-Dichloro-9,10-diethynyl-9,10- dihydroanthracene-9,10-diol. *Crystal Growth & Design* **2006,** *6* (11), 2507-2516; (d) Vangala, V. R.; Mondal, R.; Broder, C. K.; Howard, J. A. K.; Desiraju, G. R., Dianiline-Diphenol Molecular Complexes Based on Supraminol Recognition. *Crystal Growth & Design* **2005,** *5* (1), 99-104.

33. (a) Aakeröy, C. B.; Desper, J.; Helfrich, B. A., Heteromeric intermolecular interactions as synthetic tools for the formation of binary co-crystals. *CrystEngComm* **2004,** *6* (5), 19-24; (b) Aakeröy, C. B.; Beatty, A. M.; Helfrich, B. A., A High-Yielding Supramolecular Reaction. *Journal of the American Chemical Society* **2002,** *124* (48), 14425-14432; (c) Reddy, L. S.; Nangia, A.; Lynch, V. M., Phenyl-perfluorophenyl synthon mediated cocrystallization of carboxylic acids and amides. *Crystal Growth & Design* **2004,** *4* (1), 89-94; (d) Bhogala, B. R.; Basavoju, S.; Nangia, A., Tape and layer structures in cocrystals of some di-and tricarboxylic acids with 4, 4'-bipyridines and isonicotinamide. From binary to ternary cocrystals. *CrystEngComm* **2005,** *7*, 551-562; (e) Fleischman, S. G.; Kuduva, S. S.; McMahon, J. A.; Moulton, B.; Bailey Walsh, R. D.; Rodríguez-Hornedo, N.; Zaworotko, M. J., Crystal Engineering of the Composition of Pharmaceutical Phases: Multiple-Component Crystalline Solids Involving Carbamazepine. *Crystal Growth & Design* **2003,** *3* (6), 909-919.

34. (a) Bhogala, B. R.; Nangia, A., Ternary and quaternary co-crystals of 1,3-cis,5-cis-cyclohexanetricarboxylic acid and 4,4-bipyridines. *New Journal of Chemistry* **2008,** *32* (5), 800-807;

(b) Santra, R.; Ghosh, N.; Biradha, K., Crystal engineering with acid and pyridine heteromeric synthon: neutral and ionic co-crystals. *New Journal of Chemistry* **2008,** *32* (10), 1673-1676; (c) Thakur, T. S.; Desiraju, G. R., Crystal Structure Prediction of a Co-Crystal Using a Supramolecular Synthon Approach: 2-Methylbenzoic Acid–2-Amino-4-methylpyrimidine. *Crystal Growth & Design* **2008,** *8* (11), 4031-4044; (d) Aakeröy, C. B.; Hussain, I.; Forbes, S.; Desper, J., Exploring the hydrogen-bond preference of N–H moieties in co-crystals assembled via O–H (acid)··· N (py) intermolecular interactions. *CrystEngComm* **2007,** *9* (1), 46-54; (e) Lynch, D.; Smith, G.; Freney, D.; Byriel, K.; Kennard, C., Molecular Cocrystals of Carboxylic Acids. XV. Preparation and Characterization of Heterocyclic Base Adducts With a Series of Carboxylic Acids, and the Crystal Structures of the Adducts of 2-Aminopyrimidine With 2,6-Dihydroxybenzoic Acid, 4-Aminobenzoic Acid, Phenoxyacetic Acid, (2,4-Dichlorophenoxy)acetic Acid, (3,4-Dichlorophenoxy)-acetic Acid and Salicylic Acid, and 2-Aminopyridine With 2,6-Dihydroxybenzoic Acid. *Australian Journal of Chemistry* **1994,** *47* (6), 1097-1115; (f) Papaefstathiou, G. S.; Kipp, A. J.; MacGillivray, L. R., Exploiting modularity in template-controlled synthesis: a new linear template to direct reactivity within discrete hydrogen-bonded molecular assemblies in the solid state. *Chemical Communications* **2001,** (23), 2462-2463.

35. (a) Friščić, T.; Drab, D. M.; MacGillivray, L. R., A Test for Homology: Photoactive Crystalline Assemblies Involving Linear Templates Based on a Homologous Series of Phloroglucinols. *Organic Letters* **2004,** *6* (25), 4647-4650; (b) Papaefstathiou, G. S.; MacGillivray, L. R., Discrete versus Infinite Molecular Self-Assembly: Control in Crystalline Hydrogen-Bonded Assemblies Based on Resorcinol. *Organic Letters* **2001,** *3* (24), 3835-3838; (c) Vishweshwar, P.; Nangia, A.; Lynch, V. M., Supramolecular synthons in phenol-isonicotinamide adducts. *CrystEngComm* **2003,** *5* (31), 164-168; (d) Varughese, S.; Pedireddi, V. R., A Competitive Molecular Recognition Study: Syntheses and Analysis of Supramolecular Assemblies of 3,5-Dihydroxybenzoic Acid and Its Bromo Derivative with Some N-Donor Compounds. *Chemistry − A European Journal* **2006,** *12* (6), 1597-1609; (e) Zeng, Q.; Wu, D.; Liu, C.; Ma, H.; Lu, J.; Xu, S.; Li, Y.; Wang, C.; Bai, C., Crystal Engineering Based on Polymeric Hydrogen-Bonded Supramolecules by Self-Assembling of 4,4′-(9-Fluorenylidene)diphenol and 4,4′-Cyclohexylidenebisphenol with Bipyridines. *Crystal Growth & Design* **2005,** *5* (3), 1041-1047.

36. Brittain, H. G.; Grant, D. J.; Myrdal, P. B., Effects of polymorphism and solid-state solvation on solubility and dissolution rate. *Polymorphism in pharmaceutical solids* **1999,** *95*, 279-330.

37. Wöhler, F., Untersuchungen über das Chinon. *Justus Liebigs Annalen der Chemie* **1844,** *51* (2), 145-163.

38. van Niekerk, J. N.; Saunder, D. H., The crystal structure of the molecular complex of 4:4'-dinitrodiphenyl with diphenyl. *Acta Crystallographica* **1948,** *1* (1), 44.

39. Pekker, S.; Kováts, É.; Oszlányi, G.; Bényei, G.; Klupp, G.; Bortel, G.; Jalsovszky, I.; Jakab, E.; Borondics, F.; Kamarás, K.; Bokor, M.; Kriza, G.; Tompa, K.; Faigel, G., Rotor–stator molecular crystals of fullerenes with cubane. *Nature Materials* **2005,** *4*, 764.

40. Anderson, J. S., Structure of Organic Molecular Compounds. *Nature* **1937,** *140*, 583.

41. Buck, J. S.; Ide, W. S., Mixed benzoin vi. further examples of reversibility. the formation of addition compounds. *Journal of the American Chemical Society* **1931,** *53* (7), 2784-2787.

42. Stahl, P. H.; Wermuth, C. G., Handbook of pharmaceutical salts: properties, selection and use. *Chemistry International* **2002,** *24* (3), 21.

43. Blagden, N.; Coles, S. J.; Berry, D. J., Pharmaceutical co-crystals - are we there yet? *CrystEngComm* **2014,** *16* (26), 5753-5761.

44. (a) Bond, A. D., What is a co-crystal? *CrystEngComm* **2007,** *9* (9), 833-834; (b) Jones, W.; Motherwell, W. D. S.; Trask, A. V., Pharmaceutical Cocrystals: An Emerging Approach to Physical Property Enhancement. *MRS Bulletin* **2006,** *31* (11), 875-879; (c) Vishweshwar, P.; McMahon, J. A.; Bis, J. A.; Zaworotko, M. J., Pharmaceutical Co-Crystals. *Journal of Pharmaceutical Sciences 95* (3), 499-516; (d) Aakeröy, C. B.; Salmon, D. J., Building co-crystals with molecular sense and supramolecular sensibility. *CrystEngComm* **2005,** *7* (72), 439-448.

45. Cruz-Cabeza, A. J., Acid-base crystalline complexes and the pKa rule. *CrystEngComm* **2012,** *14* (20), 6362-6365.

46. Florence, A. T.; Attwood, D., *Physicochemical principles of pharmacy*. Chicago : Pharmaceutical Press: London, **2006**.

47. Babu, N. J.; Nangia, A., Solubility Advantage of Amorphous Drugs and Pharmaceutical Cocrystals. *Crystal Growth & Design* **2011**, *11* (7), 2662-2679.

48. Good, D. J.; Rodríguez-Hornedo, N., Solubility Advantage of Pharmaceutical Cocrystals. *Crystal Growth & Design* **2009**, *9* (5), 2252-2264.

49. Martínez-Alejo, J. M.; Domínguez-Chávez, J. G.; Rivera-Islas, J.; Herrera-Ruiz, D.; Höpfl, H.; Morales-Rojas, H.; Senosiain, J. P., A Twist in Cocrystals of Salts: Changes in Packing and Chloride Coordination Lead to Opposite Trends in the Biopharmaceutical Performance of Fluoroquinolone Hydrochloride Cocrystals. *Crystal Growth & Design* **2014**, *14* (6), 3078-3095.

50. Weyna, D. R.; Cheney, M. L.; Shan, N.; Hanna, M.; Zaworotko, M. J.; Sava, V.; Song, S.; Sanchez-Ramos, J. R., Improving Solubility and Pharmacokinetics of Meloxicam via Multiple-Component Crystal Formation. *Molecular Pharmaceutics* **2012**, *9* (7), 2094-2102.

51. Karki, S.; Friščić, T.; Fábián, L.; Laity, P. R.; Day, G. M.; Jones, W., Improving Mechanical Properties of Crystalline Solids by Cocrystal Formation: New Compressible Forms of Paracetamol. *Advanced Materials* **2009**, *21* (38-39), 3905-3909.

52. Sköld, O., Sulfonamide resistance: mechanisms and trends. *Drug Resistance Updates* **2000**, *3* (3), 155-160.

53. Caira, M. R., Sulfa Drugs as Model Cocrystal Formers. *Molecular Pharmaceutics* **2007**, *4* (3), 310-316.

54. Domingos, S.; Fernandes, A.; Duarte, M. T.; Piedade, M. F. M., New Multicomponent Sulfadimethoxine Crystal Forms: Sulfonamides as Participants in Supramolecular Interactions. *Crystal Growth & Design* **2016**, *16* (4), 1879-1892.

55. Caira, M. R., Molecular complexes of sulfonamides. Part 1. 1:1 complexes between sulfadimidine [4-amino-N-(4,6-dimethyl-2-pyrimidinyl)benzenesulfonamide] and 2- and 4-aminobenzoic acids. *Journal of Crystallographic and Spectroscopic Research* **1991**, *21* (5), 641-648.

56. Ghosh, S.; Bag, P. P.; Reddy, C. M., Co-Crystals of Sulfamethazine with Some Carboxylic Acids and Amides: Co-Former Assisted Tautomerism in an Active Pharmaceutical Ingredient and Hydrogen Bond Competition Study. *Crystal Growth & Design* **2011**, *11* (8), 3489-3503.

57. Adsmond, D. A.; Grant, D. J. W., Hydrogen bonding in sulfonamides. *Journal of Pharmaceutical Sciences* **2001**, *90* (12), 2058-2077.

58. (a) Caira, M. R.; Nassimbeni, L. R.; Wildervanck, A. F., Selective formation of hydrogen bonded cocrystals between a sulfonamide and aromatic carboxylic acids in the solid state. *Journal of the Chemical Society, Perkin Transactions 2* **1995**, (12), 2213-2216; (b) Elacqua, E.; Bučar, D.-K.; Henry, R. F.; Zhang, G. G. Z.; MacGillivray, L. R., Supramolecular Complexes of Sulfadiazine and Pyridines: Reconfigurable Exteriors and Chameleon-like Behavior of Tautomers at the Co-Crystal–Salt Boundary. *Crystal Growth & Design* **2013**, *13* (1), 393-403.

59. Tiwari, R. K.; Haridas, M.; Singh, T. P., Structure of 4-amino-N-(4,6-dimethyl-2-pyrimidinyl)benzenesulphonamide (sulfadimidine), $C_{12}H_{14}N_4O_2S$. *Acta Crystallographica Section C* **1984**, *40* (4), 655-657.

60. Buist, A. R.; Dennany, L.; Kennedy, A. R.; Manzie, C.; McPhie, K.; Walker, B., Eight salt forms of sulfadiazine. *Acta Crystallographica Section C* **2014**, *70* (9), 900-907.

61. Groom, C. R.; Bruno, I. J.; Lightfoot, M. P.; Ward, S. C., The Cambridge Structural Database. *Acta Crystallographica Section B* **2016**, *72* (2), 171-179.

Chapter 2

Methods and Materials

2.1   Materials

2.1.1   Pharmaceutical compounds

The Active Pharmaceutical Ingredients (API), 4-amino-N-(2-pyridinyl) benzenesulfonamide, also called sulfapyridine (SFP), and 4-amino-N-(2-pyrimidinyl) benzenesulfonamide, or sulfadiazine (SFD), were purchased from Sigma-Aldrich and were used without further purification. Table 2.1 lists their molecular formulas, molecular weight and melting points.

Table 2.1 Physical properties and formulas of the pharmaceutical compounds used.

Host	Formula	Mr (g mol^{-1})	*T_{on} (°C)	*T_{peak} (°C)
Sulfapyridine (SFP)	$C_{11}H_{11}N_3O_2S$	249.29	189.8	192.4
Sulfadiazine (SFD)	$C_{10}H_{10}N_4O_2S$	250.28	260.8	262.3

*T_{on} and *T_{peak} values were measured experimentally

2.1.2   Coformers

In this work we cocrystallized sulfonamide drugs, sulfapyridine (SFP) and sulfadiazine (SFD) with halo- and nitro-substituted aromatic acids. The six coformers, 3-nitrobenzoic acid (3NBA), 4-nitrobenzoic acid (4NBA), 5-bromosalicylic acid (5BSA), 3,5-dibromosalicylic acid (DBSA), 3,5-dinitrosalicylic acid (DNSA) and 4-dimethylaminopyridine (4DMAP) were purchased from Sigma-Aldrich and were used without further purification. Table 2.2 lists their molecular formulas, molecular weight and melting temperatures. The different solvents used in the experiments included water, methanol, ethanol, chloroform and acetonitrile and were obtained from the same source. Carboxylic acids were selected systematically to investigate the effect on packing of the position of selected functional groups. For instance, comparison of 5-bromosalicylic acid and 3,5-dibromosalicylic acid crystals of SFP may highlight the influence of the extra bromo substituent on the packing.
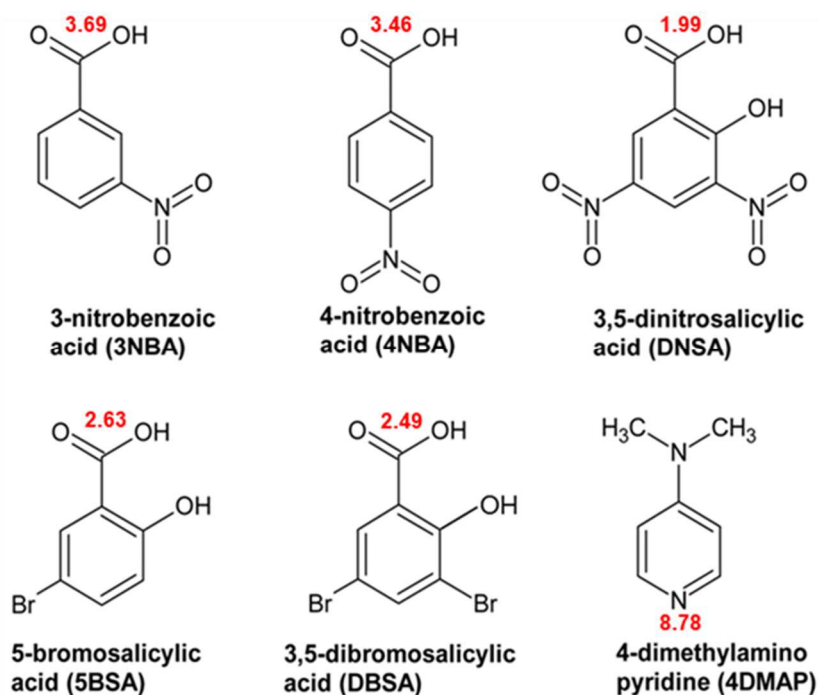
Figure 2.1 Chemical line diagrams of the coformers and their respective pK_a values.

Table 2.2 Physical properties and formulas of the coformers used.

Coformer	Formula	Mr (g mol^{-1})	*T$_{on}$ (°C)	*T$_{peak}$ (°C)
3-nitrobenzoic acid (3NBA)	$C_7H_5NO_4$	167.12	144.0	144.0
4-nitrobenzoic acid (4NBA)	$C_7H_5NO_4$	167.12	238.6	241.0
3,5-dinitrosalicylic acid (DNSA)	$C_7H_4N_2O_7$	228.12	173.0	175.0
5-bromosalicylic acid (5BSA)	$C_7H_5BrO_3$	217.02	169.1	171.1
3,5-dibromosalicylic acid (DBSA)	$C_7H_4Br_2O_3$	295.90	225.6	228.4
4-dimethylaminopyridine (4DMAP)	$C_7H_{10}N_2$	122.17	110.6	112.7
*T$_{on}$ and *T$_{peak}$ values were measured experimentally				

2.2   Preparation of multicomponent crystals

2.2.1   Crystallization from solution

The solvent evaporation method was used as the primary method for crystal growth. Crystallizations were set up by dissolving a 1:1 mixture of the API and the appropriate coformer in a minimal amount of solvent. Solvent (or solvent combinations) of different polarities were used in the crystallizations. The mixture was stirred using a magnetic stirrer on a hot plate until complete dissolution, for about 20-30 minutes. In cases of poor

solubility, mixtures were heated to temperatures about 10 °C below the estimated boiling point of the solvent system. Additionally, the sample was filtered through a micro filter into a clean vial; the vial was sealed with parafilm and perforated to allow slow evaporation of the solvent. The homogenous solution was then kept undisturbed on a bench top at room temperature.

2.2.2 Mechanochemical experiments

Multicomponent crystals can be formed by dry or solvent assisted grinding, in which the API and cocrystal formers are mixed in a known ratio and ground together manually using a mortar and pestle. To determine whether the crystals obtained can be synthesized mechanochemically, starting materials were ground with a mortar and pestle for approximately 45 to 60 minutes by neat grinding or solvent assisted grinding technique, where a few drops of solvent were added. The resulting powder was analysed on a Bruker D2 X-ray powder diffractometer with Cu Kα1 radiation. The aim of the grinding was to try and synthesize multicomponent crystals by implementing green chemistry method via reduction of solvent use.

2.3 Analytical methods

Differential scanning calorimetry, thermogravimetric analysis, single crystal X-ray diffraction, powder X-ray diffraction, nuclear magnetic resonance spectroscopy (^{1}H and ^{13}C NMR), and fourier transform infrared spectroscopy were employed to analyse and characterize the new solid forms of the APIs.

2.3.1 Single Crystal X-Ray Diffraction (SCXRD)

The SCXRD is a non-destructive technique, which precisely and accurately determines the internal lattice of the cocrystal such as bond lengths, site ordering, unit cell parameters and bond angles. X-ray diffraction studies of crystalline materials have four key steps: data collection, data reduction, structure solution and refinement.

Good quality crystals were selected for analysis from the bulk; covered with Paratone N oil to prevent loss of possible incorporated solvent and mounted on a nylon loop on a goniometer head. Data was collected on a Bruker APEX II diffractometer with a graphite monochromated Mo Kα = 0.71073 (Å) radiation at 173 (2) K using an Oxford Cryostream 700. The programme Siemens Area Detector Absorption Corrections (SADABS[1]) was used to correct data for Lorentz-polarisation effects. SADABS is an application in the APEX suite used to scale and correct data for absorption collected on a Bruker AXS area detector.[2] The program is designed to exploit data redundancy, corrects for errors resulting from the variation in the volume of the crystal, absorption by the crystal support and crystal decay during the measurement. SAINT[3] was used to perform unit cell refinement and data-reduction. XPREP[4] was used to determine the unit cells from the cell parameters specified by SAINT, and from the collected X-ray intensity data. Data obtained from X-ray analysis was refined and interpreted in order to solve crystal structures. The structure was solved using SHELXS-97[5] which has run under a graphical user interface, X-Seed.[6] The space groups were determined using the program XPREP and SHELXL-97 was used to solve the structures by direct methods, and for refinement by employing full-matrix least-squares against F^2 for unique reflections given by equation (1):

$$\sum w(F_0^2 - kF_C^2)^2 \qquad (eqn\ 1)$$

The agreement between the observed structure factors (F_0) and the calculated structure factors (F_c) is expressed by the residual index R_1. The residual index R_1 represents the agreement between the observed and calculated structure factors based on F, whereas residual index, wR_2, is the agreement based on F^2 given by the equations (2) and (3).

$$R_1 = \frac{\sum \left\| F_0 \right| - \left| F_c \right\|}{\sum \left| F_0 \right|} \qquad (eqn\ 2)$$

$$wR_2 = \left[\frac{\sum w(F_0^2 - F_C^2)^2}{\sum w(F_0^2)^2} \right]^{1/2} \qquad (eqn\ 3)$$

The weighing scheme (*w)* in wR_2 was used to yield a constant distribution in terms of *a* and *b*, where the parameters were refined for each structure using expressions (4) and (5):

$$w = \frac{1}{\sigma^2(F_0^2) + (aP)^2 + bP} \qquad (eqn\ 4)$$

$$P = \frac{\max(0, F_0^2) + 2F_C^2}{3} \qquad (eqn\ 5)$$

The goodness of fit (S) is defined by the expression 6, where n is the number of reflections and p is the total number of parameters refined.

$$S = \left[\frac{\sum w \left(|F_0|^2 - |F_C|^2 \right)^2}{(n - p)} \right]^{1/2} \qquad (eqn\ 6)$$

The hydrogen atoms bound to carbon atoms were placed at idealized positions and refined as riding atoms. Hydrogen atoms bonded to the carboxylic acid, amine or amide groups were located in the difference electron density map and their coordinates refined freely but their isotropic displacement parameters were fixed where necessary. Structure solution and refinement details for all individual structures are described in Chapter 3.

2.3.2   Powder X-Ray Diffraction (PXRD)

PXRD analysis was done to compare whether the bulk material was representative of the collected single crystal. The starting materials and the bulk material were analyzed on a Bruker D2 Phaser X-ray powder diffractometer with Cu Kα_1 radiation. The technique describes structural characterization of the materials based on the diffraction of X-rays by the crystals.[7] Mercury was used to generate a computed PXRD pattern for each newly synthesized multicomponent crystal. When a match between the experimental PXRD plot and the computed PXRD pattern was observed, it was concluded that the structure of the bulk material was correctly represented by that of the crystal selected for single crystal X-ray analysis.

2.3.3 Thermogravimetric Analysis (TGA)

TGA is a technique in which the mass of a substance is monitored as a function of temperature or time, as the sample is subjected to controlled temperature program or atmospheric environments.[8] This technique can characterize materials that exhibit weight loss or gain due to desolvation, decomposition or oxidation.[9]

The thermogravimetric instrument consists of a furnace, a temperature programmer, a microgram balance, sample holder and a thermobalance where the curves are recorded. The sample under study is placed in a crucible, which is attached to the weighing arm of the microgram balance; also, the thermobalance has a clamp which is used to hold the microbalance arm. As the sample is heated, the change in weight of the sample is measured by the microbalance while temperature is checked by a thermobalance.

A thermogravimetric analysis study was performed using a Perkin Elmer Pyris 6 Instrument. Crystals were lightly crushed and blotted dry on a filter paper to remove surface solvent. A sample mass of about 3 to 5 mg was placed in a tared crucible for analysis. Samples were heated at a rate of 10 °C min^{-1} up to a final temperature of 360 °C under nitrogen (purge rate of 10 mL min^{-1}). In this study thermogravimetric analysis was used to confirm that the TGA thermograms of all new solid forms exhibit no weight loss attributable to residual solvents.

2.3.4 Differential Scanning Calorimetry (DSC)

Differential scanning calorimetry (DSC) is an experimental technique to measure the heat energy uptake that takes place in a sample in a temperature controlled environment. There are two main types of DSCs; power compensated DSC and heat-flux DSC. In our laboratory we use the heat-flux DSC, hence only that will be discussed.

Heat-flux DSC: Thermocouples are attached to the base of the sample and reference material vessels (a single heat source is employed to heat both the reference material and the sample). A second set of thermocouples measures the temperature of the furnace and of the heat-sensitive plate. The temperature difference between the sample and reference material is measured as a function of time or temperature. This temperature difference is

proportional to the change in the heat flux (energy input per unit time). As phase change occurs heat is absorbed or emitted by the sample, changing the heat flux through the heat-sensitive plate. The variation in heat flux causes an increase in temperature difference to be measured between the heat-sensitive plate and the furnace.

DSC analysis was performed on a Perkin Elmer Pyris 6000 DSC, using sealed and crimped vented aluminium pans for all samples. For reference, an empty pan sealed in the same way as the sample was used. Using inert nitrogen gas conditions (flow rate of 20 mL min^{-1}), samples were heated in the DSC cell from 30 °C to 300 °C at a heating rate of 10 °C min^{-1}. 1-3 mg of sample was taken from the mother liquor, dried on a filter paper, lightly crushed and crimped into a vented aluminium pan for analysis. Calibration of the DSC was performed by running indium and zinc. Peaks (endothermic or exothermic) appearing in the DSC were analysed with respect to onset temperatures, temperature range of the peak and the enthalpy of the peak (J g^{-1}).

In this study DSC was used to determine thermal transition (decomposition) temperatures for the starting material and newly synthesised crystals to see if there is a difference in thermal behaviour between the crystals and the starting material. The various endothermic and exothermic peaks observed in the DSC trace were analysed together with the TGA thermograms.

2.3.5   Fourier Transform Infrared Spectroscopy (FTIR)

The infrared spectroscopy is a useful tool to monitor cocrystal or salt formation especially when carboxylic acids are cocrystallized. This technique has been successfully used by Aakeröy and co-workers[10] as a screening tool in the synthesis of diclofenac cocrystals with pyrimidines. Fourier Transform Infrared (FTIR) was used to characterize the resultant multicomponent crystals. Samples of pure API, pure coformer and crystal were analysed using a Perkin Elmer Spectrum fitted with UATR. Averages of 5 scans at 4 cm^{-1} resolutions were taken for each sample, scanning the 4000–400 cm^{-1} range. An instrumental correction of the baseline of the spectra was applied. The transmittance signal was used for data analysis.

2.3.6 Nuclear Magnetic Resonance Spectroscopy (^{1}H NMR and ^{13}C NMR)

Nuclear Magnetic Resonance Spectroscopy is a spectroscopic technique that distinguishes between atoms from their difference in magnetic properties. It is a useful method in determining the type and number of unique atoms; additionally, we obtain information about the environment around the atoms.[11] The most common atoms investigated are hydrogen and carbon through ^{1}H NMR and ^{13}C NMR. NMR analysis was used to identifying proton transfer within the multicomponent crystals. Also, we aimed to investigate the existence of ion pairs in solution, and consequently justifying the investigation of intermolecular interactions of ion pairs. The spectra were acquired on a Bruker Avance III HD Nanobay 400 MHz spectrometer equipped with a 5 mm BBO probe at room temperature (298 K) using standard 1D and 2D pulse programs.

2.4 ConQuest

ConQuest[12] is the primary program for searching and recovering information from the Cambridge Structural Database (CSD).[13]

2.5 Mercury

All the crystal packing diagrams were generated with Mercury[14] together with Pov-Ray[15]. X-ray powder patterns were calculated using Mercury and compared to experimental powder patterns for characterization. In addition, this software provides vast options to aid the investigation and analysis of crystal structures. It can import chemical bond types, generates molecular packing diagrams, defines and visualises Miller planes, and take a slice through a crystal in any direction. Also, it displays space group symmetry elements, generates powder diffraction pattern for the single crystal, calculates voids based either on contact surface or solvent accessible surface and intermolecular potentials.

2.6   CrystalExplorer

CrystalExplorer[16] is a computer package that utilizes calculated Hirshfeld surfaces[17] of molecules within a crystal structure to determine the intermolecular interactions between particular molecules or for the crystal structure in its entirety. Hirshfeld surfaces are created by an extension of the weight function describing an atom in a molecule, to include the function of a molecule in a crystal.[18] The isosurfaces generated from these calculations, with a specified weight function *w*(r)=0.5, surrounds the molecule and by partitioning the electron density of the molecular fragments, delineates the space occupied by a molecule in a crystal.[19] Hirshfeld surfaces can provide information about intermolecular interactions in the crystal as the surface is determined by both the enclosed molecule and its closest neighbours.[16] Fused sphere van der Waals (or CPK), smoothed Connelly surfaces or other molecular surfaces can be used to visualise and quantify molecular geometries and designated only by the molecule itself.[16] The only prerequisite for quality data regarding intermolecular interactions to be extracted from Hirshfeld surfaces is that the crystal structures imported into the program are well-characterised with all hydrogen atoms located accurately. The equation used to define a Hirshfeld surface is *w* (r) = 0.5 where *w* (r) is the weight function given by:

$$w_A(\mathrm{r}) = \sum_{i\,\epsilon\ molecule\ A} \rho_i\,(r) \; / \sum_{i\,\epsilon\ crystal} \rho_i\,(r) \qquad (eqn\ 6)$$

Where ρ_i(r) is a spherical atomic electron distribution located at the ith nucleus. The surfaces integrated in this study are all calculated using the d_{norm} function so that the contact distance is normalised according to the formula:

$$d_{norm} = \frac{d_i - r_i^{vdW}}{r_i^{vdW}} + \frac{d_e - r_e^{vdW}}{r_e^{vdW}} \qquad (eqn\ 7)$$

Where d_i is the distance from the surface to the nearest atom interior to the surface; d_e is the distance from the surface to the nearest atom exterior to the surface. The sum of the two distances gives an approximate contact distance.

The calculated Hirshfeld surface is a 3D representation of the intermolecular interactions, and is a complex way of illustrating the observed contacts. Therefore, fingerprint plots, a 2D representation of these surfaces are used. Fingerprint plots are graphs of the internal distance (d_i) vs external distance (d_e), and are ideal tools for directly comparing crystal structures.[20] Several examples can be found in literature where fingerprint plots have been used to compare crystal packing,[21] and so we will also employ the same tool to compare intermolecular interaction and packing variations in the synthesised multicomponent crystals.

2.7   References

1. Sheldrick, G., SADABS, Version 2.10. *University of Göttingen, Germany* **2003**.
2. Sheldrick, G., SADABS software for empirical absorption correction. *University of Gottingen, Institut fur Anorganische Chemieder Universitat, Tammanstrasse* **1996, 4**, 1999-2003.
3. Bruker AXS Inc. *Madison, Wisconsin, USA* **2004**.
4. Sheldrick, G., Bruker-Nonius AXS, . **2003**.
5. Sheldrick, G., Shelxs-97 and Shelxl-97, Software for Crystal Structure Analysis. *Siemens Analyical X-ray Instruments Inc., Madison, Wisconsin* **1997**.
6. Barbour, L. J., X-Seed — A Software Tool for Supramolecular Crystallography. *Journal of Supramolecular Chemistry* **2001, 1** (4), 189-191.
7. Suryanarayana, C.; Norton, M. G., *X-Ray Diffraction: A Practical Approach*. Springer US: **2013**.
8. Hatakeyama, T.; Quinn, F., *Thermal analysis: fundamentals and applications to polymer science*. [sl]: **1999**.
9. Coats, A. W.; Redfern, J. P., Thermogravimetric analysis. A review. *Analyst* **1963, 88** (1053), 906-924.
10. Aakeröy, C. B.; Grommet, A. B.; Desper, J., Co-Crystal Screening of Diclofenac. *Pharmaceutics* **2011, 3** (3), 601-614.
11. Pavia, D. L.; Lampman, G. M.; Kriz, G. S.; Vyvyan, J. A., *Introduction to Spectroscopy*. Engage Learning: **2014**.
12. Bruno, I. J.; Cole, J. C.; Edgington, P. R.; Kessler, M.; Macrae, C. F.; McCabe, P.; Pearson, J.; Taylor, R., New software for searching the Cambridge Structural Database and visualizing crystal structures. *Acta Crystallographica Section B* **2002, 58 (1)** , 389-397.
13. Groom, C. R.; Bruno, I. J.; Lightfoot, M. P.; Ward, S. C., The Cambridge Structural Database. *Acta Crystallographica Section B* **2016, 72** (2), 171-179.
14. Macrae, C. F.; Bruno, I. J.; Chisholm, J. A.; Edgington, P. R.; McCabe, P.; Pidcock, E.; Rodriguez-Monge, L.; Taylor, R.; van de Streek, J.; Wood, P. A., Mercury CSD 2.0 - new features for the visualization and investigation of crystal structures. *Journal of Applied Crystallography* **2008, 41** (2), 466-470.
15. Pov-Ray for Windows. *Version 3.6.watcom.win32. The persistence of vision development team* **1991-1999**.
16. Wolff, S.; Grimwood, D.; McKinnon, J.; Turner, M.; Jayatilaka, D.; Spackman, M., CrystalExplorer. The University of Western Australia Perth, Australia: **2012**.
17. Hirshfeld, F. L., Bonded-atom fragments for describing molecular charge densities. *Theoretica chimica acta* **1977, 44** (2), 129-138.
18. Spackman, M. A.; Jayatilaka, D., Hirshfeld surface analysis. *CrystEngComm* **2009, 11** (1), 19-32.
19. McKinnon, J. J.; Jayatilaka, D.; Spackman, M. A., Towards quantitative analysis of intermolecular interactions with Hirshfeld surfaces. *Chemical Communications* **2007,** (37), 3814-3816.
20. Wood, P. A.; McKinnon, J. J.; Parsons, S.; Pidcock, E.; Spackman, M. A., Analysis of the compression of molecular crystal structures using Hirshfeld surfaces. *CrystEngComm* **2008, 10** (4), 368-376.
21. (a) Báthori, N. B.; Nassimbeni, L. R.; Oliver, C. L., Quininium mandelates-a systematic study of chiral discrimination in crystals of diastereomeric salts. *Chemical Communications* **2011, 47** (9), 2670-2672; (b) Batisai, E.; Ayamine, A.; Kilinkissa, O. E.; Báthori, N. B., Melting point–solubility–structure correlations in multicomponent crystals containing fumaric or adipic acid. *CrystEngComm* **2014, 16** (43), 9992-9998; (c) Báthori, N. B.; Kilinkissa, O. E. Y., Are gamma amino acids promising tools of crystal engineering? - Multicomponent crystals of baclofen. *CrystEngComm* **2015, 17** (43), 8264-8272; (d) J. McKinnon, J.; S. Mitchell, A.; A. Spackman, M., Visualising intermolecular interactions in crystals: naphthalene vs. terephthalic acid. *Chemical Communications* **1998,** (19), 2071-2072.

Chapter 3

Results

3.1 Multicomponent crystals of sulfapyridine (SFP) and sulfadiazine (SFD)

Ionisable compounds were cocrystallized in this work and the quantitative pK_a rule by Cruz-Cabeza[1] was used to investigate the ionization state of the newly formed complexes. In acids, smaller pK_a values show a stronger capability as proton donors while for bases, larger pK_a values signify the stronger capability to accept protons.[2] In her paper Cruz-Cabeza mentions some limitations of the pK_a rule and states that the ΔpK_a can be implemented in compounds with only one donor or acceptor site. Additionally, it is affected by the type of solvent used.

Sulfa drugs exhibit tautomerism as proton transfer from the sulfonamide NH to the N (heterocyclic), shown in Figure 3.1.[3-3b] The pK_as (pK_{a1}, pK_{a2}, pK_{a3} and pK_{a4}) of the amidine and imidine tautomeric forms (Figure 3.1) were calculated using Marvin.[4] Systematic structural studies of hydrogen bonds show that the strongest hydrogen bond donor interacts with the strongest hydrogen bond acceptor.[5] Following that, in this study, it is anticipated that the N (heterocyclic) or the $-NH_2$ sites would participate as strong hydrogen bond acceptors with the carboxylic acid coformers. However, owing to the multiple hydrogen bond acceptor sites present on SFP and SFD, we were unable to apply the quantitative pK_a rule for predicting salt or cocrystal.
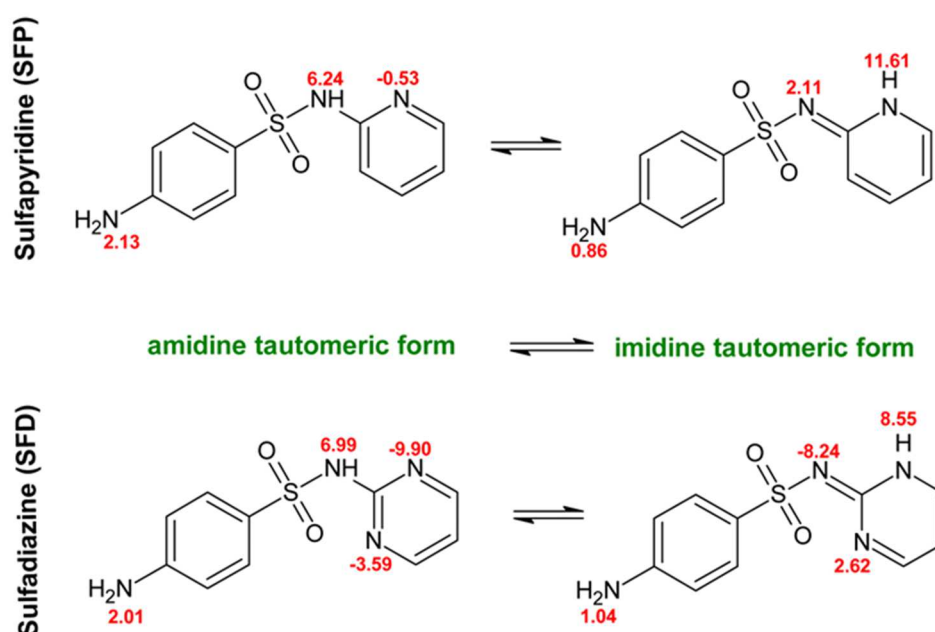
Figure 3.1 Tautomeric forms of the APIs, with pK_a values highlighted in red.

3.1.1 Effect of the substituent position on the crystal packing: SFP·3NBA and [SFP⁺][4NBA⁻]

Equimolar amounts of sulfapyridine with 3-nitrobenzoic acid and 4-nitrobenzoic acid were dissolved in a 1:1 mixture of ethanol/water solution separately and crystals were obtained within 2 weeks via the slow evaporation method. The crystallographic details and hydrogen bonds for SFP·3NBA and [SFP⁺][4NBA⁻] are summarized in Table 3.1 and Table 3.2 respectively.

Table 3.1 Crystallographic data and structure refinement parameters for SFP·3NBA and [SFP⁺][4NBA⁻].

Compounds	SFP·3NBA	[SFP⁺][4NBA⁻]
Molecular formula	$C_{18}H_{16}N_4O_6S$	$C_{18}H_{16}N_4O_6S$
Formula weight (g mol⁻¹)	416.41	416.41
Crystal system	monoclinic	monoclinic
Space group (No.)	$P2_1/n$ (No. 14)	Cc (No. 9)
a (Å)	8.3648 (17)	8.2589 (17)
b (Å)	19.064 (4)	19.011 (4)
c (Å)	11.763 (2)	12.093 (2)
α (°)	90	90
β (°)	91.81 (3)	92.10 (3)
γ (°)	90	90
V (Å³)	1874.9 (7)	1897.4 (7)
Z	4	4
ρ_{calc} (g cm⁻³)	1.475	1.458
μ (Mo Kα) (mm⁻¹)	0.218	0.216
F (000)	864	864
Crystal size (mm)	0.11x0.21x0.27	0.09x0.21x0.34
Temperature (K)	173 (2)	173 (2)
Radiation (Å)	MoKα, 0.71073	MoKα, 0.71073
Theta min/max (°)	2.035, 27.973	2.143, 27.976
Dataset	-11:11; 0:25; 0:15	-10:10; -24:24; -15:15
Final R indices [I>2.0 σ(I)]	R_1=0.0482, wR_2=0.1137	R_1= 0.0339, wR_2= 0.0773
R indices [all data]	R_1=0.0676, wR_2= 0.1239	R_1= 0.0383, wR_2= 0.0796
Tot., uniq. data, R (int)	4532, 3590, 0.0496	3893, 3585, 0.0291
N_{ref}, N_{par}	4532; 267	3893; 264
S	1.033	1.062
Max. and av. Shift/error	0.000, 0.000	0.000, 0.000
Min. and max. resd. dens. (Å³)	-0.428, 0.348	-0.257, 0.182

Table 3.2 Hydrogen bonding of SFP·3NBA and [SFP⁺][4NBA⁻].

D-H···A	d(D-H)(Å)	d(H···A)(Å)	d(D···A) (Å)	<DH···A (°)	Symmetry operator
SFP·3NBA					
C5-H5···O9	0.95	2.62	3.451	146.2	x-1, y, z
N7-H7A···O10	0.88	2.16	3.031	172.7	x-1/2, -y+1/2, z+1/2
N7-H7B···O9	0.90	2.50	3.301	148.3	x-1, y, z
N11-H11···O19	0.92	1.86	2.782	176.5	
O18-H18···N13	1.10	1.53	2.613	171.2	
[SFP⁺][4NBA⁻]					
C5-H5···O9	0.95	2.57	3.381	143.1	x+1, y, z
C6-H6···O29	0.95	2.58	3.462	154.1	x+1, y, z-1
N7-H7B···O9	0.91	2.29	3.153	158.3	x+1, y, z
N7-H7A···O10	0.86	2.23	3.035	155.9	x+1/2, -y+1/2, z+1/2
N11-H11···O19	0.96	1.76	2.707	174.0	
N13-H13···O18	0.91	1.78	2.673	167.2	
C25-H25···O9	0.95	2.66	3.489	146.4	x-1/2, -y+1/2, z+1/2

The SFP·3NBA structure was solved in the monoclinic $P2_1/n$ space group (No. 14), with one molecule of sulfapyridine and 3-nitrobenzoic acid in the asymmetric unit (Figure 3.2). The carboxylic acid proton (H18), amine protons (H7A & H7B) and amidine proton (H11) were located in the electron density map and allowed to refine freely. No proton transfer was observed from the carboxylic acid group of the 3NBA to the SFP, thus a cocrystal was formed. The two components interact in a discrete assembly forming the amidine-carboxylic acid heterodimer, constructed by the (acid) O18-H18···N13 (pyridine) [2.61 Å, 171°] and (amidine) N11-H11···O19 (acid) [2.78 Å, 176°] hydrogen bonds, classified as a $R_2^2(8)$ graph set.
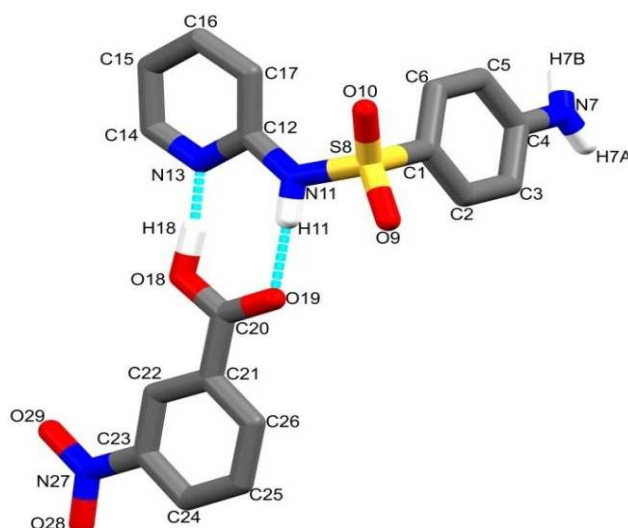
Figure 3.2 Asymmetric unit of SFP·3NBA with primary interaction between SFP and 3NBA molecules, (Some hydrogen atoms are omitted for clarity).

As observed in the extended 2D structure, the amine group participates in NH_2···SO_2 intermolecular hydrogen bonds via (amine) N7-H7A···O10 (sulfoxide) [3.03 Å, 173°], (amine) N7-H7B···O9 (sulfoxide) [3.30 Å, 148°] that may be described with a $R_4^4(22)$ graph set (Figure 3.3).
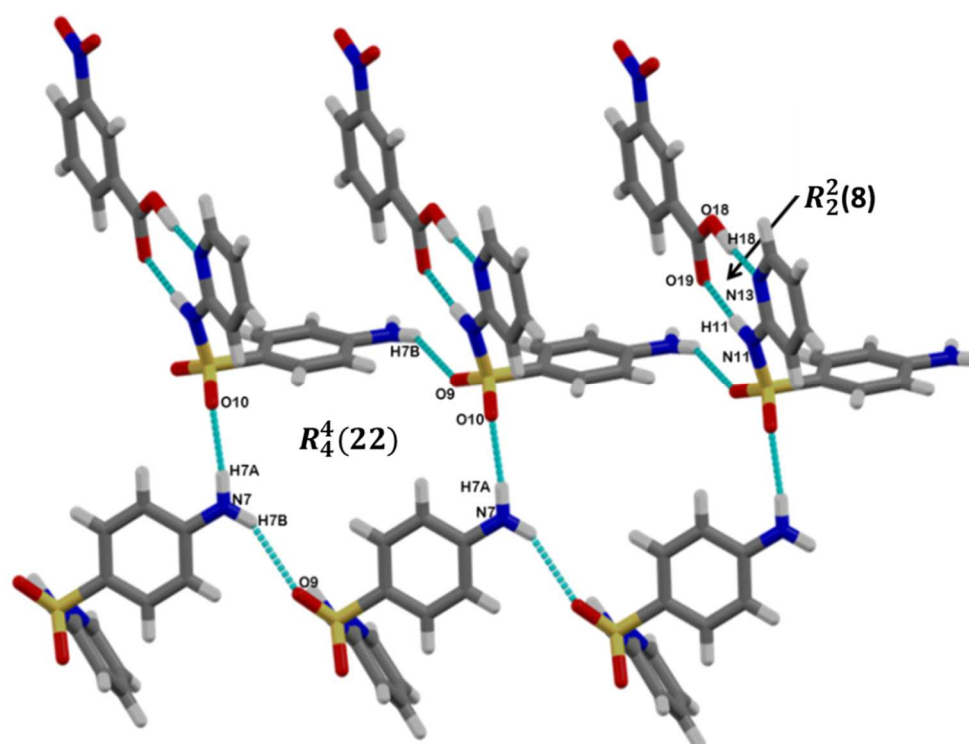
Figure 3.3 Extended 2D structure of SFP·3NBA showing hydrogen bonding and graph sets.

35

The SFP molecules form a 2D network via alternating (amine) N7-H7A⋯O10 (sulfoxide) and (amine) N7-H7B⋯O9 (sulfoxide) hydrogen bonds forming infinite $C_2^2(16)$ zig-zag chains (Figure 3.4a). Furthermore, the SFP molecules (red) form a honeycomb network with channels, which are filled by 3NBA molecules (blue), as shown in Figure 3.4b. Additional weak hydrogen bonds (C-H⋯O) and face-to-face π-π interactions between the aromatic rings of the carboxylic acid and pyridine rings (centroid-centroid distance of 3.69 Å) contribute to the overall structure.
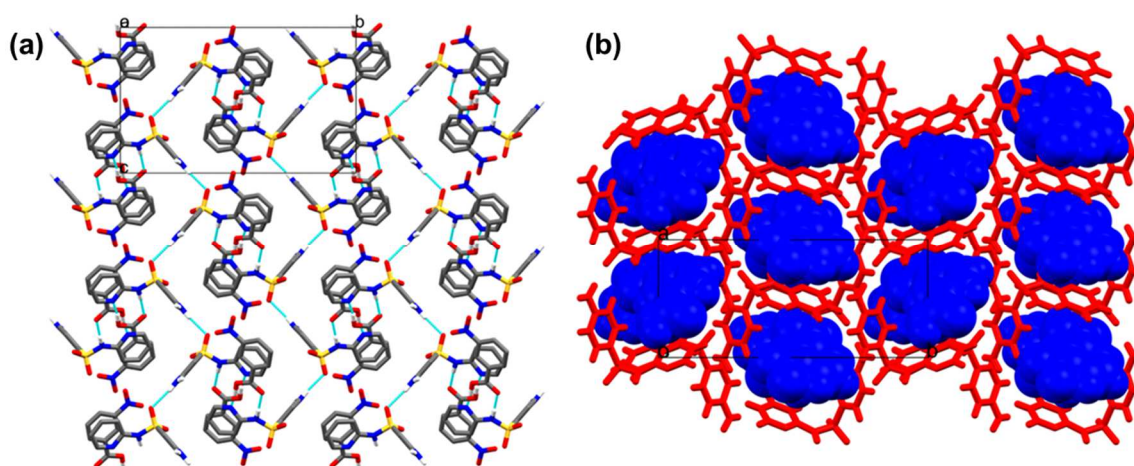
Figure 3.4 View of SFP·3NBA packing highlighting (a) wave-like hydrogen bonded chains between SFP moieties and (b) the honeycomb pattern of SFP molecules (red) filled with 3NBA (blue).

[SFP⁺][4NBA⁻] crystallized in the monoclinic crystal system having the space group *C*c (No. 9) as a salt in a 1:1 ratio. Although 4NBA (pK_a= 3.46) is a stronger acid than 3NBA (pK_a = 3.69) by 0.23 pK_a units, the difference in acidity did not cause any variance in the overall packing and hydrogen bonding. Interestingly, the two complexes possess the same main intermolecular interaction sites, except the locations of the acidic protons are different (as shown in the asymmetric unit figures). The two-component assembly of [SFP⁺][4NBA⁻] (Figure 3.5) is sustained by the robust amidine pyridinium-carboxylate supramolecular heterodimer as the primary interaction. The API and the coformer formed charge assisted hydrogen bond via (amidine) N11-H11⋯O19 (carboxylate) [2.71 Å, 174°] and (pyridinium) N13⁺-H13⋯O18⁻ (carboxylate) [2.67 Å, 167°], depicted by $R_2^2(8)$ graph set.
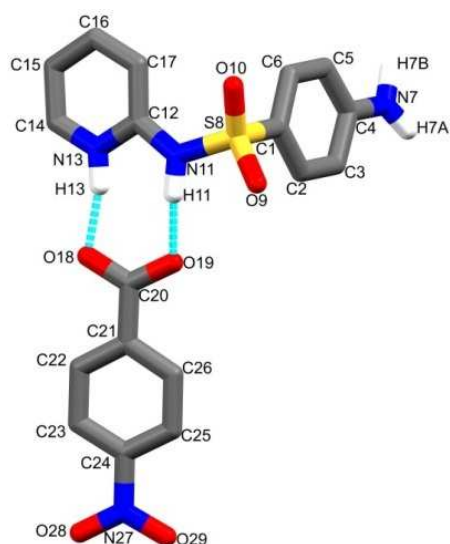
Figure 3.5 Asymmetric unit of [SFP⁺][4NBA⁻] showing the primary synthon between the SFP⁺ and 4NBA⁻ moieties, (Some H atoms are omitted for clarity).

The amine donates its protons in intermolecular hydrogen bonds constructed by (amine) N7-H7A···O10 (sulfoxide) [3.04 Å, 156°], (amine) N7-H7B···O9 (sulfoxide) [3.15 Å, 158°] and their symmetry generated counterparts forming a $R_4^4(22)$ ring (Figure 3.6).
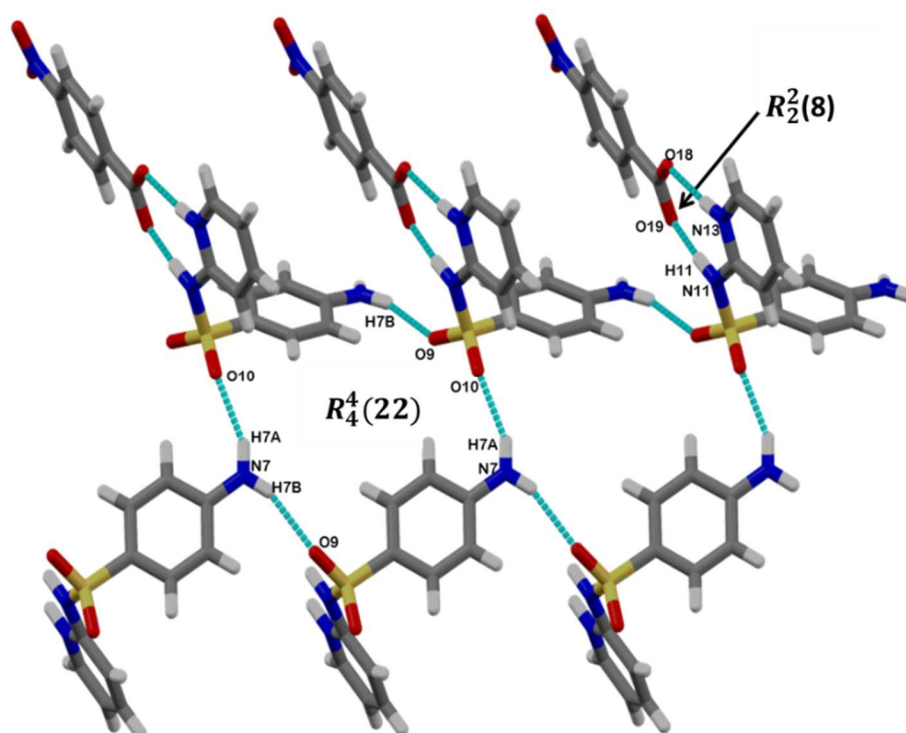
Figure 3.6 Hydrogen bonding motif of [SFP⁺][4NBA⁻] highlighting the most prominent synthons and graph sets.

Similar to SFP·3NBA, the sulfapyridine molecules form infinite wave-like $C_2^2(16)$ chains by means of alternating (amine) N7-H7A···O10 (sulfoxide) and (amine) N7-H7B···O9 (sulfoxide) hydrogen bonds (Figure 3.7a). The SFP molecules (red) form square shaped channels where the 4NBA molecules (blue) are located (Figure 3.7b). In addition, there are several weak interactions such as C-H···O, C-H···N and face-to-face π-π interaction between the carboxylic acid and pyridine aromatic systems (minimal ring centroid separation = 4.27 Å) which contribute to the packing of the solid.
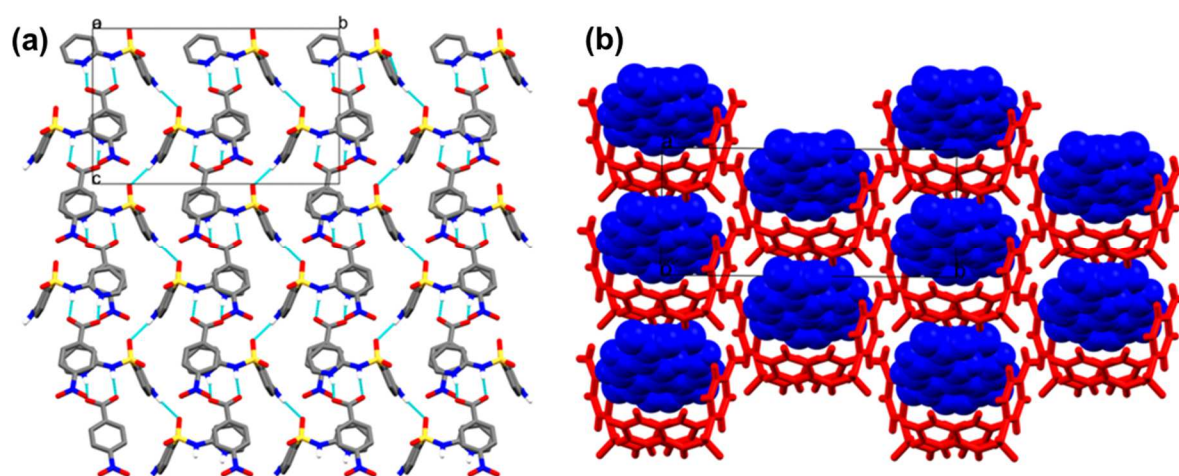
Figure 3.7 View of [SFP⁺][4NBA⁻] highlighting (a) wave-like chains formed between adjacent SFP⁺ moieties and (b) square shape channels formed by SFP⁺ (red) filled with 4NBA⁻ (blue), view down the c-axis.

Although the space groups for SFP·3NBA and [SFP⁺][4NBA⁻] differ, the unit cell parameters are very similar and the network built from the SFP molecules shows a similar pattern (Figure 3.8). In both cases, the SFP molecules adopt an approximate L shape conformation (the angle between the planes of the six membered rings is 85.11° for SFP·3NBA and 80.88° for [SFP⁺][4NBA]). Overall, the arrangement of SFP molecules in both structures gives rise to the honeycomb pattern. In conclusion, the nitro substituent did not participate in the intermolecular bonding; however, it imparted steric factors to the crystal structures. Also, that the two isomers of nitrobenzoic acid (3NBA and 4NBA) disrupted the amidine dimers between the sulfapyridine molecules and formed the heterosynthons: amidine-carboxylic acid and amidine pyridinium-carboxylate.
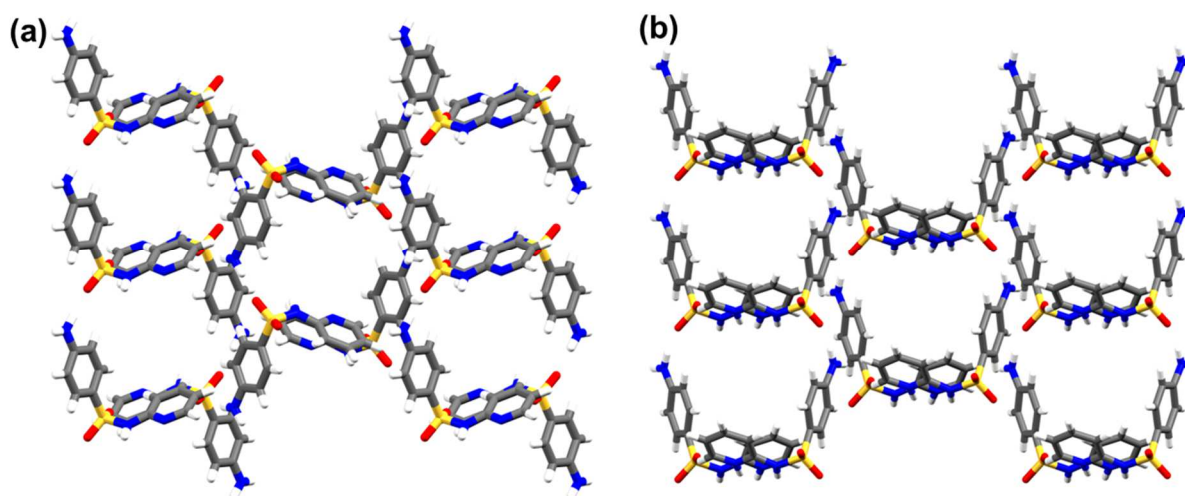
Figure 3.8 Similarity of the arrangement of the SFP moieties in; (a) SFP·3NBA, and (b) [SFP⁺][4NBA⁻].

CrystalExplorer was used to take a closer look at the intermolecular interactions in the very similar crystal structures of SFP·3NBA and [SFP⁺][4NBA⁻]. Full and partial fingerprint plots for all crystal structures are presented in appendix A (Figure A.1 and A.2). The assessment was done by calculating the 3D Hirshfeld surfaces of the asymmetric unit and representing them as 2D fingerprint plots (Figure 3.9). The fingerprint plots are essentially the same with the same symmetrical spikes due to O···H hydrogen bonds.

The percentage contributions of the various intermolecular interactions are summarised in the bar chart (Figure 3.9). A partial difference in the O···H interactions is observed, with [SFP⁺][4NBA⁻] having approximately 2 % more % O···H interactions than SFP·3NBA. Thus, despite a slight difference in the orientation of the SFP molecules and the difference in protonation in the two structures, the structures have very similar stabilising intermolecular interactions.
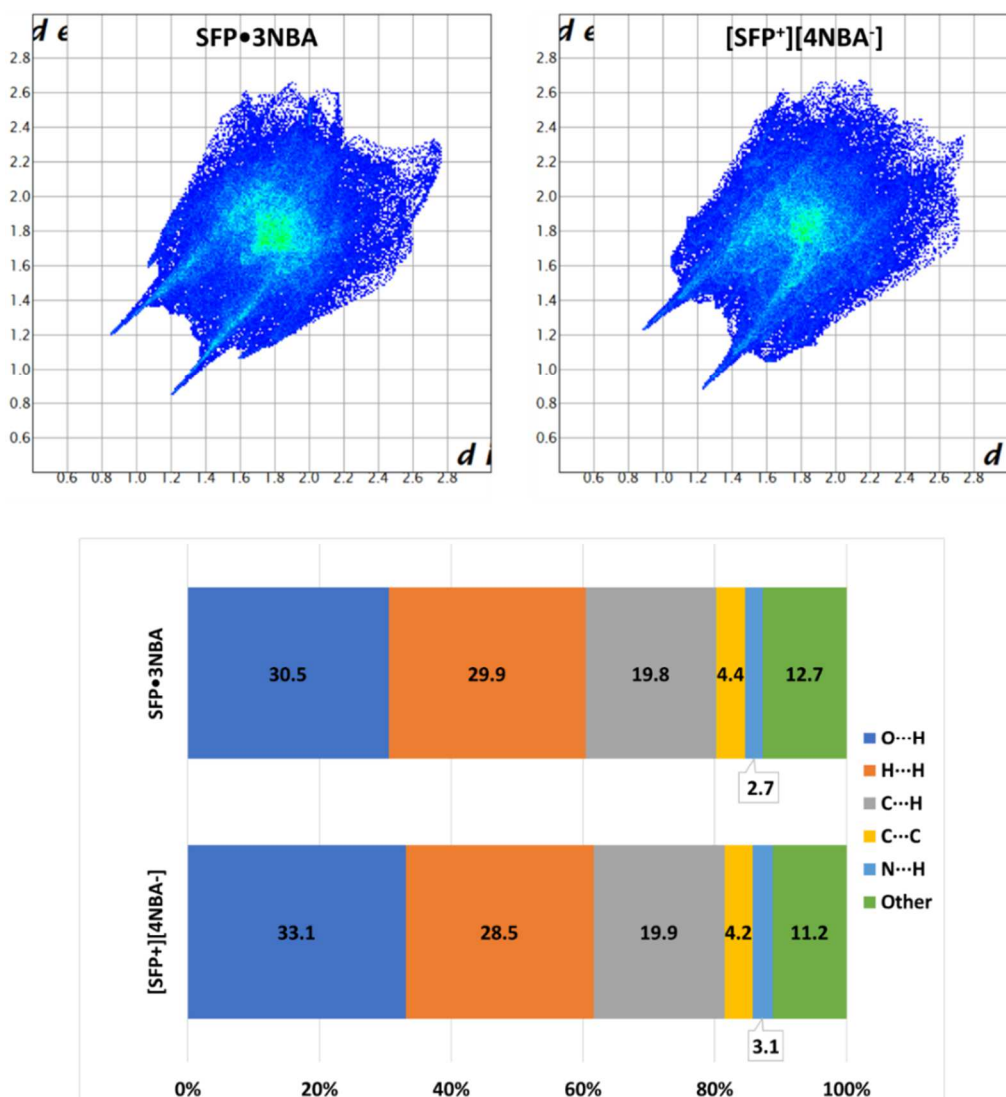
Figure 3.9 Fingerprint plots and summary of the % contributions of the different interactions for SFP·3NBA and [SFP+][4NBA-].

3.1.2 Effect of the number of substituents on the crystal packing: SFP·5BSA and [SFP+][DBSA-]

SFP·5BSA and [SFP+][DBSA-] were synthesized by dissolving equimolar amounts of sulfapyridine with 5-bromosalicylic acid or 3,5-dibromosalicylic acid in a 1:1 mixture of ethanol/water solution. Crystals were obtained within 2 weeks via the slow evaporation method. The crystallographic details and hydrogen bonds for SFP·5BSA and [SFP+][DBSA-] are summarized in Table 3.3 and Table 3.4, respectively.

Table 3.3 Crystallographic data and structure refinement parameters for SFP·5BSA and [SFP⁺][DBSA⁻].

Compounds	SFP·5BSA	[SFP⁺][DBSA⁻]
Molecular formula	$C_{18}H_{16}BrN_3O_5S$	$C_{18}H_{14}Br_2N_3O_5S$
Formula weight (g mol^{-1})	466.31	544.20
Crystal system	monoclinic	monoclinic
Space group (No.)	$P2_1/n$ (No. 14)	$P2_1/c$ (No. 14)
a (Å)	12.506 (3)	14.239 (3)
b (Å)	6.8403 (14)	9.0520 (18)
c (Å)	21.308 (4)	15.820 (3)
α (°)	90	90
β (°)	93.99 (3)	106.98 (3)
γ (°)	90	90
V ($Å^3$)	1818.4 (6)	1950.2 (7)
Z	4	4
ρ_{calc} (g cm^{-3})	1.703	1.854
μ (Mo Kα) (mm^{-1})	2.413	4.301
F (000)	944	1076
Crystal size (mm)	0.14x0.16x0.18	0.25x0.29x0.35
Temperature (K)	173 (2)	173 (2)
Radiation (Å)	MoKα, 0.71073	MoKα, 0.71073
Theta min-max (°)	1.834, 27.981	1.495, 28.319
Dataset	-16:16;-9:9;-28:28	-18:18;-12:12;-21:21
Final R indices [$I>2.0\sigma(I)$]	R_1= 0.0306, wR_2=0.0673	R_1= 0.0252, wR_2= 0.0593
R indices [all data]	R_1= 0.0437, wR_2=0.0726	R_1= 0.0347, wR_2=0.0627
Tot., uniq. data, R (int)	4370, 3546, 0.0671	4845, 4039, 0.0431
Nref, Npar	4370; 264	4845; 277
S	1.041	1.044
Max. and av. Shift/error	0.002, 0.000	0.001, 0.000
Min. and max. resd. dens. ($Å^3$)	-0.400, 0.340	-0.413, 0.440

Table 3.4 Hydrogen bonds of SFP·5BSA and [SFP⁺][DBSA⁻].

D-H···A	d(D-H) (Å)	d(H···A) (Å)	d(D···A) (Å)	<DH···A (°)	Symmetry operator
SFP·5BSA					
C6-H6···Br18	0.95	3.02	3.871	149.3	x-1, y, z
N13-H13···S8	0.85	3.02	3.761	145.9	-x+1, -y+1, -z+1
N13-H13···N11	0.85	2.05	2.897	171.4	-x+1, -y+1, -z+1
C14-H14···O9	0.95	2.46	3.182	132.4	-x+1, -y+1, -z+1
C17-H17···O10	0.95	2.38	2.995	121.7	
C17-H17···Br18	0.95	3.05	3.990	170.6	x-1, y, z
O26-H26···N7	0.88	1.87	2.733	168.8	
O28-H28···O27	0.84	1.86	2.599	145.6	
[SFP⁺][DBSA⁻]					
C3-H3···O10	0.95	2.63	3.401	139.1	x, -y+1/2, z+1/2
N7-H7A···O10	0.80	2.39	3.129	155.2	x, -y+1/2, z+1/2
N11-H11···O19	0.87	1.87	2.742	175.0	
N13-H13···O18	0.89	1.72	2.592	166.1	
N13-H13···O19	0.89	2.65	3.358	137.0	
C14-H14···Br29	0.95	2.99	3.906	162.3	x, y+1, z
O27A-H27A···O18	0.84	1.71	2.485	153.6	
O27B-H27B···O19	0.84	1.67	2.445	152.4	

The SFP·5BSA structure was solved in the monoclinic crystal system having the space group $P2_1/n$ (No.14), with one molecule of sulfapyridine and 5-bromosalicylic acid in the asymmetric unit (Figure 3.10). The acidic proton (H26), the imidine proton (H13) and amine protons (H7A & H7B) were located in the electron density map and their coordinates refined freely. SFP and 5BSA interact to form a discrete assembly via $D_1^1(2)$ constructed by (acid) O26-H26···N7 (amine) [2.73 Å, 169°]. The hydroxyl group of the 5BSA forms an intramolecular $S_1^1(6)$ synthons via (hydroxyl) O28-H28···O27 (carbonyl) [2.60 Å, 146°] hydrogen bonds. An interesting feature is the non-planarity of the NH₂ group. H7A and H7B hydrogens are positioned out of the plane and this suggests some kind of 'transition state towards' the protonation of the group by the carboxylic acid.
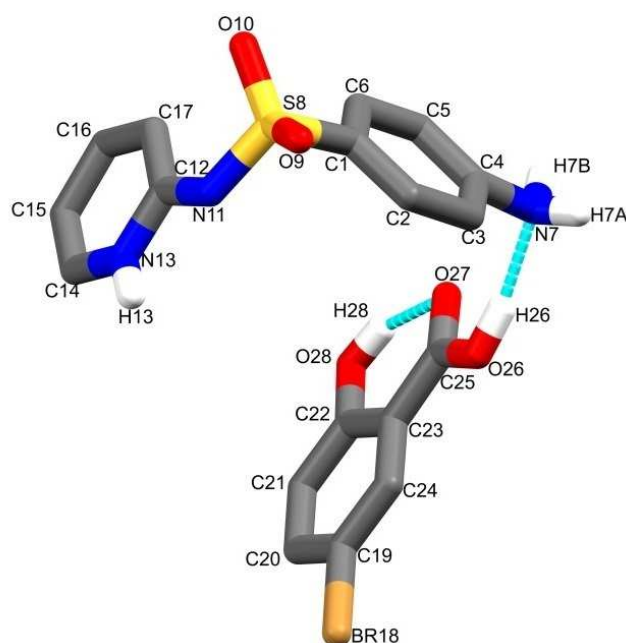
Figure 3.10 Asymmetric unit of SFP·5BSA, (Some hydrogen atoms on carbons are omitted for clarity).

The robust $R_2^2(8)$ imidine homodimer between the SFP molecules is preserved, and is constructed via N13-H13···N11 [2.90 Å, 171°] hydrogen bonds. The main supramolecular unit of the crystal is the tetramer formed from the two SFP molecules and two acids (Figure 3.11). These S shaped molecular associates interact with each other via face-to-face $\pi\cdots\pi$ interactions with the minimal ring centroid separation of 3.64 Å.

The crystal packing is stabilized by halogen interactions in the form of C-H···Br and Br···O. The Br···O interactions between the neighbouring units are prominent in the crystal packing and are highlighted with pink-dashed lines in Figure 3.12a. The Hirshfeld plot further illustrates the flat surface of the Br sigma hole pointing to the sulfoxide oxygen in order to facilitate the Br···O interactions (Figure 3.12b).
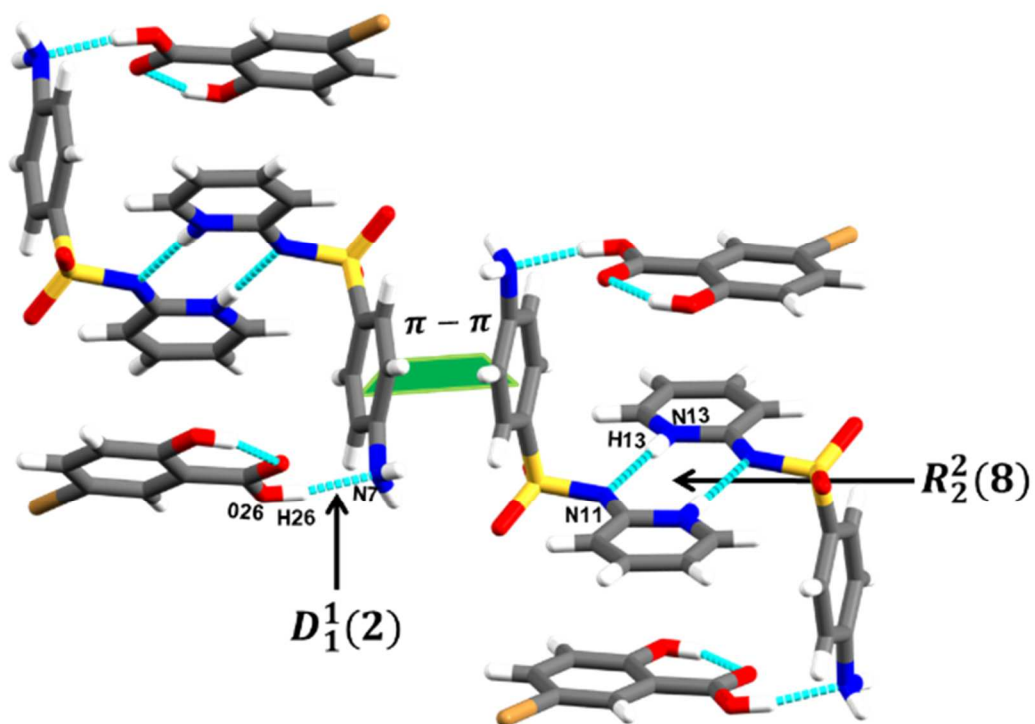
Figure 3.11 Extended motif SFP·5BSA highlighting hydrogen bonding and $\pi\cdots\pi$ interactions.
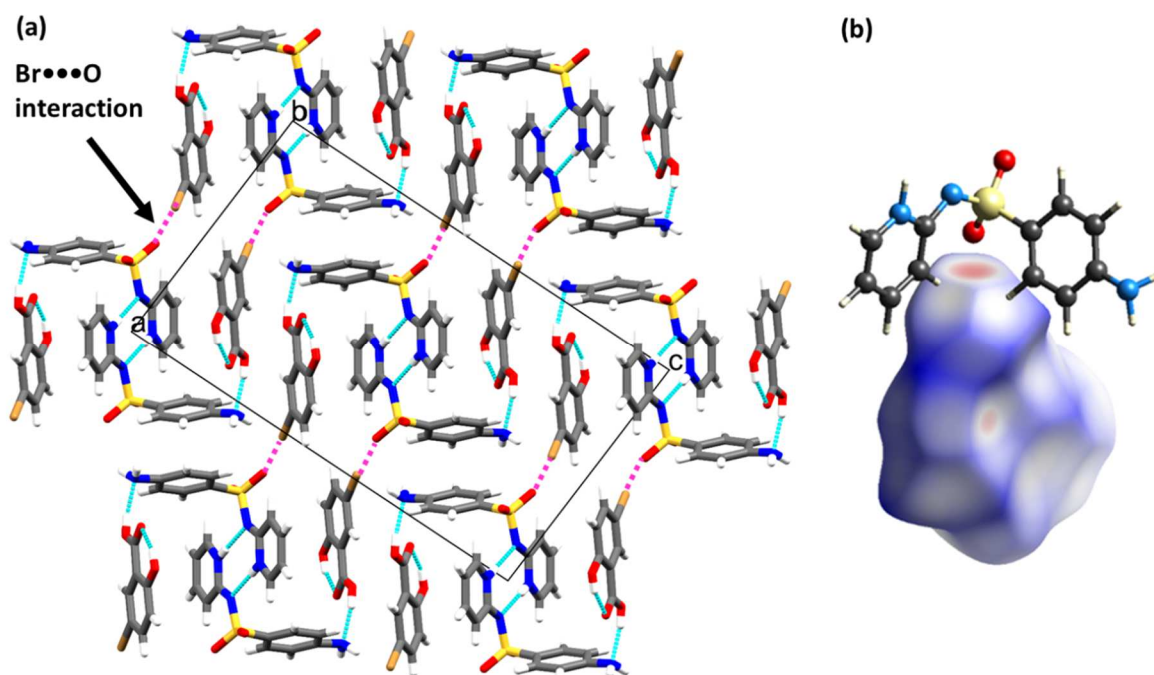
Figure 3.12 (a) View of SFP·5BSA highlighting the Br···O interactions (pink) and (b) Hirshfeld surface showing the sigma hole of the bromine pointing to the oxygen atom.

[SFP+][DBSA-] crystallized in the monoclinic crystal system having the space group $P2_1/c$ (No. 14) with one SFP+ cation and one DBSA- anion in the asymmetric unit (Figure 3.13). The hydroxyl group in the dibromosalicylate anion is disordered over two positions: 61.2% (O27A-H27A) and 38.8% (O27B-H27B). The addition of a second bulky bromo substituent to the system resulted in the formation of different hydrogen bonding between the SFP ion and the acid. The amidine dimers are disrupted by the acid and, an amidine pyridinium-carboxylate interaction is formed.
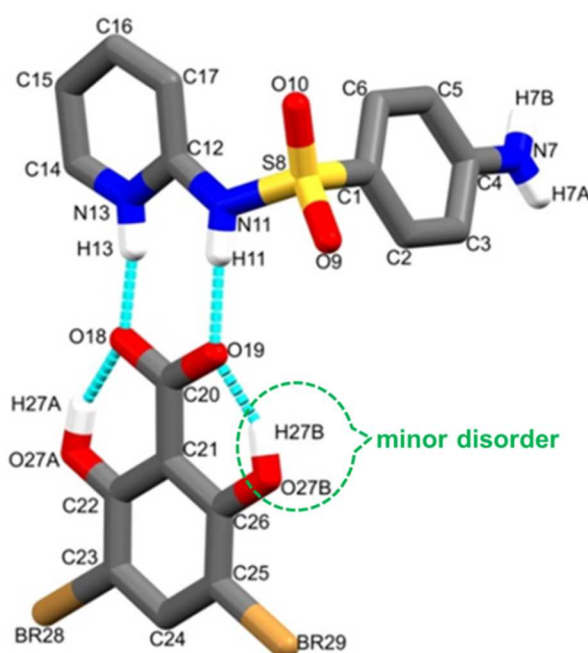
Figure 3.13 Asymmetric unit of [SFP+][DBSA-], (Some hydrogen atoms are omitted for clarity).

In SFP·5BSA, the acid proton of 5BSA bonds to the amine and the imidine homodimer between the SFP molecules is preserved. However, in [SFP+][DBSA-], similar to the [SFP+][4NBA-] structure, the amidine pyridinium-carboxylate heterodimer is observed.

The amidine pyridinium-carboxylate $R_2^2(8)$ supramolecular synthon formed from (amidine) N11-H11···O19 (carboxylate) [2.74 Å, 175°] and (pyridinium) N13-H13···O18 (carboxylate) [2.59 Å, 166°] hydrogen bonds. The extended packing is sustained by $C_1^1(8)$ chains (Figure 3.14) created by (amine) N7-H7A···O10 (sulfoxide) [3.12 Å, 155°]. In addition, the disordered hydroxyl protons, H27A & H27B, of the DBSA form intramolecular (hydroxyl) O27A-H27A···O18 (carboxylate) [2.49 Å, 154°] and (hydroxyl) O27B-H27B···O19 (carboxylate) [2.45 Å, 152°] hydrogen bonds.
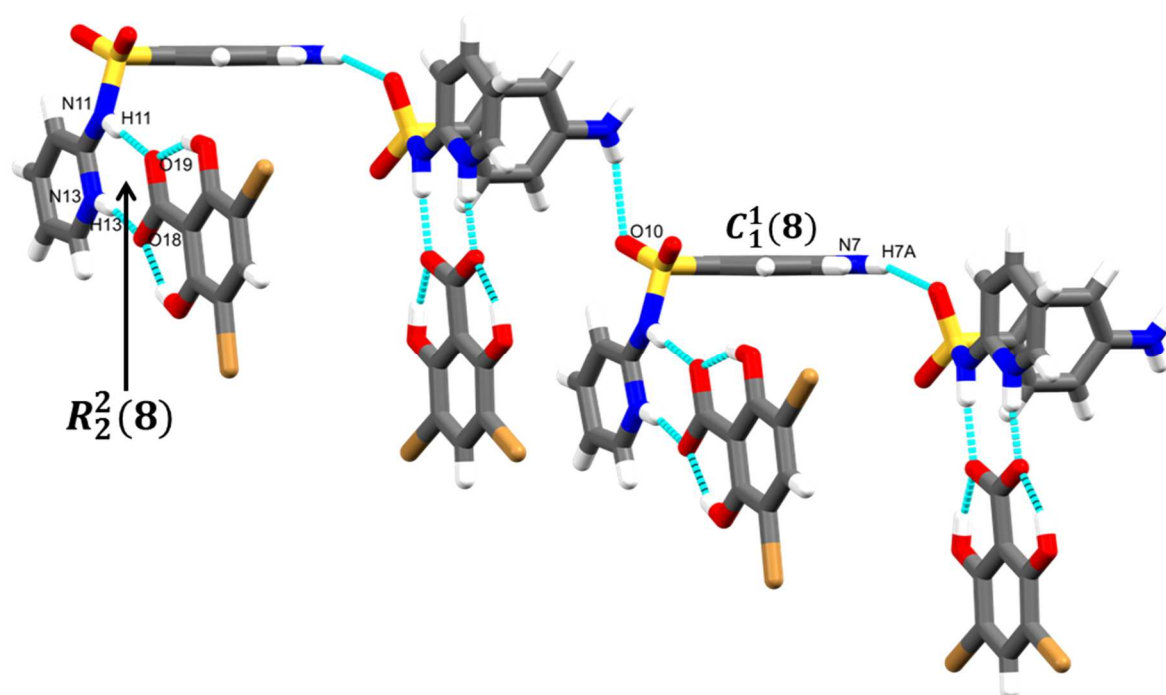
Figure 3.14 Extended hydrogen bonding of [SFP⁺][DBSA⁻].

The packing of the crystal resembles a staircase as a result of the finite chains formed between SFP molecules (Figure 3.15a). The anionic coformer, DBSA⁻, is interleaved into the staircase, forming hydrogen bonds with the SFP⁺ cations. The adjacent chains are held together by C-H⋯π interactions, shown as green dotted lines with $d_{C-H⋯π}$ 3.30 Å. This structure is also stabilised by weak C-H⋯O, halogen (C-H⋯Br) and $π ⋯ π$ interactions. The sigma hole of the bromine atoms (pointing towards oxygen atoms) are not that obvious as in the SFP·5BSA (Figure 3.12a), but the Hirshfeld surface of [DBSA⁻] (Figure 3.15b) showed its weak existence.
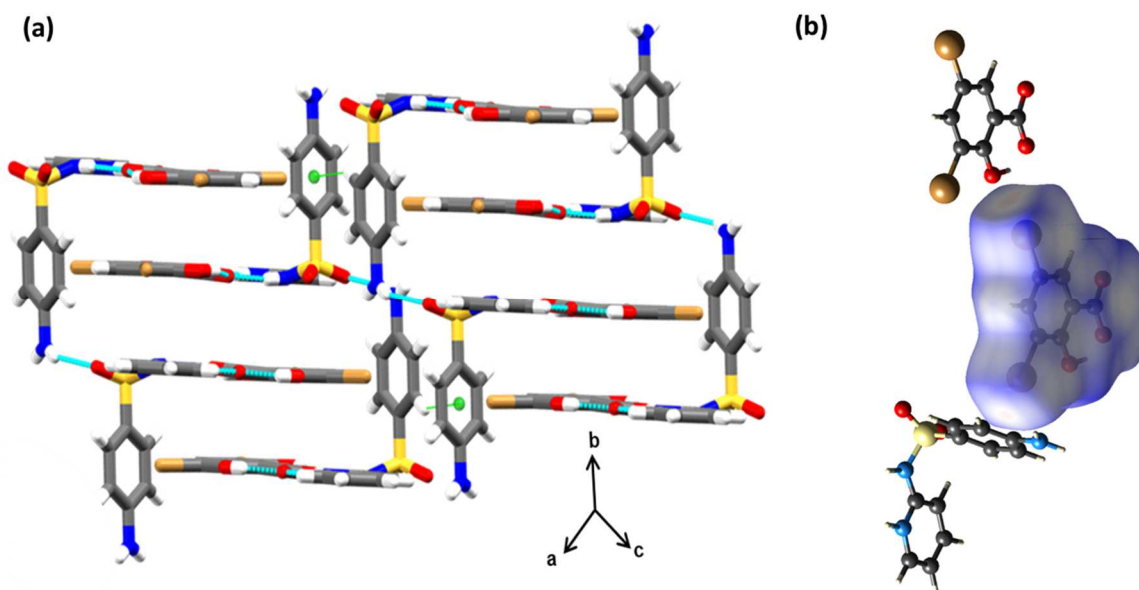
Figure 3.15 (a) Packing of [SFP⁺][DBSA⁻] highlighting interlocked chains and C-H⋯π interactions formed between SFP molecules and (b) Hirshfeld surface showing the weak Br⋯O interactions; with the sigma hole of the bromine pointing to the OH group.

Figure 3.16 is an illustration of the arrangement of the sulfapyridine molecules in the packing structures of SFP·5BSA and [SFP⁺][DBSA⁻]. The black symbols represent the asymmetric unit in SFP·5BSA (U shape) and [SFP⁺][DBSA⁻] (L shape). While in SFP·5BSA (Figure 3.16a) a sandwich-like assembly was observed, the [SFP⁺][DBSA⁻] structure (Figure 3.16b) displays a different pattern altogether which resembles a staircase.
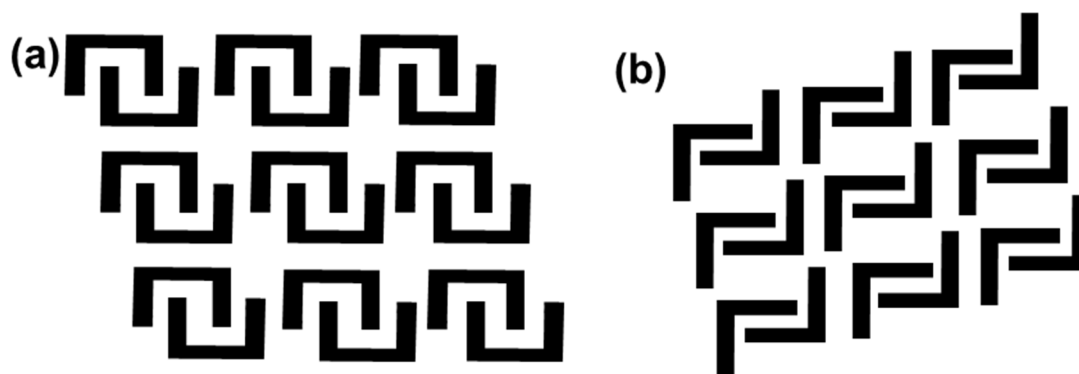
Figure 3.16 Comparison of packing patterns observed in (a) SFP·5BSA illustrating sandwich-like assembly and (b) [SFP⁺][DBSA⁻] resembling a staircase.

The Hirshfeld surfaces of the 5BSA and DBSA⁻ ion, in SFP·5BSA and [SFP⁺][DBSA⁻] respectively, were generated to compare the environment around the acids in the crystal structures. The fingerprint plots (Figure 3.17) were then used to quantitatively and qualitatively compare the intermolecular interactions around these acids. The full interaction plots A and B represent the major and minor disorder of the DBSA⁻ ions. The percentage contributions of the various intermolecular interactions are summarised in Figure 3.17. The shapes of the fingerprint plots are strikingly different. Firstly, the shortest contacts in DBSA⁻ A and B are the O···H interactions, whilst N···H contacts are the shortest in 5BSA. This is because the two acids have different bonding functionality; DBSA⁻ acts as a hydrogen bond acceptor and 5BSA as a hydrogen bond donor.

Quantitatively, the H···H contacts have a higher percentage contribution to the Hirshfeld surface in 5BSA (23.4 %) and contribute less in DBSA⁻ (11.5%). C···Br contacts have a percentage contribution of 8.8 in DBSA⁻, and are absent from 5BSA. These contacts are attributed to C-Br···π interactions; in Figure 3.15b, one of the bromines on DBSA⁻ can be seen pointing towards the aniline ring. Comparatively, the O···Br contacts are higher in DBSA ion (7.0%) compared to 5BSA (2.3%). However, interestingly these contacts are not picked up as short contacts in the crystal packing of [SFP⁺][DBSA⁻], while in SFP·5BSA they can be clearly seen. This indicates that these interactions are stronger in SFP·5BSA (despite having less percentage contribution) than in [SFP⁺][DBSA⁻]. Thus, it can be concluded that adding an additional bromo substituent from 5BSA to DBSA resulted in different stabilising interactions and subsequently significant difference in the crystal packing was observed.
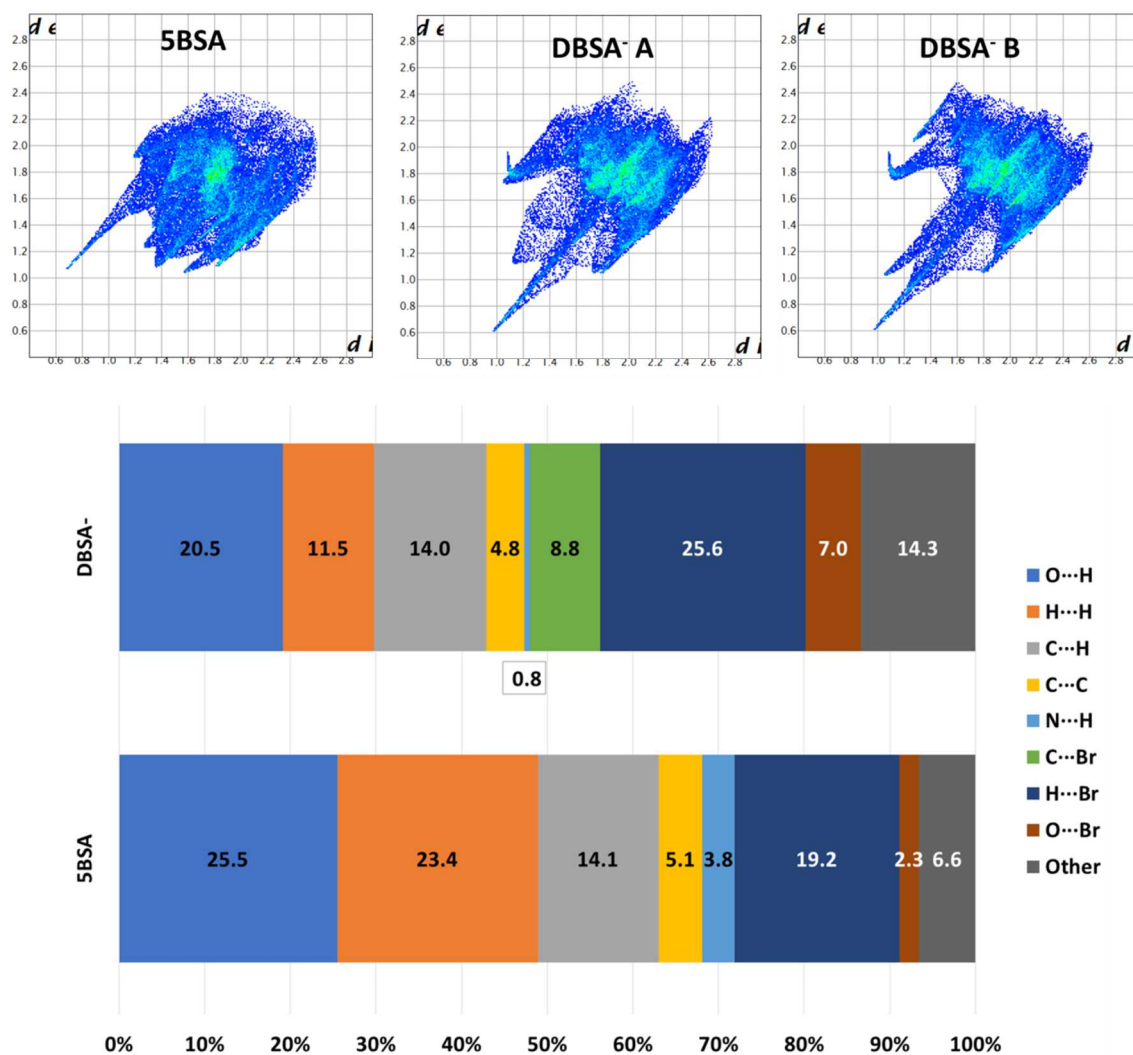
Figure 3.17 Fingerprint plots and summary of the % contributions of the different interactions for 5BSA and DBSA⁻.

3.1.3 Minimal change in the structure of the API: [SFP⁺][DNSA⁻] and [SFD⁺][DNSA⁻]

[SFP⁺][DNSA⁻] and [SFD⁺][DNSA⁻] were synthesized by dissolving equimolar amounts of sulfapyridine or sulfadiazine with 3,5-dinitrosalicylic acid in 1:1 mixture of methanol/chloroform solution or acetonitrile. Crystals were obtained within 2 weeks via the slow evaporation method. The crystallographic details and hydrogen bonds for [SFP⁺][DNSA⁻] and [SFD⁺][DNSA⁻] are summarized in Table 3.5 and Table 3.6 respectively.

Table 3.5 Crystallographic data and structure refinement parameters for [SFP+][DNSA-] and [SFD+][DNSA-].

Compound	[SFP+][DNSA-]	[SFD+][DNSA-].
Molecular formula	$C_{18}H_{15}N_5O_9S$	$C_{17}H_{14}N_6O_9S$
Formula weight (g mol^{-1})	477.41	478.40
Crystal system	Triclinic	Triclinic
Space group (No.)	$P\bar{1}$ (No. 2)	$P\bar{1}$ (No. 2)
a (Å)	7.1170 (14)	6.5978 (13)
b (Å)	11.520 (2)	11.955 (2)
c (Å)	12.656 (3)	12.619 (3)
α (°)	72.82 (3)	74.78 (3)
β (°)	89.85 (3)	86.18 (3)
γ (°)	80.97 (3)	82.69 (3)
V (Å^3)	978.0 (4)	952.1 (4)
Z	2	2
ρ_{calc} (g cm^{-3})	1.621	1.669
μ (Mo Kα) (mm^{-1})	0.233	0.241
F (000)	492	492
Crystal size (mm)	0.04x0.11x0.14	0.03x0.21x0.37
Temperature (K)	173 (2)	173 (2)
Radiation (Å)	MoKα, 0.71073	MoKα, 0.71073
Theta min-max (°)	1.686, 27.920	1.673, 27.992
Dataset	-9:9;-15:15;-16;16	-8:8;-15:15;-16;16
Final R indices [I>2.0σ(I)]	R_1= 0.0423, wR_2=0.0993	R_1= 0.0410, wR_2= 0.1045
R indices [all data]	R_1= 0.0652, wR_2= 0.1114	R_1= 0.0539, wR_2= 0.1128
Tot., uniq. data, R (int)	4673, 3436, 0.0534	4574, 3662, 0.0367
Nref, Npar	4673, 303	4574, 303
S	1.017	1.043
Max. and av. Shift/error	0.000, 0.000	0.000, 0.000
Min. and max. resd. dens. (Å^3)	-0.524, 0.396	-0.490, 0.514

Table 3.6 Hydrogen bonds of [SFP⁺][DNSA⁻] and [SFD⁺][DNSA⁻].

D-H···A	d(D-H) (Å)	d(H···A) (Å)	d(D···A) (Å)	<DH···A (°)	Symmetry operator
[SFP⁺][DNSA⁻]					
C3-H3···O19	0.95	2.46	3.119	126.8	
N7-H7A···O18	0.94	2.43	2.990	118.5	
N7-H7A···O19	0.94	1.96	2.868	161.4	
N7-H7C···O27	0.88	1.90	2.745	161.1	-x+1, -y+1, -z-1
N7-H7C···O30	0.88	2.36	2.935	122.7	-x+1, -y+1, -z-1
N7-H7B···S8	0.95	2.94	2.775	142.2	-x+1, -y+1, -z
N7-H7B···O9	0.95	1.86	3.733	161.3	-x+1, -y+1, -z
N13-H13···N11	0.87	2.06	2.924	174.0	-x+1, -y, -z
C14-H14···O30	0.95	2.65	3.455	143.2	-x+1, -y, -z-1
C15-H15···O29	0.95	2.43	3.287	150.2	-x+1, -y, -z-1
C17-H17···O10	0.95	2.35	2.983	123.8	
O27-H27···O18	0.84	1.66	2.432	152.33	
[SFD⁺][DNSA⁻]					
N7-H7A···O27	0.94	1.85	2.765	164.4	-x, -y, -z+1
N7-H7A···O30	0.94	2.33	2.885	117.4	-x, -y, -z+1
N7-H7B···S8	0.97	2.87	3.688	142.8	-x, -y, -z+2
N7-H7B···O10	0.97	1.87	2.811	163.2	-x, -y, -z+2
N7-H7C···O19	0.92	1.99	2.872	158.6	
C14-H14···O33	0.95	2.42	3.205	140.1	x-2, y, z
C15-H15···O29	0.95	2.42	3.151	133.2	-x, -y-1, -z+1
C16-H16···O30	0.95	2.58	3.439	151.4	-x, -y-1, -z+1
N17-H17···N11	0.85	2.04	2.887	175.9	-x, -y-1, -z+2
O27-H27···O18	0.84	1.66	2.435	152.2	

[SFP⁺][DNSA⁻] crystallized in the triclinic crystal system, having the space group $P\bar{1}$ (No. 2). The asymmetric unit consists of one SFP⁺ cation and one DNSA⁻ anion (Figure 3.18). The hydroxyl proton, H27 of the DNSA forms an intramolecular hydrogen bond via (hydroxyl) O27-H27···O18 (carboxylate) [2.50 Å, 163°]. The asymmetric unit is held together by the (amino) N7-H7A···O19 (carboxylate) [3.10 Å, 125°] hydrogen bond.
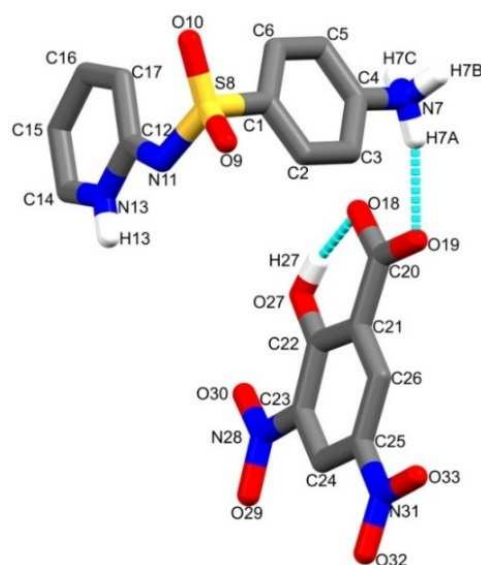
Figure 3.18 Asymmetric unit of [SFP⁺][DNSA⁻], (Some hydrogen atoms are omitted for clarity).

The hydrogen bonding pattern in the [SFP⁺][DNSA⁻] can be described by the $R_6^6(16)$ graph set constructed by (amino) N7-H7A···O19 (carboxylate) [3.10 Å, 125°], (amino) N7-H7C···O27 (hydroxyl) [2.77 Å, 161°] and their symmetry generated counterparts. The ring $R_2^2(16)$ is formed by (amino) N7-H7C···O9 (sulfoxide) [2.75 Å, 159°] hydrogen bonds. The smallest ring, $R_2^2(8)$, formed a homodimer between SFP molecules via (imidine) N13-H13···N11 [3.17 Å, 176°] interactions. All the available hydrogen bond acceptors and donors are fully utilized in this structure (Figure 3.19).

The crystal of [SFP⁺][DNSA⁻] forms from alternating layers of the SFP⁺ (blue) and DNSA⁻ (yellow) ions (Figure 3.20) linked via hydrogen bonding. Face-to-face π-π interactions between the aniline rings of the SFP molecules sustain the assembly, with centroid-to-centroid distance of 3.63 Å. Additional weak C-H···O intermolecular interactions also contribute to the overall structure.
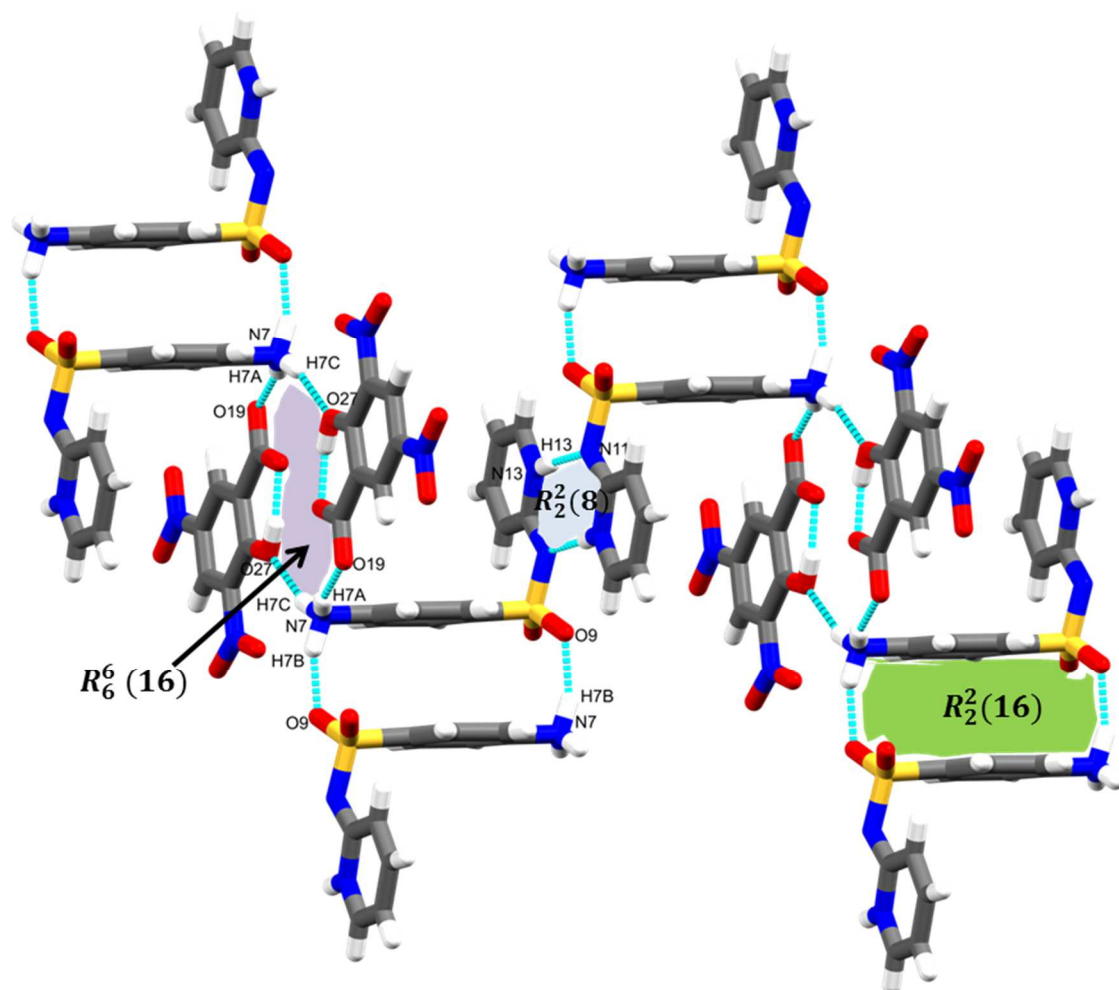
Figure 3.19 Extended structure of [SFP⁺][DNSA⁻] showing hydrogen bonding.
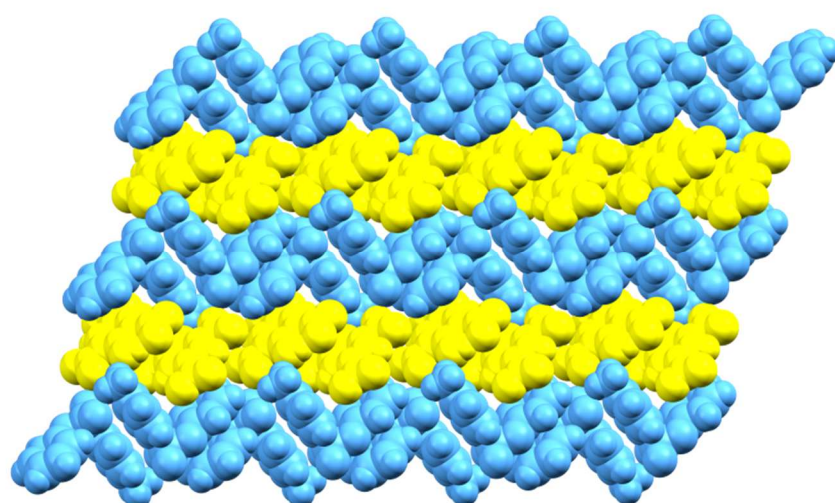
Figure 3.20 Packing diagram of [SFP⁺][DNSA⁻]. Symmetry equivalent SFP⁺ ions are coloured blue and DNSA⁻ ions yellow.

SFD is a sulfonamide that is structurally similar to SFP. It differs by having an extra nitrogen atom; changing a pyridine ring to a pyrimidine ring (Figure 1.10). Sulfadiazine was selected to determine whether using the same coformer to cocrystallize a sulfa drug with a closely related structure would change the crystal packing and hydrogen bonding network significantly. [SFD⁺][DNSA⁻] crystallized in the same triclinic crystal system, having the space group $P\bar{1}$ (No. 2) as [SFP⁺][DNSA⁻] with one SFD⁺ cation and one DNSA⁻ anion in the asymmetric unit (Figure 3.21).
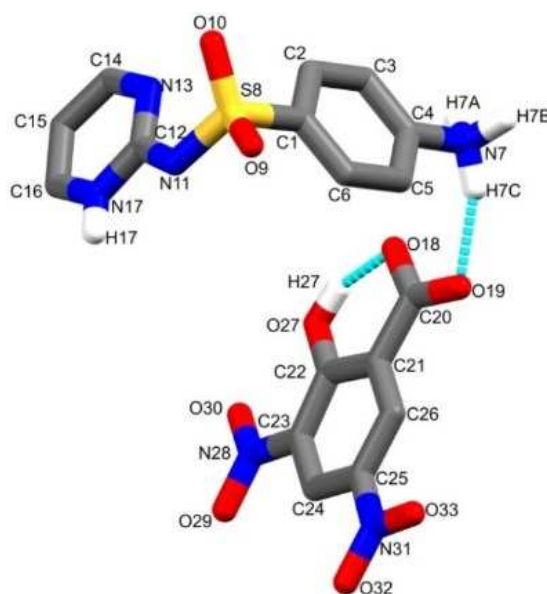

Figure 3.21 Asymmetric unit of [SFD⁺][DNSA⁻], (Some hydrogen atoms are omitted for clarity).

Similar to [SFP⁺][DNSA⁻], identical synthons are observed in this crystal structure and their point of interaction is the same (Figure 3.22). The largest ring $R_6^6(16)$ is constructed by (amino) N7-H7A···O30 (carboxylate) [2.77 Å, 164°], (amino) N7-H7C···O28 (hydroxyl) [2.87 Å, 159˚] hydrogen bonds and their symmetry generated counterparts. The ring $R_2^2(16)$ is formed by (amino) N7-H7B···O10 (sulfoxide) [2.81 Å, 163°] interactions. The smallest ring, $R_2^2(8)$, is generated via (imidine) N17-H17···N11 (imidine) [2.89 Å, 176°] interactions and its symmetry generated counterparts. While all the displacement ellipsoid of [SFD⁺][DNSA⁻] look normal, the shape of the displacement ellipsoid of O29, shown in Figure 3.23, suggests a disorder. SHELX also suggested a split position for this atom. The structure was refined with suggested parameters for the possible disorder, but the refinement did not converge, thus the existence of the disorder cannot be supported with the current data set.

Figure 3.22 Extended structure of [SFD⁺][DNSA⁻] showing hydrogen bonding and graph sets.
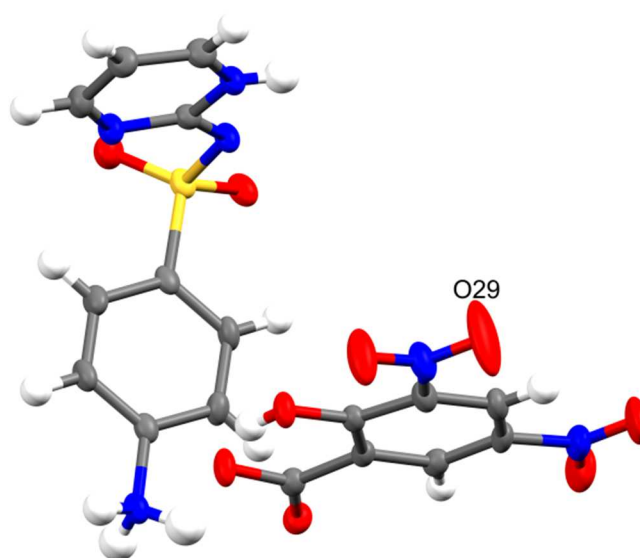
Figure 3.23 [SFD⁺][DNSA⁻] with displacement ellipsoids at the 50% probability level.

Similar to [SFP$^+$][DNSA$^-$], the salt of sulfadiazine packs in alternating layers of the SFD$^+$ (blue) and DNSA$^-$ (yellow) (Figure 3.24). The packing in this structure is mostly dominated by the N-H···O hydrogen bonds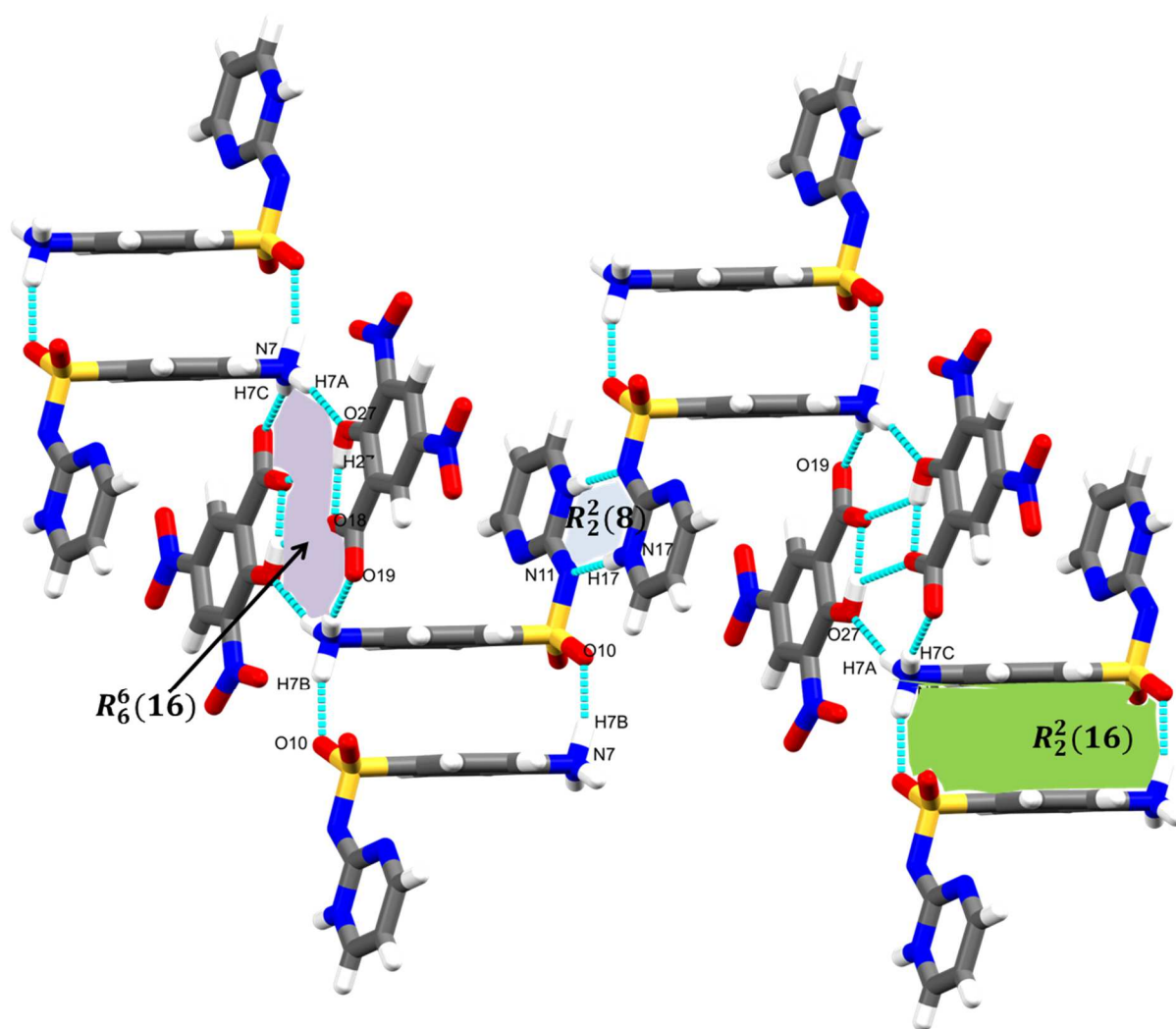 formed between SO$_2$, OH and NH$_2$ groups. Additional forces in the form of C-H···O (sulfoxide), C-H···O (nitro) and (imidine) N-H···O (sulfoxide) as well π-π stacking (centroid-to-centroid distance of 3.68 Å) contributed to the overall structure. All the available donors and acceptors are fully utilized in this structure with the exception of the ortho N on the SFD$^+$.
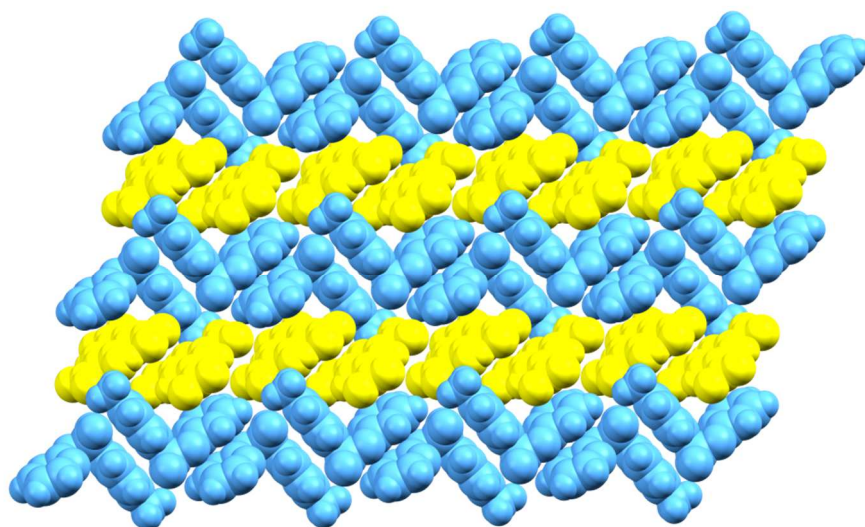
Figure 3.24 Packing of [SFD$^+$][DNSA$^-$] viewed down the a-axis. Symmetry equivalent SFD$^+$ moieties are coloured blue and DNSA$^-$ moieties in yellow.

Isostructurality analysis was carried out in order to study the crystal packing similarities between [SFP$^+$][DNSA$^-$] and [SFD$^+$][DNSA$^-$]. Figure 3.25 was generated by the structure comparison tool of Mercury, which fits 15 out of 15 molecules with an RMS value of 0.65. Although the APIs are slightly different, the crystal structures obtained hardly differ in molecular position or conformation within the crystalline lattice. It is clear from the overlay that the packing arrangement and nature of the intermolecular interactions are identical. [SFP$^+$][DNSA$^-$] and [SFD$^+$][DNSA$^-$] are isostructural and the slight structural differences between the SFP and SFD do not alter the hydrogen bond patterns or the crystal packing.
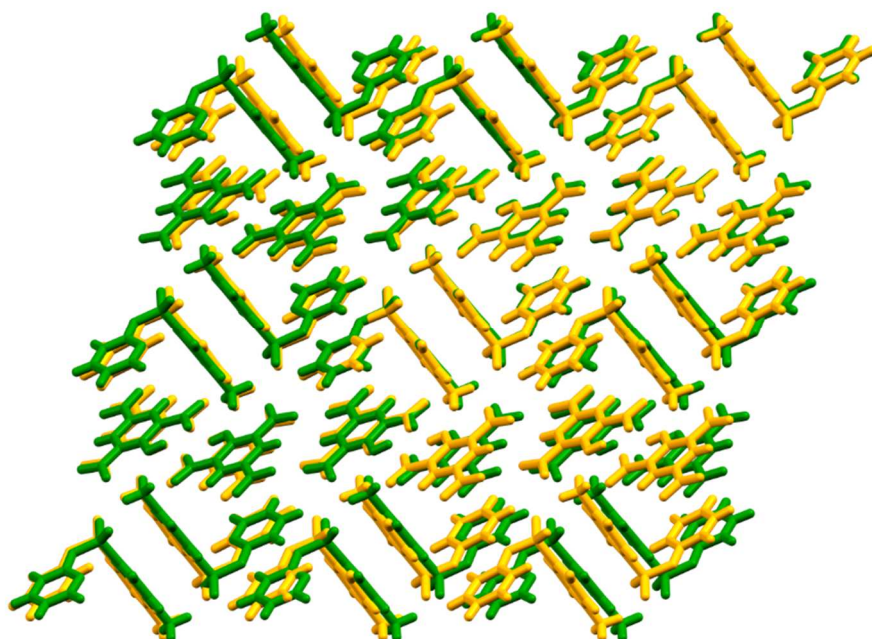
Figure 3.25 Structure overlay of [SFP⁺][DNSA⁻] in orange, and [SFD⁺][DNSA⁻] in green.

The fingerprint plots of the ion pairs are presented in Figure 3.26 for the two isostructural crystals. The plots are symmetrical, indicating that both supramolecular units donate and accepts hydrogen bonds to the procrystal. The crystal structure of [SFP⁺][DNSA⁻] is less efficiently packed when compared to [SFD⁺][DNSA⁻]; this is indicated by the presence of long range H⋯H contacts (highlighted by a red circle in Figure 3.26). In addition, the spike labeled 1, which is also due to short range H⋯H contacts, is less prominent in [SFP⁺][DNSA⁻]. The length of the O⋯H interactions are very similar in both structures, but [SFD⁺][DNSA⁻] has more O⋯H % interactions. There is difference in the length and the % contribution of the N⋯H interactions, favouring [SFD⁺][DNSA⁻]. These O⋯H and N⋯H interactions are represented as double spikes on the fingerprint plots (Figure 3.26).

Due to the slight changes in packing efficiency, small differences in the percentage contributions of the intermolecular interactions are observed. These observations show how even isostructural compounds may have slight differences in their stabilising interactions.
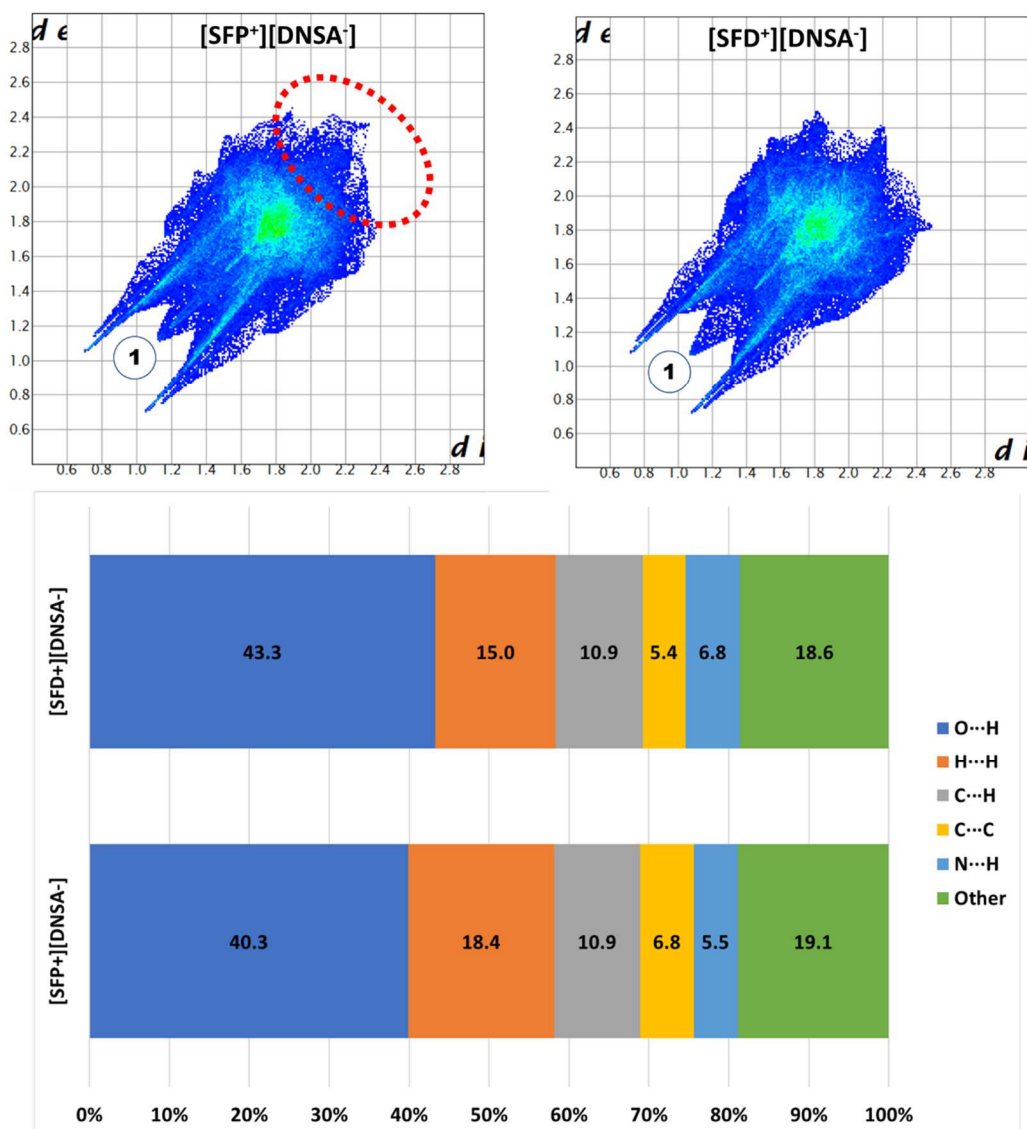
Figure 3.26 Fingerprint plots and summary of the % contributions of the different interactions for [SFP⁺][DNSA⁻] and [SFD⁺][DNSA⁻].

3.1.4 Evaluation of the effect of acidity change in coformer: SFP·4DMAP

A pyridine derivative coformer was employed to evaluate if a change in acidity of the coformer would result in a solid form with different intermolecular interactions, hydrogen bonding patterns or crystal packing, when compared to carboxylic acids. SFP·4DMAP was synthesized by dissolving equimolar amounts of sulfapyridine with 4-dimethylaminopyridine in 1:1 mixture of ethanol/water solution. The crystallographic details and hydrogen bonds are summarized in Table 3.7 and Table 3.8 respectively.

Table 3.7 Crystal structure data of SFP·4DMAP.

Compound	SFP·4DMAP
Molecular formula	$C_{18}H_{21}N_5O_2S$
Formula weight (g mol^{-1})	371.46
Crystal system	Orthorhombic
Space group (No.)	$P2_12_12_1$ (No. 19)
a (Å)	6.7496 (13)
b (Å)	15.211 (3)
c (Å)	17.933 (4)
α (°)	90
β (°)	90
γ (°)	90
V (Å^3)	1841.1 (7)
Z	4
ρ_{calc} (g cm^{-3})	1.340
μ (Mo Kα) (mm^{-1})	0.199
F (000)	784
Crystal size (mm)	0.06x0.12x0.17
Temperature (K)	173 (2)
Radiation (Å)	MoKα, 0.71073
Theta min-max (°)	1.756, 27.954
Dataset	-7:8;-20:20;-23;23
Final R indices [I>2.0σ(I)]	R$_1$=0.0628, wR$_2$=0.1285
R indices [all data]	R$_1$=0.0920, wR$_2$=0.1397
Tot., uniq. data, R (int)	4409, 3311, 0.0519
Nref, Npar	4409, 239
S	1.042
Max. and av. Shift/error	0.000, 0.000
Min. and max. resd. dens. (Å^3)	-0.353, 0.607

Table 3.8 Hydrogen bonds of SFP·4DMAP.

D-H⋯A	d(D-H) (Å)	d(H⋯A) (Å)	d(D⋯A) (Å)	<DH⋯A (°)	Symmetry operator
C5-H5⋯S8	0.95	3.02	3.912	157.2	-x+1, y+1/2, -z+1/2
C5-H5⋯O9	0.95	2.65	3.582	166.8	-x+1, y+1/2, -z+1/2
N7-H7A⋯O9	0.80	2.14	2.895	158.9	-x, y+1/2, -z+1/2
N7-H7B⋯O10	0.86	2.07	2.921	171.5	-x+1, y+1/2, -z+1/2
N13-H13⋯N18	0.88	1.81	2.687	175.3	
C17-H17⋯O10	0.95	2.39	2.973	119.4	
C19-H19⋯O9	0.95	2.44	3.247	143.0	-x+1/2, -y, z+1/2
C20-H20⋯O10	0.95	2.41	3.318	160.3	-x+1/2, -y, z+1/2

The cocrystal SFP·4DMAP crystallizes in the orthorhombic crystal system, having space group $P2_12_12_1$ (No. 19). The asymmetric unit contains one molecule of sulfapyridine and one molecule of 4-dimethylaminopyridine (Figure 3.27). The imidine proton (H13) and amine protons (H7A & H7B) were located in the electron density map and their coordinates refined freely. The asymmetric unit molecules associate via (imidine) N13-H13···N18 (pyridine) [2.69 Å, 175°] represented by $R_2^2(7)$ graph set.
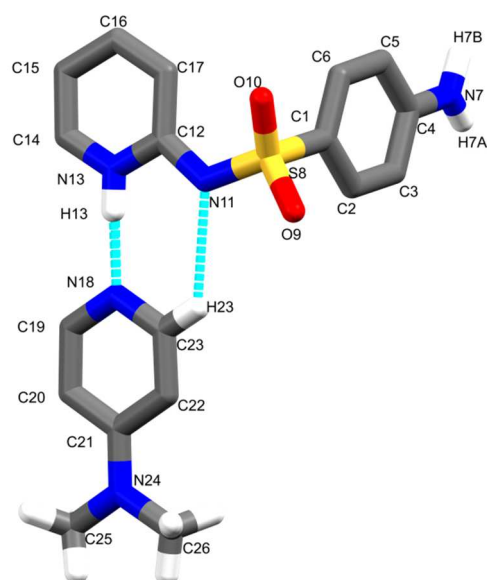
Figure 3.27 Asymmetric unit of SFP·4DMAP.

The extended motif, Figure 3.28, built by (amine) N7-H7A···O9 (sulfoxide) [2.90 Å, 159°], (amine) N7-H7B···O10 (sulfoxide) [2.92 Å, 171°] and their symmetry generated counterparts is illustrated by $R_4^4(22)$ graph set. Like in the case of SFP·3NBA and [SFP⁺][4NBA⁻], the structure forms wave-like chains via alternating (amine) N7-H7A···O9 (sulfoxide) and (amine) N7-H7B···O10 (sulfoxide) interactions to form $C_2^2(16)$ chains.

The packing is stabilised by formation of wave-like chains, shown in Figure 3.29. Additional interactions such as C-H···O (sulfoxide), C-H···O (nitro) and (imidine) N-H···O (sulfoxide) contribute to the 3D hydrogen bonded structure. Contrary to the rest of the structures described herein, the coformer in SFP·4DMAP has a hydrogen bond acceptor functional group. Despite this difference, the crystal structure adopted similar crystal packing to crystals formed with acid coformers, such as SFP·3NBA and [SFP⁺][4NBA⁻].

Figure 3.28 Hydrogen bonding motifs of SFP·4DMAP, view down the a-axis.

Figure 3.29 Crystal packing of SFP·4DMAP depicting stacked wave-like infinite chains (purple) formed between SFP molecules and the 4DMAP molecules which have been omitted for clarity.
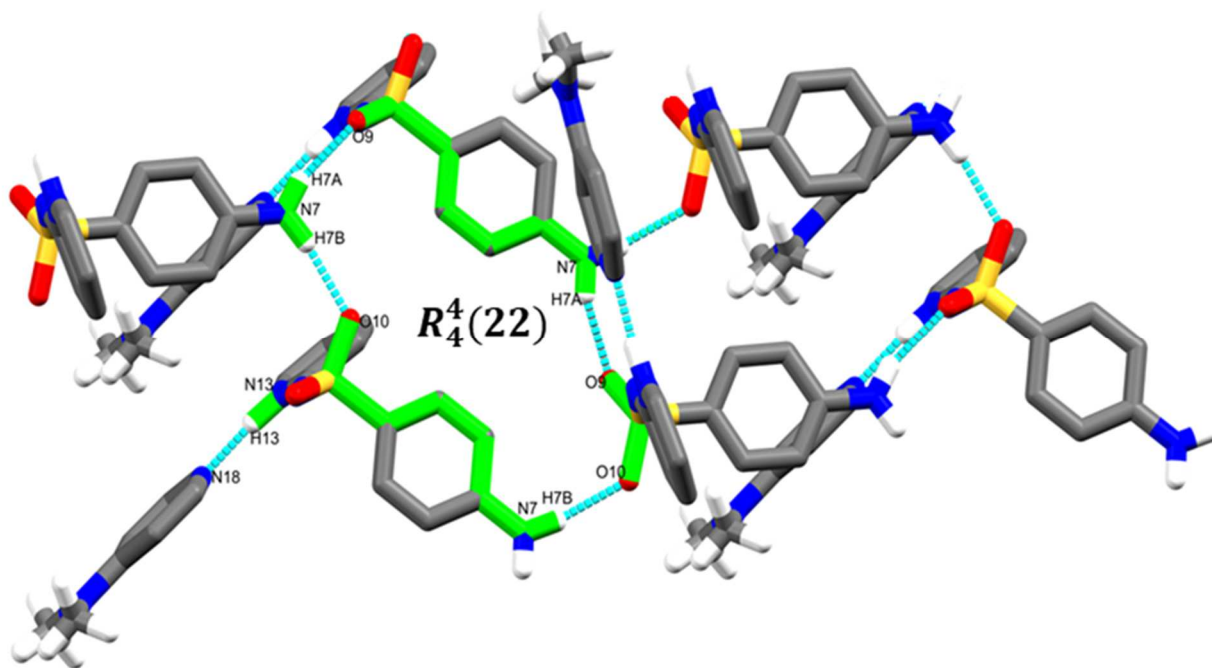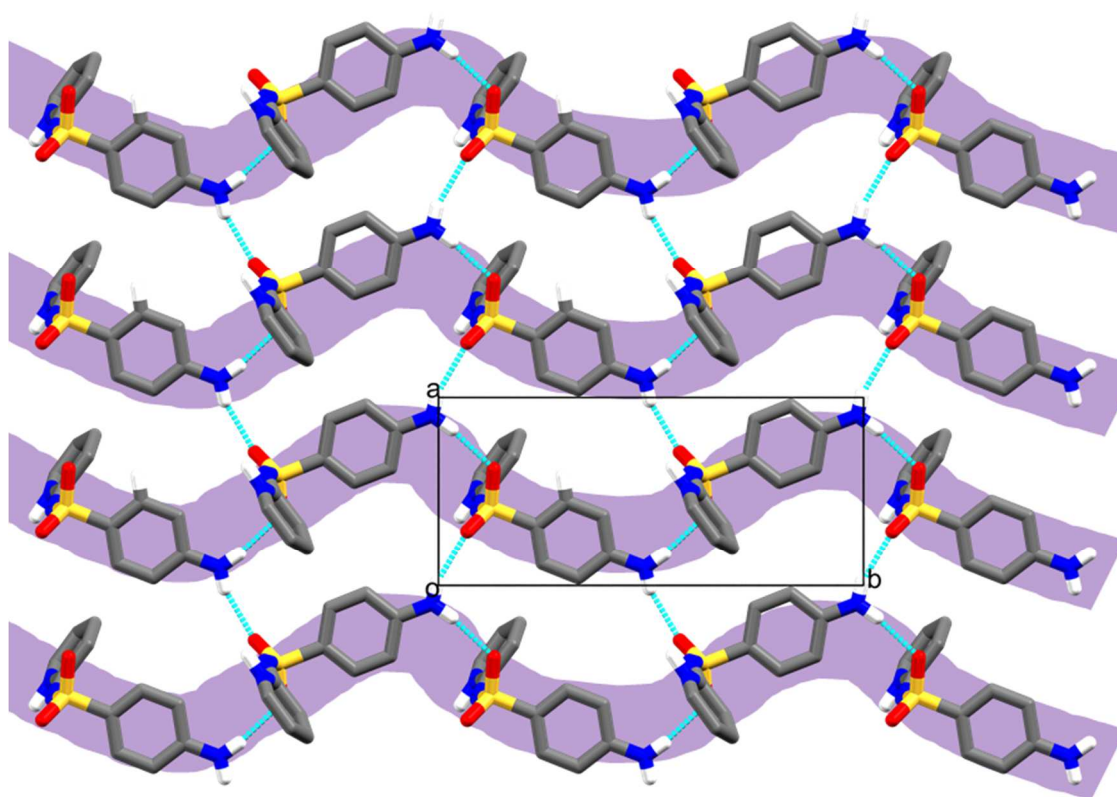
Unlike in the crystals containing acid coformers where the quantitative ΔpK_a rule could not be applied. In this case, since a pyridine coformer was employed, we could easily identify the strong hydrogen bond donor site in the two forms of SFP. In the amidine form, the ΔpK_a was calculated as 1.04, suggesting the formation of a cocrystal or salt. On the other hand, the ΔpK_a in the imidine form was calculated as -2.83 suggesting the formation of a cocrystal. The calculated results agreed well with our experimental results as we observed a cocrystal in the imidine tautomeric form. In conclusion the quantitative ΔpK_a rule can be used to assess compounds containing one hydrogen bond acceptor and one donor interactive site

Despite changing the coformer from an acid to a base, it was observed that the fingerprint plot of SFP·4DMAP (Figure 3.30) is similar to that of SFP·3NBA and [SFP+][4NBA-]. One noticeable similarity is the symmetrical shape of the fingerprint plots, indicating that the SFP·4DMAP pair has equal donor and acceptor functionality. However, the fingerprint plot of SFP·4DMAP shows the 'chicken wing' feature which indicates that this structure has more pronounced C···H interactions. As such, more % C···H interactions are observed in SFP·4DMAP (25.4%) as compared to SFP·3NBA (19.8%) and [SFP+][4NBA-] (19.9%).

Another difference is the significantly higher % H···H interactions in SFP·4DMAP, this can be expected because of the methyl groups on 4DMAP. In addition, the H···H contacts (peak 1, Figure 3.30) are at shorter contact distance, which suggests unfavourable packing in SFP·4DMA. Remarkably, despite the difference in stabilising interactions, similar packing is observed in SFP·4DMAP, SFP·3NBA and [SFP+][4NBA-]. This suggests that, in these structures, hydrogen bonding plays a more central role in directing the packing.
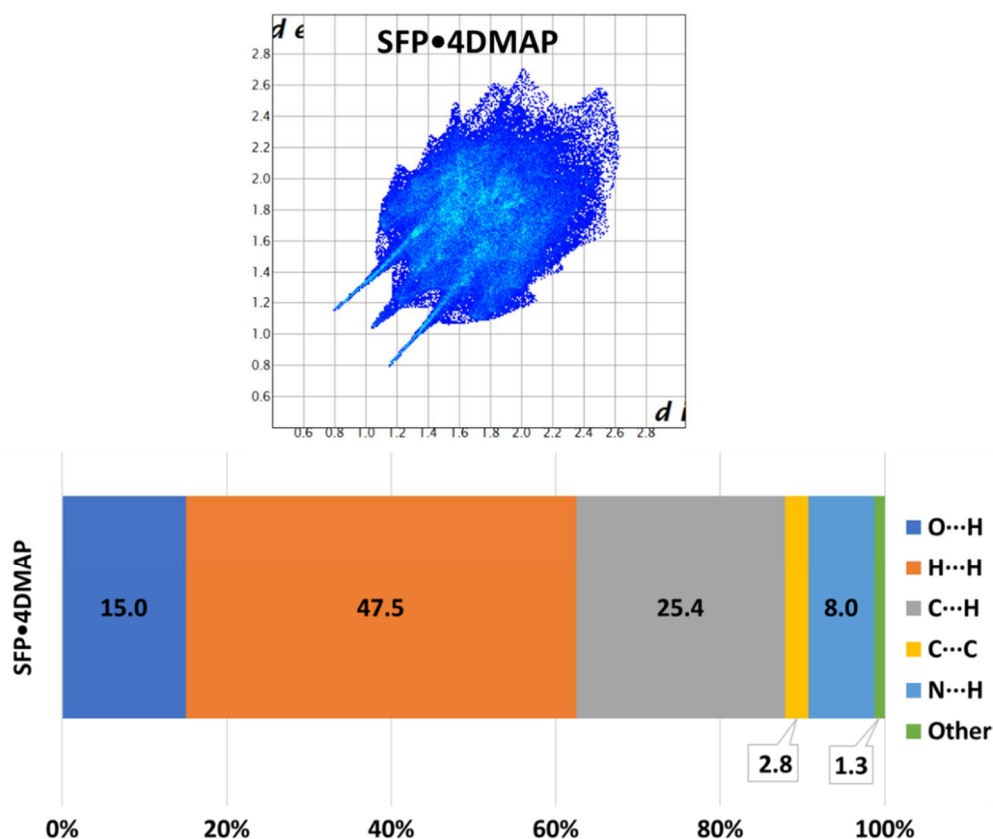
Figure 3.30 Fingerprint plots and summary of the % contributions of the different interactions for SFP·4DMAP.

3.2   Bulk property analysis of (DSC, TGA, PXRD and NMR)

Detailed DSC and TGA experiments were carried out for each novel multicomponent crystal to study the thermal behaviour. The TGA data and DSC traces for all cocrystals and salts are presented in Appendix B; Figure B1-B7. TGA thermograms exhibited no weight loss attributable to included solvents.

The DSC thermograms for all seven complexes of sulfadiazine and sulfapyridine showed a single endotherm corresponding to the melting point. The melting transition temperature of all solid forms was distinct from the individual components confirming the formation of a new compound. It is interesting that although SFP·3NBA and [SFP$^+$][4NBA$^-$] have similar crystal packing, they show a huge difference in melting points i.e. 155.9 °C and 196.7 °C respectively. This is due to differences in the nature of hydrogen bonds. i.e. the normal hydrogen bonds in SFP·3NBA, and the much stronger charge assisted hydrogen bonds in [SFP$^+$][4NBA$^-$]. Hence [SFP$^+$][4NBA$^-$] has a higher melting point.

Table 3.9 Melting point measurements for multicomponent crystals.

coformer	DSC			
	Onset (°C)	Peak (°C)	ΔH (J g^{-1})	H (J mol^{-1})
SFP·3NBA	155.9	157.3	153.22	0.37
[SFP$^+$][4NBA$^-$],	196.7	198.4	183.16	0.44
SFP·5BSA	141.7	144.4	84.23	0.18
[SFP$^+$][DBSA$^-$],	201.9	205.5	88.02	0.16
[SFP$^+$][DNSA$^-$],	193.4	197.8	36.42	0.08
SFP·4DMAP	173.4	175.1	171.74	0.46
[SFD$^+$][DNSA$^-$]	212.5	218.5	40.55	0.09

The homogeneity of the bulk material was also tested with PXRD and was compared to the single crystal structures (Appendix Fig. C1-C7). Good correlation between the single crystal structure and the bulk material was found in all seven compounds: SFP·3NBA, [SFP$^+$][4NBA$^-$], SFP·5BSA, [SFP$^+$][DBSA$^-$], [SFP$^+$][DNSA$^-$], [SFD$^+$][DNSA$^-$] and SFP·4DMAP.

The crystalline solids were characterised by proton and carbon nuclear magnetic resonance spectroscopy (^{1}H NMR and ^{13}C NMR). The spectrum showed signals representing both the starting materials and all the spectra are presented in Appendix E; Figure E1-E14. NMR study was used to investigate if the salts synthesised herein; [SFP$^+$][4NBA$^-$], [SFP$^+$][DBSA$^-$], [SFP$^+$][DNSA$^-$] and [SFD$^+$][DNSA$^-$] exist as ion pairs in solution. From the signal allocation, it was observed that all salt forms, except [SFP$^+$][4NBA$^-$], exist as ion pairs in solution. This was confirmed by a broad peak at 12.25 ppm which is the chemical shift of the acid proton.

The ^{1}H NMR and ^{13}C NMR of [SFP$^+$][DNSA$^-$] was difficult to assign, therefore 2D HSQC and HMBC were used to help with the assignment of the protons and carbons. The 2D HSQC Spectrum (Appendix E: Figure E.15) was generated to provide information on the direct C-H coupling in [SFP$^+$][DNSA$^-$]. That is, how protons are attached directly to carbons; and therefore we only observe correlations where carbons are protonated. Here some of the missing protonated carbons, such as C14 and C6/C2, were located.

The HMBC spectrum (Figure E.16) provides information on the neighbouring carbons of a particular proton. Here other carbons (not necessarily protonated carbons i.e. quaternary carbons) are also observed, e.g. C4, C20. As such, HMBC confirmed that those carbons that we were not quite sure of were actually present.

3.3 References

1. Cruz-Cabeza, A. J., Acid-base crystalline complexes and the pKa rule. *CrystEngComm* **2012,** *14* (20), 6362-6365.
2. Fu, X.; Li, J.; Wang, L.; Wu, B.; Xu, X.; Deng, Z.; Zhang, H., Pharmaceutical crystalline complexes of sulfamethazine with saccharin: same interaction site but different ionization states. *RSC Advances* **2016,** *6* (31), 26474-26478.
3. (a) Jetti, R. K. R.; Boese, R.; Sarma, J. A. R. P.; Reddy, L. S.; Vishweshwar, P.; Desiraju, G. R., Searching for a Polymorph: Second Crystal Form of 6-Amino-2-Phenylsulfonylimino-1,2-Dihydropyridine. *Angewandte Chemie International Edition* **2003,** *42* (17), 1963-1967; (b) Bingham, A. L.; Threlfall, T. L.; Gelbrich, T.; Hursthouse, M. B., Polymorph VI of sulfapyridine: interpenetrating two- and three-dimensional hydrogen-bonded nets formed from two tautomeric forms. *Acta Crystallographica Section C* **2007,** *63* (6), o323-o326.
4. Calculator Plugins were used for structure property prediction and calculation, M., 2016, ChemAxon(http://www.chemaxon.com). #The pKa prediction is done on the basis of the partial charge distribution calculated for the atoms in the molecule and this method provides an efficient and robust way to locate the most acidic and basic sites."
5. Etter, M. C.; MacDonald, J. C.; Bernstein, J., Graph-set analysis of hydrogen-bond patterns in organic crystals. *Acta Crystallogr B* **1990,** *46 (Pt 2)*, 256-262

Chapter 4

Discussion

4.1   Synthon competition study

Sulfapyridine contains multiple hydrogen bond acceptor and donor sites: two S=O groups from the sulfoxide, an imidine (–NH) group, the amine (-NH$_2$), and the imidine N atom. On the other hand, sulfadiazine has all the previously mentioned functional groups plus an additional pyrimidine N atom. The introduction of coformers with competing hydrogen bond acceptor and donor sites creates multiple synthons and can possibly disrupt the preferred dimer formation between the sulfonamides. Carboxylic acids and a pyridine derivative were employed to compete with the dimer formation.

An analysis of the synthons formed in the current and previously reported structures of multicomponent crystals of SFP in the CSD was carried out. The commonly observed interactions/synthons are the amidine dimer, depicted as synthon 6 (Figure 4.1), synthon 5 formed from NH$_2$···O (sulfoxide), NH$_2$···N (amidine) and (imidine) N−H ···O (sulfoxide). From all the synthons observed in the multicomponent crystals of SFP in this study, the most resilient interaction is the NH$_2$···O (sulfoxide) (synthon 5), which was observed in six of the new solid forms: namely SFP·3NBA, [SFP$^+$][4NBA$^-$], [SFP$^+$][DBSA$^-$], [SFP$^+$][DNSA$^-$], [SFD$^+$][DNSA$^-$] and SFP·4DMAP, except SFP·5BSA. The amidine dimer (synthon 6) was preserved in three of the seven crystals, namely: SFP·5BSA, [SFP$^+$][DNSA$^-$] and [SFD$^+$][DNSA$^-$].

Additionally, synthons 1 and 2 were observed in SFP·3NBA, [SFP$^+$][4NBA$^-$] and [SFP$^+$][DBSA$^-$] multicomponent crystals. The amidine carboxylic acid or the amidine pyridinium carboxylate heterodimers were formed in these three latter structures, thus disrupted the formation of the amidine dimer (synthon 6). Moreover, synthon 10, (imidine) N−H···N (pyridine) formed in the SFP·4DMAP also disrupted the formation of the amidine dimer. Synthons 3 and 4 were observed in SFP·5BSA, [SFP$^+$][DNSA$^-$] and [SFD$^+$][DNSA$^-$]. In addition, in the latter structures, the amidine dimer (synthon 6) was also observed. It is worth mentioning that whenever synthon 3 and 4 are observed, concurrently synthon 6 is observed. Synthon 7 was only observed in the cocrystal of SFP·4DMAP. Synthon 8 and 9 were only observed in [SFP$^+$][DNSA$^-$] and [SFD$^+$][DNSA$^-$].

To conclude, employing carboxylic acids and amines as coformers can disrupt the formation of the most popular synthon, i.e. (amidine) N−H···N (pyridine) dimer in sulfapyridine. In

addition, we observed that the imidine/amidine dimer was disrupted in SFP·3NBA, [SFP⁺][4NBA⁻], [SFP⁺][DBSA⁻] and SFP·4DMAP while it was maintained in SFP·5BSA, [SFP⁺][DNSA⁻] and [SFD⁺][DNSA⁻].
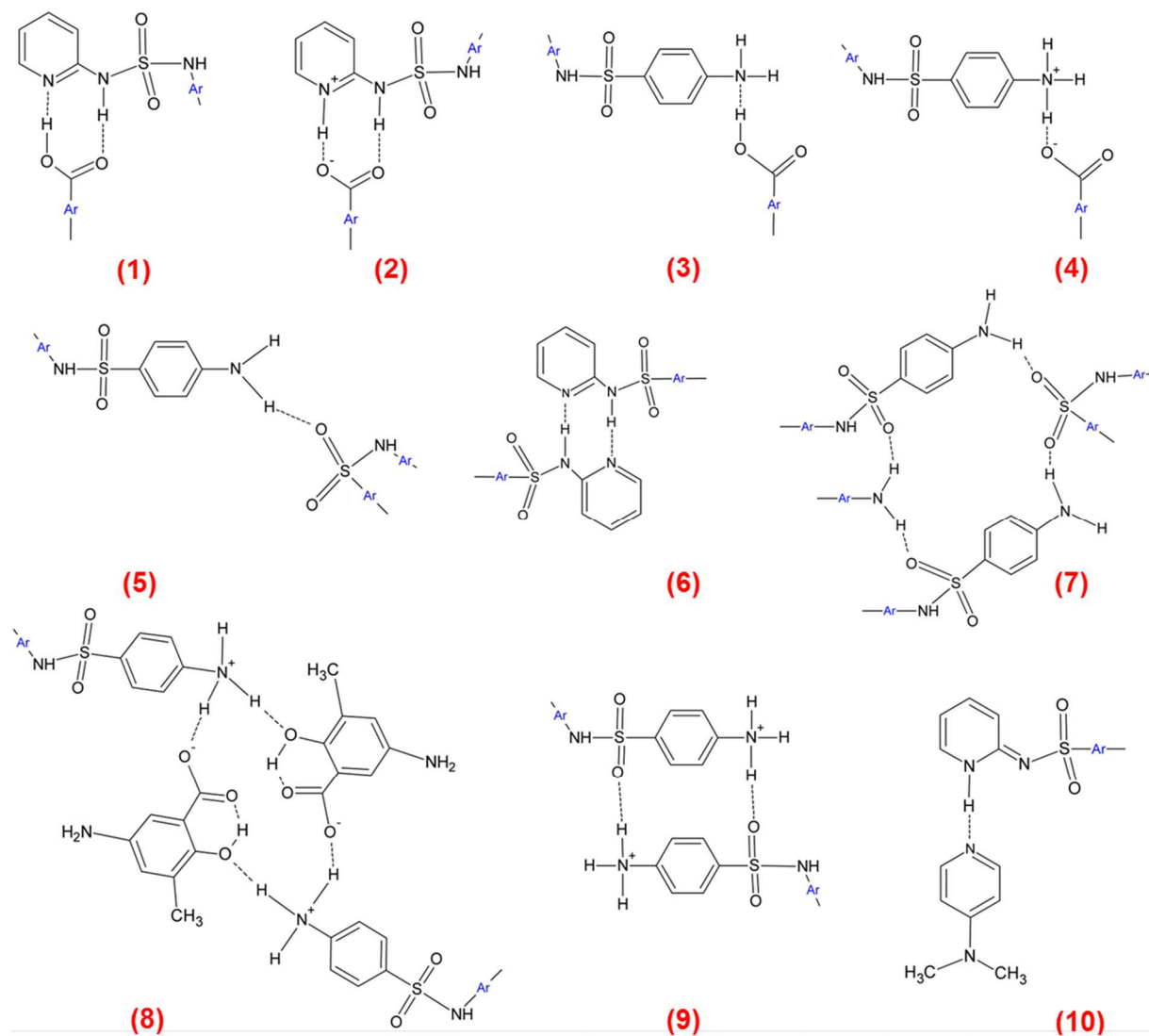

Figure 4.1 Synthons observed in the multicomponent crystals of SFP and SFD.

4.2   Conformational Analysis

The presence of the sulfonamide group in SFP and SFD suggests that these molecules can potentially adopt different conformations and have tautomers in the crystal structures due to the flexible rotation around the single bond of the sulfonamide group.[1] A comparison in the bond rotation was completed to get a more precise measure of the conformational differences of the molecules in the different crystal structures.

The main conformational changes of the SFP and the SFD molecules can be described by three torsion angles: τ_1 = C-C-S-N (yellow on Figure 4.2), τ_2 = S-N-C-C (green) and τ_3 = O-S-N-C (purple). The values of the torsion angles for the seven multicomponent crystals presented in this work are listed in Table 4.1. The values for τ_1, which describe the rotation of the aniline moiety, show small variation (from -70° to -89°). Similarly, τ_2 describing the movement of the pyridine ring presents small differences (from -2° to -28°). τ_3 , defining the amidine or the imidine moiety position relative to the S=O group, varies from 40° to 47°.

The torsion angles of the sulfapyridine and sulfadiazine molecules suggest that all API molecules in the multicomponent crystals adopt a similar conformation. This was verified by the molecular overlay of SFP and SFD molecules in the crystals which show similar conformation (Figure 4.3).
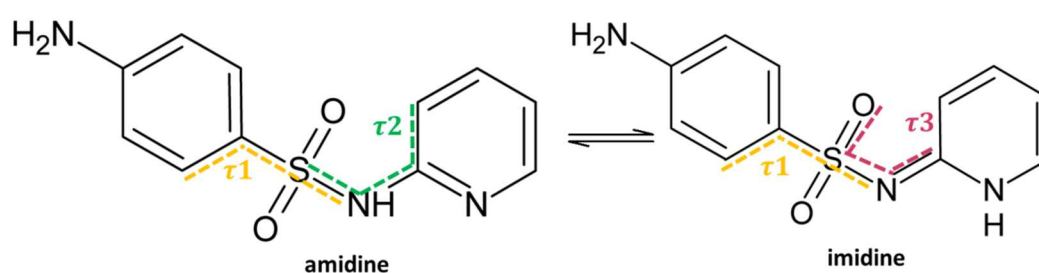

Figure 4.2 Graphical representations of the torsion angles of SFP.

Table 4.1 Related torsion angles of SFP and SFD from current and previously reported multicomponent crystals.

	$\tau_1/°$	$\tau_2/°$	$\tau_3/°$
SFP·3NBA	-89.1	-20.1	43.9
[SFP$^+$][4NBA$^-$]	-79.0	-14.9	42.5
SFP·5BSA	-84.3	-7.7	40.9
[SFP$^+$][DBSA$^-$]	-88.3	-28.4	43.3
[SFP$^+$][DNSA$^-$]	-71.5	-12.5	41.4
SFP·4DMAP	-70.4	-2.7	40.7
[SFD$^+$][DNSA$^-$]	-81.6	-2.2	47.4

SFP·3NBA
[SFP$^+$][4NBA$^-$]
[SFP$^+$][DNSA$^-$]
SFP·5BSA
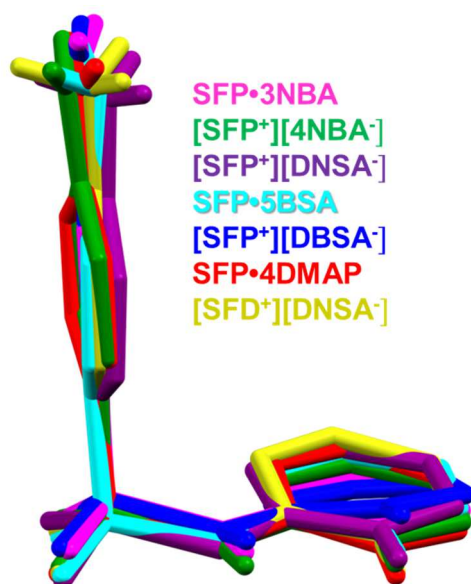[SFP$^+$][DBSA$^-$]
SFP·4DMAP
[SFD$^+$][DNSA$^-$]

Figure 4.3 The superimposed molecules of sulfapyridine and sulfadiazine from structures formed.

4.3 Tautomers in sulfa drugs

In our work we employed a base and carboxylic acids as coformers, which yielded cationic salts and cocrystals. We measured the S-N and C12-N11 bond lengths (Figure 4.4) of our new solid forms in order to determine the range of values in which the imidine and amidine tautomers lie in each solid form.

Additionally, the bond lengths S-N and C12-N11 of the cationic based salts and sulfapyridine cocrystals available from literature were analyzed and the ranges of values obtained were compared to those recorded from this study.

Figure 4.4 Tautomers of sulfapyridine with the atomic numbering of sections of interest.

From the CSD study of the amidine based complexes, the measured bond lengths S-N and C12-N11, range between 1.63-1.68 Å and 1.35-1.41 Å, respectively. In the imidine based structures, both bond lengths (S-N and C12-N11) range from 1.60-1.61 Å and 1.34-1.36 Å. In this work, the multicomponent crystals containing the amidine tautomer showed S-N and C12-N11 bond length of 1.62-1.65 Å and 1.39 Å respectively. While, the imidine based solid forms exhibited S-N and C12-N11with ranges between 1.58-1.61 Å and 1.34-1.36 Å respectively. All measured bond lengths from this work are given in Table 4.2.

It was noted that if the sum of (S-N) and (C12-N11) is below 2.99 then the imidine tautomer is observed in the complex, and if above 2.99, then it is amidine form (Figure 4.5). The analysis of the structures obtained from the CSD show that in certain cases the amidine and the imidine tautomers have very similar selected bond length. (This can be the result of uncertainty of the published values or uncertainty in the allocation of the hydrogen atom in these structures.) The values observed in the seven new multicomponent crystals are laying in the regions based according to their tautomeric form, and the amidine tautomers are clustered, displaying very similar values for the two bond lengths investigated.

Table 4.2 Geometric parameters and tautomeric forms of cationic SD complexes and SFP based cocrystals.

Sulfa drug	coformer	S-N (Å)	C12-N11 (Å)	tautomer	refcode
sulfisomidine	HCl, H2O	1.653	1.372	amidine	CITYEJ10[3]
sulfapyridine	1,3-dioxane	1.600	1.356	imidine	ODIGAL[2]
sulfapyridine	piperidine	1.624	1.404	†amidine	ODIGIT[2]
sulfamethazine	2,4,6-trinitrophenol	1.679	1.367	amidine	RILQOU[4]
sulfamethazine	5-nitrosalicylic acid	1.677	1.352	amidine	RILQUA[4]
sulfamethaxole	HCl	1.631	1.393	amidine	SIMJEE[5]
sulfamethaxole	3,5-dinitrosalicylic acid	1.626	1.388	amidine	TUJPEV[6]
sulfamethazine	3,5-dinitrosalicylic acid	1.673	1.357	amidine	WIHJAA[7]
sulfapyridine	oxalic acid dibutyl ester	1.644	1.413	amidine	XIFKUT01[8]
sulfapyridine	THF	1.614	1.351	imidine	XIFPAE01[2]
sulfapyridine	THF	1.604	1.353	imidine	XIFPAE02[9]
sulfamethazine	saccharin	1.657	1.363	imidine	XOBCOH01[11]
sulfapyridine	nitromethane	1.597	1.343	imidine	YAWQIY[12]
Sulfadiazine	ethane sulfonic acid	1.633	1.387	amidine	YONKUJ[13]
Sulfadiazine	4-hydroxybenzenesulfonic acid, H2O	1.642	1.386	amidine	YONLAQ[13]
SFP·3NBA	3-nitrobenzoic acid	1.627	1.386	amidine	this work
[SFP⁺][4NBA⁻]	4-nitrobenzoic acid	1.624	1.386	amidine	this work
SFP·5BSA	5-bromosalicylic acid	1.605	1.354	imidine	this work
[SFP⁺)][DBSA⁻]	3,5-dibromosalicylic acid	1.650	1.387	amidine	this work
[SFP⁺][DNSA⁻]	3,5-dinitrosalicylic acid	1.588	1.343	imidine	this work
SFP·4DMAP	4-dimethylaminopyridine	1.577	1.363	imidine	this work
[SFD⁺][DNSA⁻]	3,5-dinitrosalicylic acid	1.607	1.342	imidine	this work

† Denotes salt containing anionic SD and cationic coformer (excluded from geometry study)
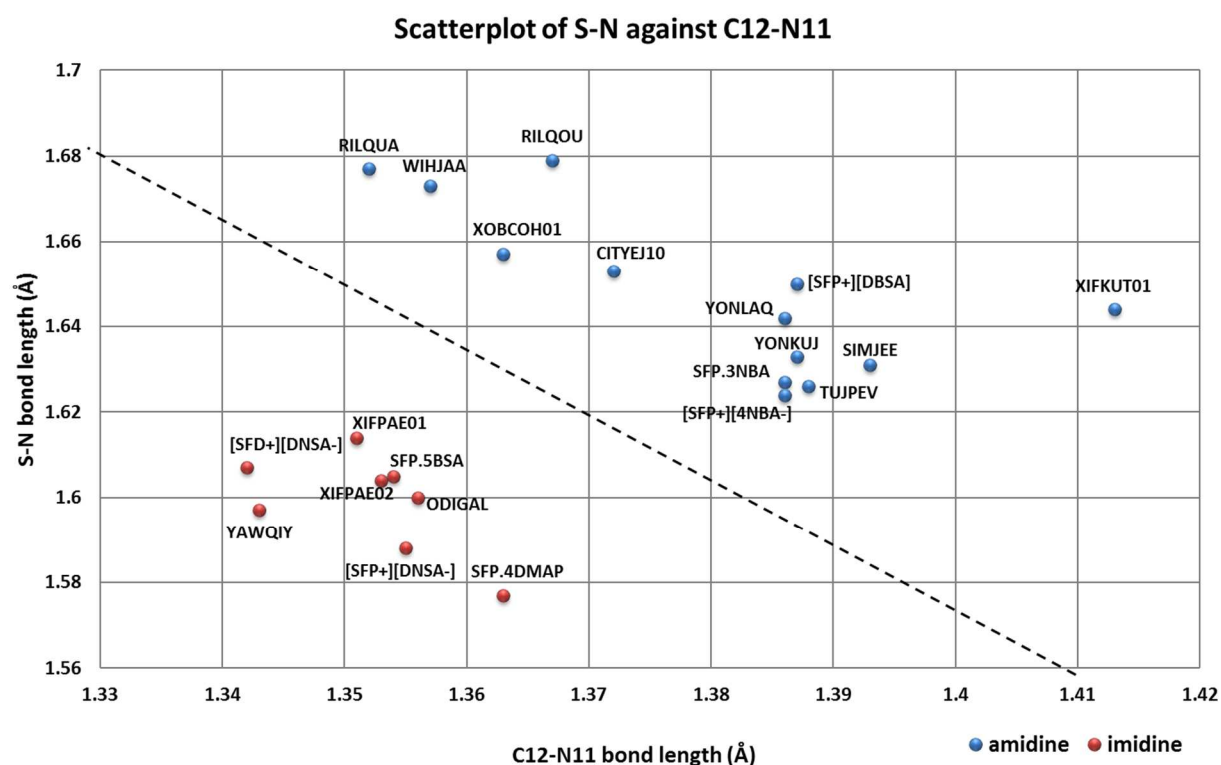
Figure 4.5 Plot of S-N bond length vs. C12-N11 bond length for cationic based CSD complexes (light coloured squares or diamonds) and SFP and SFD based multicomponent crystals obtained from this work (dark coloured squares or diamonds).

To further investigate tautomerism of the sulfa drugs, the S-N bond length and SNC bond angles were also analyzed to see if they could serve as a tool to identify amidine or imidine tautomers. The amidine tautomers have S-N bond lengths within a range of 1.63-1.65 Å and SNC bond angles between 125.6-127.5°. The imidine tautomeric forms revealed shorter S-N bond lengths of (1.58-1.62 Å) and smaller SNC bond angles (115.2-122.7°). The values are listed in Table 4.3. The graphs summarizing the S-N bond length vs. the SNC angle shows the different tautomeric forms in two distinct regions (Figure 4.6), thus the measured SNC bond angles and S-N bond lengths can aid to classify the tautomeric forms obtained in the different multicomponent crystals.

Table 4.3 Geometric parameters of our newly synthesized structures.

Compounds	θ/°	d/ Å	tautomer
SFP·3NBA	127.45	1.627	amidine
[SFP$^+$][4NBA$^-$]	125.81	1.624	amidine
[SFP$^+$][DNSA$^-$]	115.29	1.620	imidine
[SFD$^+$][DNSA$^-$]	120.38	1.607	amidine
SFP·5BSA	122.30	1.605	imidine
[SFP$^+$)][DBSA$^-$]	125.56	1.650	imidine
SFP·4DMAP	122.70	1.577	imidine
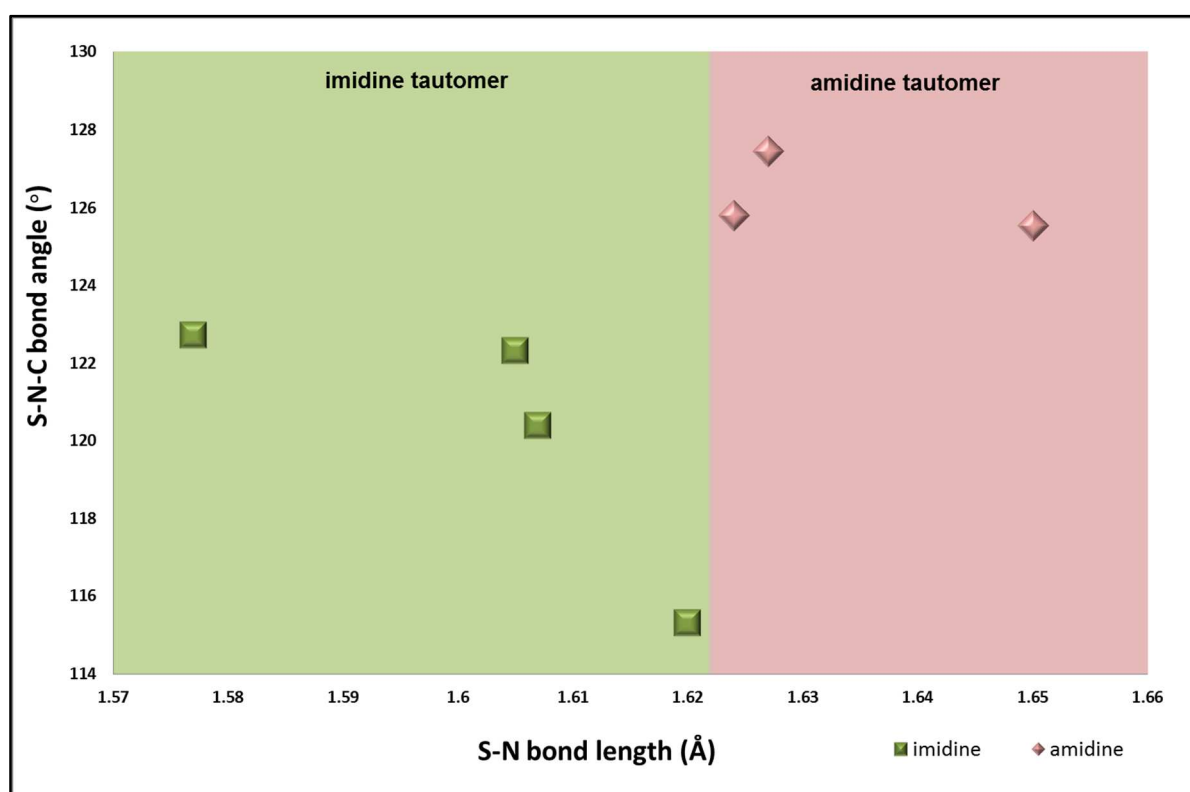
Figure 4.6 Plot of S–N bond length vs. SNC angle for the seven new solid forms.

4.4 Confirmation of cocrystal or salt formation from FTIR data

FTIR is a reliable technique to investigate the interactions occurring between the API and coformer; especially when a carboxylic acid is used as a coformer. The salts and cocrystals were screened using FTIR Spectroscopy. A clear distinction, in the spectra can be made between a carboxylate anion and a neutral carboxylic acid moiety. Typically, a strong C=O stretching band around 1700 cm^{-1} and a weaker C-O stretch around 1200 cm^{-1} indicates the presence of a neutral carboxylic group.[14] On the other hand, when an acidic proton is transferred to a base, a carboxylate, COO$^-$ is formed. Thus, hydrogen bonding of the C=O is known to lengthen the bond and lowers the stretching force constant resulting in lower absorption frequency.[15]

Schultheiss and Newman[16] suggested that the state of the carboxylic moiety (neutral or ionic) can also be confirmed by measuring the C-O and C=O bond distances from the single crystal data. Characteristically, a C=O bond length is about 1.2 Å, with the C-O bond distance at about 1.3 Å; if deprotonation has occurred, the resonance stabilised C-O bond distance will still be very similar. Therefore, to determine unequivocally if a cocrystal or salt forms requires mutually FTIR data and single crystal data.

The significant functional groups, identified by the FTIR spectra, are presented for each API and coformer in (Appendix D) Table D1 and all the FTIR spectra for the new solid forms are presented in Appendix D (Figure D1- D7). Of the seven complexes, three formed cocrystals and four formed salts and the important peak data is listed in Table 4.4.

Table 4.4 Results of IR screening.

Compound	C=O (cm^{-1})	C-O (cm^{-1})	COO$^-$ (cm^{-1})	Outcome
SFP·3NBA	1669	1274	n/a	cocrystal
[SFP$^+$][4NBA$^-$]	n/a	n/a	1681	salt
SFP·5BSA	1672	1274	n/a	cocrystal
[SFP$^+$][DBSA$^-$]	n/a	n/a	1680	salt
[SFP$^+$][DNSA$^-$]	n/a	n/a	1667	salt
[SFD$^+$][DNSA$^-$]	n/a	n/a	1672	salt
The SFP·4DMAP cocrystal generates a peak at 3411cm^{-1} indicative of the N-H··· N (heterocyclic) hydrogen bond.				

In cocrystal formation; the C=O stretching frequency band was observed at 1669 cm^{-1} and 1672 cm^{-1} for SFP·3NBA and SFP·5BSA, while the C-O stretching frequencies appeared at 1274 cm^{-1} for both cocrystals. In addition, the bond lengths of C=O and C-O are distinctly different, indicative of neutral C=O and C-O bonds. These bond lengths are consistent with the assignment from the FTIR and verify that the acidic proton has not been transferred to SFP. In contrast to SFP·3NBA and SFP·5BSA, the SFP·4DMAP cocrystal utilizes a base coformer so no proton transfer is expected. The spectrum generates a peak at 3411cm^{-1} indicative of the N-H··· N (heterocyclic) hydrogen bond.

In salt formation, the carbonyl peak is converted into a carboxylate moiety (-COO$^-$). For the salts [SFP$^+$][4NBA$^-$] and [SFP$^+$][DBSA$^-$] proton transfer was to the amidine/imidine N-atom, and similar asymmetric COO$^-$ stretching frequency bands were observed at 1681 cm^{-1} and 1680 cm^{-1} respectively. Furthermore, the bond lengths between C(20)-O(19) and C(20)-O(18) are almost equal suggestive of the carboxylate moiety. These bond lengths emphasize that the acidic proton was transferred to SFP.

Unlike in the [SFP$^+$][4NBA$^-$] and [SFP$^+$][DBSA$^-$] where proton transfer was to the amidine/imidine N-atom, in [SFP$^+$][DNSA$^-$] and [SFD$^+$][DNSA$^-$], the amine (-NH$_2$) group was protonated. The asymmetric COO$^-$ stretching frequency bands were observed at 1667 cm^{-1} and 1672 cm^{-1} respectively.

While the peaks at 1667 cm^{-1} and 1672 cm^{-1} were assigned as the asymmetric (COO$^-$) stretching frequency bands, the bond length for C(20)-O(19) and C(20)-O(18) are distinctly different suggesting the presence of neutral acid C=O and C-O bands (where d C=O≈1.2Å, d C-O≈1.3Å). However, protonation was confirmed by the absence of characteristic asymmetric -NH$_2$ and symmetric -NH$_2$ peaks of SFP, which is typical behaviour in sulfa drugs when this amine group is protonated. In conclusion, the FTIR data was successful in confirming salt and cocrystal formation in this study.

4.5   References

1. Suresh, K.; Minkov, V. S.; Namila, K. K.; Derevyannikova, E.; Losev, E.; Nangia, A.; Boldyreva, E. V., Novel Synthons in Sulfamethizole Cocrystals: Structure–Property Relations and Solubility. *Crystal Growth & Design* **2015,** *15* (7), 3498-3510.
2. Pratt, J.; Hutchinson, J.; Klein Stevens, C. L., Sulfapyridine (polymorph III), sulfapyridine dioxane solvate, sulfapyridine tetra-hydro-furan solvate and sulfapyri-dine piperi-dine solvate, all at 173 K. *Acta Crystallographica Section C: Crystal Structure Communications* **2011,** *67* (Pt 12), o487-o491.
3. Ghose, S.; Dattagupta, J. K., Struture of sulfisomidine dihydrochloride dihydrate. *Acta Crystallographica Section C* **1986,** *42* (11), 1563-1566.
4. Smith, G.; Wermuth, U. D., Proton-transfer compounds with 4-amino-N-(4,6-dimethylpyrimidin-2-yl)benzenesulfonamide (sulfamethazine): the structures and hydrogen bonding in the salts with 5-nitrosalicylic acid and picric acid. *Acta Crystallographica Section C* **2013,** *69* (5), 538-543.
5. Subashini, A.; Muthiah, P. T.; Bocelli, G.; Cantoni, A., Hydrogen-bonding patterns in 4-[(5-methylisoxazol-3-yl)aminosulfonyl]anilinium chloride. *Acta Crystallographica Section E* **2007,** *63* (11), o4312-o4313.
6. Malathy, S.; Nirmalram, J. S.; Muthiah, P. T., Crystal structure of 4-[(5-methylisoxazol-3-yl)aminosulfonyl]anilinium 3,5-dinitrosalicylate. *Acta Crystallographica Section E* **2015,** *71* (6), 618-620.
7. Smith, G.; Wermuth, U. D., 2-(4-Aminobenzenesulfonamido)-4,6-dimethylpyrimidin-1-ium 2-carboxy-4,6-dinitrophenolate. *Acta Crystallographica Section E* **2013,** *69* (4), o472.
8. Coles, S. J.; Hursthouse, M. B.; Mayer, T. A.; Threlfall, T. L., 4-Amino-N-Pyridin-2-yl-benzenesulfonamide with Formic acid butyl ester. 2000.
9. Threlfall, T. L.; Coles, S. J.; Hursthouse, M. B.; Mayer, T. A., 4-Amino-N-(1H-pyridin-2-ylidene)-benzenesulfonamide and tetrahydro-furan solvate. 2000.
10. Lu, E.; Rodriguez-Hornedo, N.; Suryanarayanan, R., A rapid thermal method for cocrystal screening. *CrystEngComm* **2008,** *10* (6), 665-668.
11. Fu, X.; Li, J.; Wang, L.; Wu, B.; Xu, X.; Deng, Z.; Zhang, H., Pharmaceutical crystalline complexes of sulfamethazine with saccharin: same interaction site but different ionization states. *RSC Advances* **2016,** *6* (31), 26474-26478.
12. Ghorab, M. M.; Al-Said, M. S.; Ghabbour, H. A.; Chantrapromma, S.; Fun, H.-K., (E)-4-Amino-N-(1,2-dihydropyridin-2-ylidene)benzenesulfonamide   nitromethane   monosolvate. *Acta Crystallographica Section E* **2012,** *68* (4), o1030.
13. Buist, A. R.; Dennany, L.; Kennedy, A. R.; Manzie, C.; McPhie, K.; Walker, B., Eight salt forms of sulfadiazine. *Acta Crystallographica Section C* **2014,** *70* (9), 900-907.
14. Aakeröy, C. B.; Grommet, A. B.; Desper, J., Co-Crystal Screening of Diclofenac. *Pharmaceutics* **2011,** *3* (3), 601-614.
15. Pavia, D. L.; Lampman, G. M.; Kriz, G. S.; Vyvyan, J. A., *Introduction to Spectroscopy*. Cengage Learning: 2008.
16. Schultheiss, N.; Newman, A., Pharmaceutical Cocrystals and Their Physicochemical Properties. *Crystal Growth & Design* **2009,** *9* (6), 2950-2967.

Chapter 5

Summary and Conclusion

In this contribution, four salts and three cocrystals of sulfapyridine (SFP) and sulfadiazine (SFD) were synthesized with an amine and aromatic carboxylic acid coformers. The effect of substituent position on the coformer on crystal packing and hydrogen bonding was investigated by utilising 3-nitrobenzoic acid (3NBA) and 4-nitrobenzoic acid (4NBA). Next, the effect of the number of substituent/s groups was investigated by using 5-bromosalicylic acid (5BSA) and 3,5-dibromosalicylic acid (DBSA) as coformers. Thirdly, the influence of small structural changes on the crystal structure was studied by cocrystalizing structurally similar compounds (SFP and SFD) with the same coformer (3,5-dinitrosalicylic acid, DNSA). Moreover, the effect of acidity of the coformer was explored by cocrystallizing SFP with 4-dimethylaminopyridine (4DMAP). We also performed conformational analysis and investigated how the interconversion of tautomers promotes crystal formation by conforming to the geometric demands of the different coformers.

When the position of the nitro-substituent on the coformer was changed from the meta-(3NBA) position to para-position (4NBA), a cocrystal and a salt were produced respectively. The two structures, SFP·3NBA and [SFP$^+$][4NBA$^-$], have very similar crystal packing, and also have the same main intermolecular interaction sites; although the locations of the acidic protons are different. Intermolecular interaction analysis of the asymmetric units with CrystalExplorer also showed that the % interaction contributions are similar for both complexes. It was concluded, that the nitro-substituent did not participate in the intermolecular bonding, however it imparted steric factors to the crystal structures.

The addition of a second bulky bromo substituent to the [SFP$^+$][DBSA$^-$] system resulted in the formation of different crystal packing and hydrogen bonding, compared to what was found in the SFP·5BSA cocrystal. While in SFP·5BSA a sandwich-like assembly was observed, the [SFP$^+$][DBSA$^-$] structure displayed a different pattern altogether, which resembled a staircase style. Halogen interactions (Br⋯O) were present in both structures, however they are more distinct in SFP·5BSA than in [SFP$^+$][DBSA$^-$]. The Hirshfeld surface analysis indicates that these interactions are stronger in SFP·5BSA, despite having a lower percentage contribution, than in [SFP$^+$][DBSA$^-$].

To investigate the influence of small structural changes on the API, [SFP⁺][DNSA⁻] and [SFD⁺][DNSA⁻] were formed. SFD is a sulfonamide, and it has a pyrimidine ring instead of a pyridine. It was observed that although the APIs are slightly different, the crystal structures obtained hardly differ at all. It is clear from the packing similarity analysis that the packing arrangement and nature of the intermolecular interactions are identical, i.e. the crystals are isostructural and the slight structural difference between the SFP and SFD does not alter the hydrogen bond patterns or the crystal packing.

The effect of possible change in the acidity of the coformer was analyzed by employing a pyridine derivative, 4-dimethylaminopyridine (4DMAP) as a coformer. The crystal structure adopted similar crystal packing to crystals formed with acid coformers, such as SFP·3NBA and [SFP⁺][4NBA⁻]. The identification of the hydrogen bond donor site on the two SPF tautomers is obvious, i.e. NH amidine and NH pyridinium. The ΔpK_a prediction suggested the formation of a cocrystal and the experimental result supported this by observing the cocrystal of the imidine tautomeric form.

In bulk property analysis the DSC of SFP·3NBA and [SFP⁺][4NBA⁻], showed huge difference in the physicochemical properties, i.e. the melting points are 155.9 °C and 196.7 °C respectively. This was attributed to the nature of the observed hydrogen bonds. SFP·3NBA is a cocrystal, while in [SFP⁺][4NBA⁻] the interactions are much stronger because of the charge assisted hydrogen bonds. NMR study was used to investigate if the salts synthesised herein: [SFP⁺][4NBA⁻], [SFP⁺][DBSA⁻], [SFP⁺][DNSA⁻] and [SFD⁺][DNSA⁻] exist as ions in solution. From the signal allocation, it was observed that all salts, except [SFP⁺][4NBA⁻], exist as charged species in solution. This was confirmed by a broad peak at 12.25 ppm chemical shift indicative of the acidic proton, which means that the SFP and 4NBA exist as neutral molecules in solution. Also, the FTIR data was successful in confirming salt or cocrystal formation in our study. This was achieved by careful analysis of the C=O stretching band and C-O stretch, and it was confirmed by measuring the C-O and C=O bond distances from the single crystal data.

The aim of the synthon competition study was to investigate how introduction of coformers with competing hydrogen bond acceptor and donor sites can possibly disrupt the preferred dimer formation between the sulfonamides. The $NH_2 \cdots O$ (sulfoxide) hydrogen bond was found to be the most resilient synthon as it was preserved in all structures, except SFP·5BSA. The imidine/amidine homodimers were disrupted in SFP·3NBA, [SFP$^+$][4NBA$^-$] and [SFP$^+$][DBSA$^-$], but were maintained in structures of SFP·5BSA, [SFP$^+$][DNSA$^-$] and [SFD$^+$][DNSA$^-$]. Although the dimers were preserved in the latter structures, it was observed that multiple synthons were also formed in the structures together with the dimers. It was concluded that cocrystallisation with carefully selected coformers the dimer formation can be disrupted.

By studying the tautomerism for the newly synthesized solid forms, as well as existing selected sulfa drug complexes in the CSD, we were able to determine the range of bond lengths in which the amidine and imidine tautomeric forms exist. The S-N and C12-N11 bond lengths for amidine and imidine tautomeric forms do not overlap. All imidine and amidine complexes, from both this work and the literature clearly lie in the distinct imidine and amidine regions.

The geometric parameters S-N bond length and SNC bond angles were investigated to see whether they can serve to identify the new solid forms as either an amidine or imidine tautomer. A plot of the S-N bond length against SNC angle shows that the different tautomers fall into two distinct regions. From these results, it was concluded that the measurements of the SNC bond angles and S-N bond lengths can also aid in classifying the tautomeric forms obtained in the different multicomponent crystals.

Finally, the values of the torsion angles of the sulfapyridine and sulfadiazine molecules suggest that all API molecules in the multicomponent crystals adopt similar conformation, which was also proven by the molecular overlay of SFP and SFD molecules of all seven structures.

Appendices

Appendix A

	SFP·3NBA	[SFP+][4NBA-]	SFP·4DMAP	[SFP+][DNSA-]	[SFD+][DNSA-]
FULL					
O···H	30.5 %	33.1 %	15 %	40.3 %	43.3 %
H···H	29.9 %	28.5 %	47.5 %	18.4 %	15.0 %
C···H	19.8 %	19.9 %	25.4 %	10.9 %	10.9 %
N···H	2.7 %	3.1 %	8.0 %	5.5 %	6.8 %
C···C	4.4 %	4.2 %	2.8 %	6.8 %	5.4 %
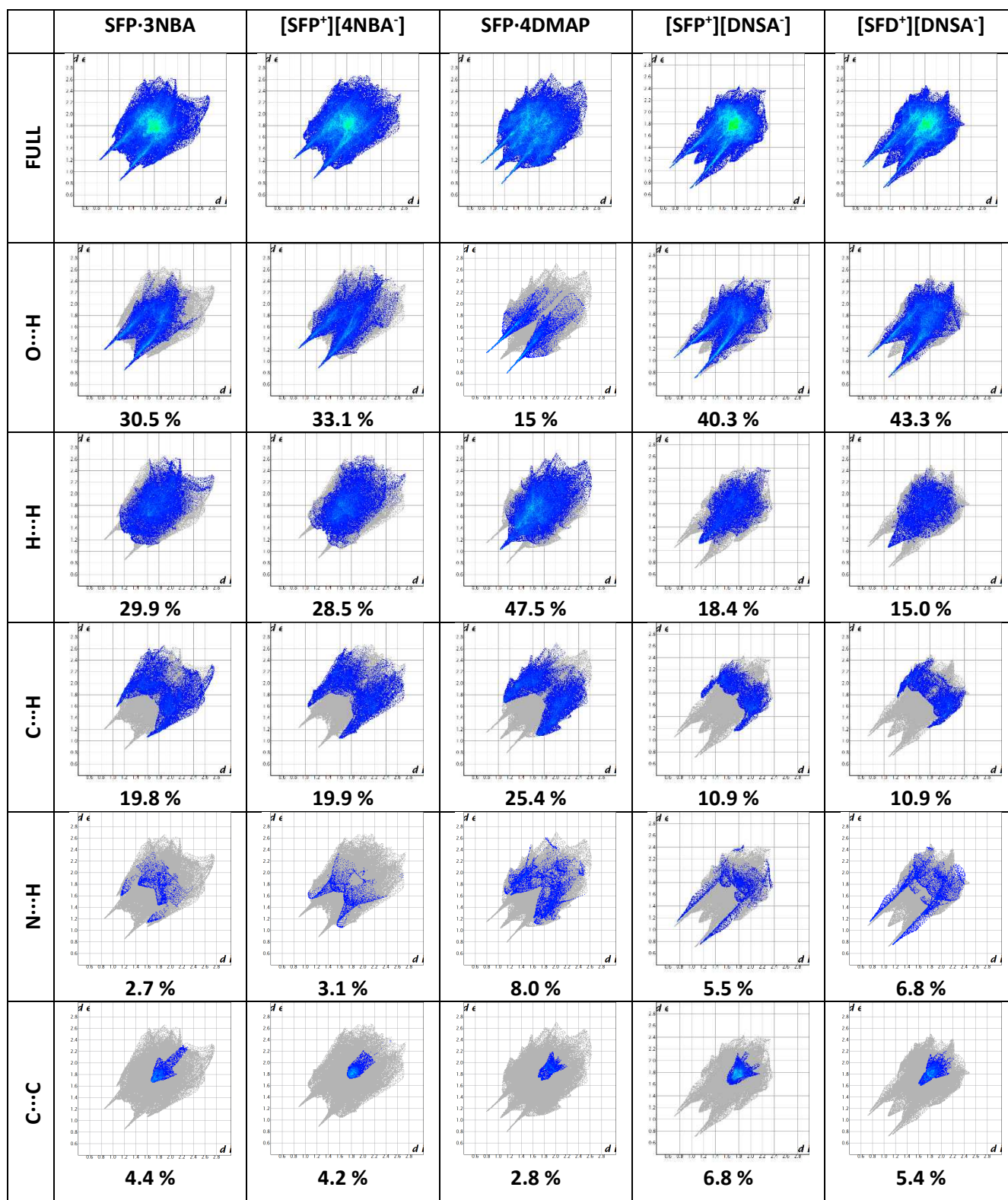
Figure A.1 Hirshfeld fingerprint plots for our newly synthesized forms.

	SFP·5BSA	[SFP⁺][DBSA⁻] A	[SFP⁺][DBSA⁻] B
FULL			
O···H	25.5 %	21.4 %	18.1 %
H···H	23.4 %	2.8 %	6.8 %
C···H	14.1 %	20.2 %	15.9 %
N···H	3.8 %	0.8 %	0.2 %
C···C	5.1 %	4.9 %	5.5 %
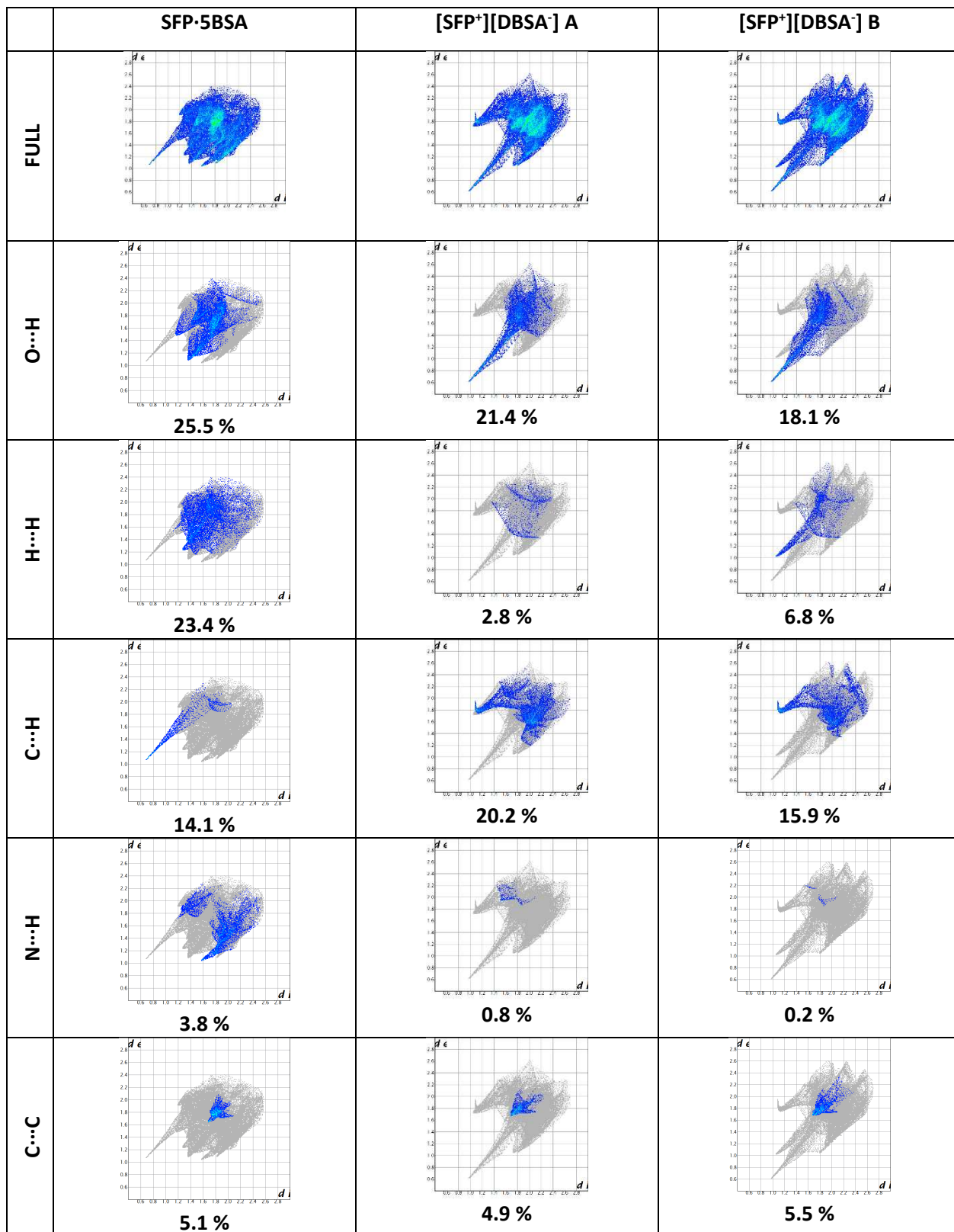
Figure A.2 Hirshfeld fingerpint plots fora our newly synthesized forms (part 1).

Figure A.2 continued.

	SFP·5BSA	[SFP⁺][DBSA⁻] A	[SFP⁺][DBSA⁻] B
O···Br	2.3 %	7.5 %	8.3 %
H···Br	19.2 %	26.1 %	23.7 %
C···Br	0.0 %	9.1 %	10.8 %
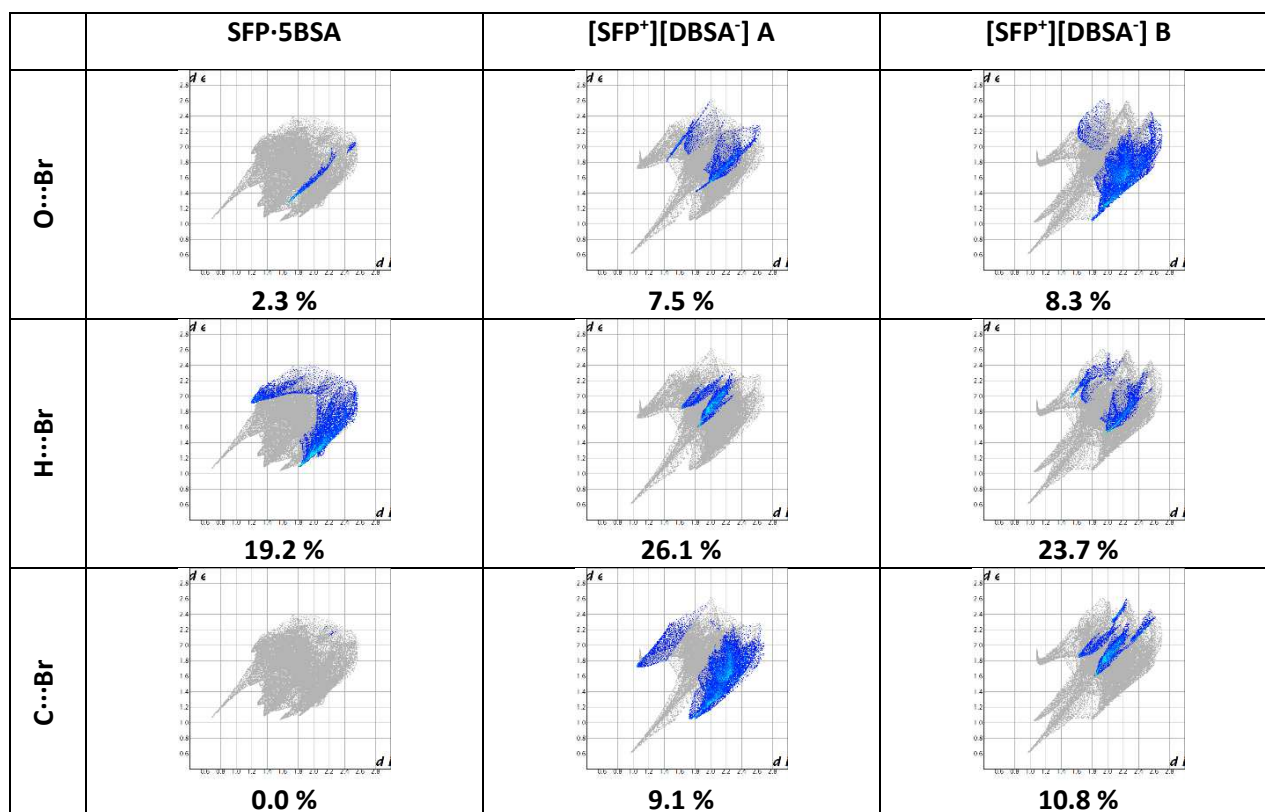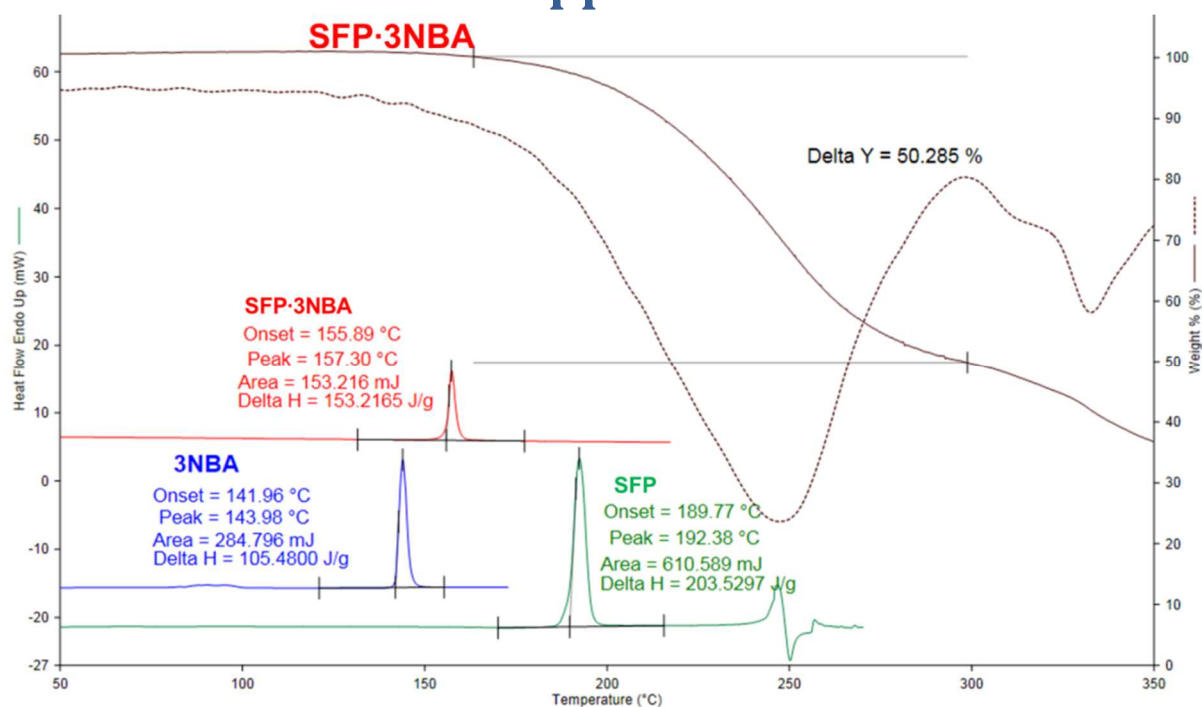
Appendix B

Figure B.1 DSC curve of SFP·3NBA.
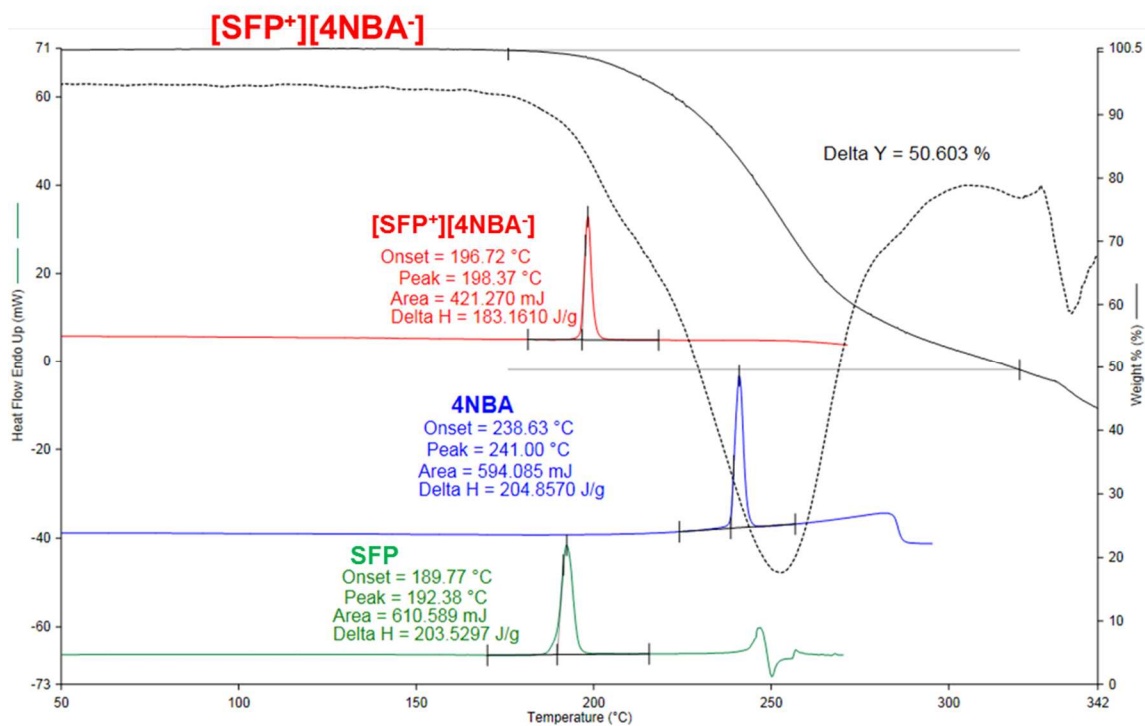
Figure B.2 DSC curve of [SFP+][4NBA-].
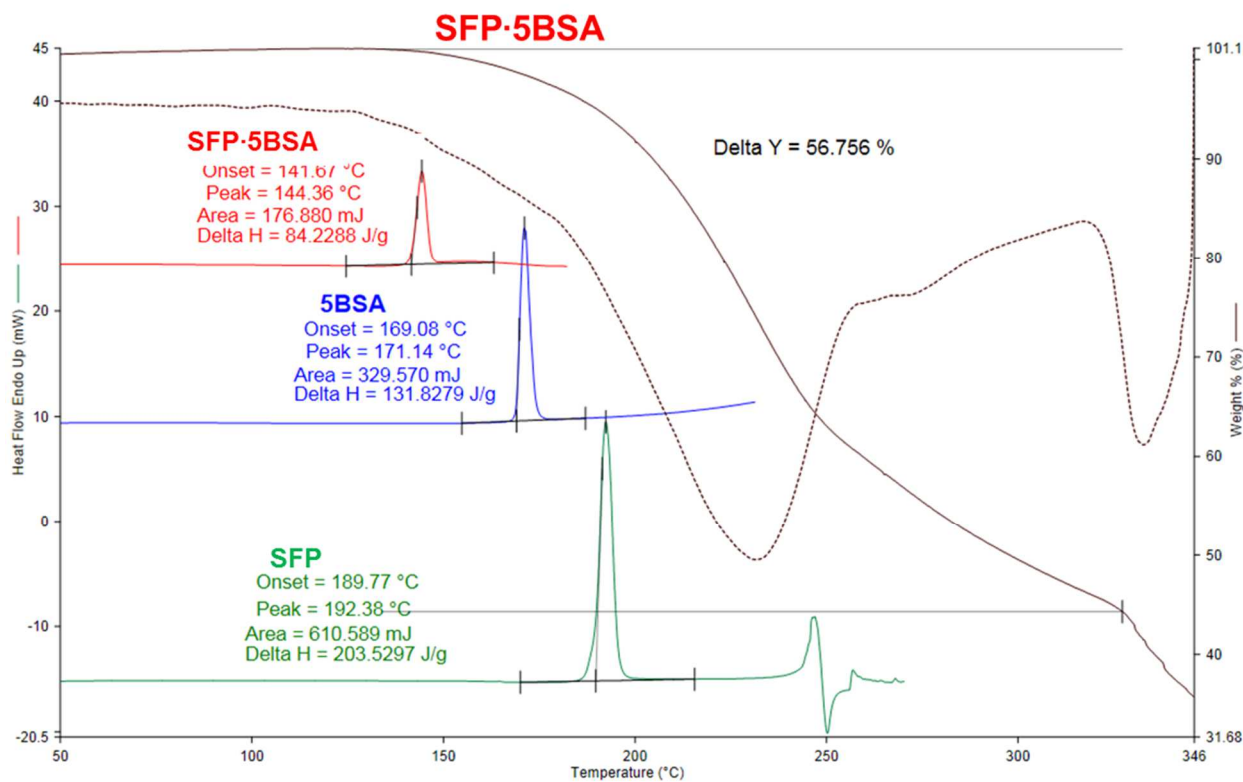
Figure B.3 DSC curve of SFP·5BSA.
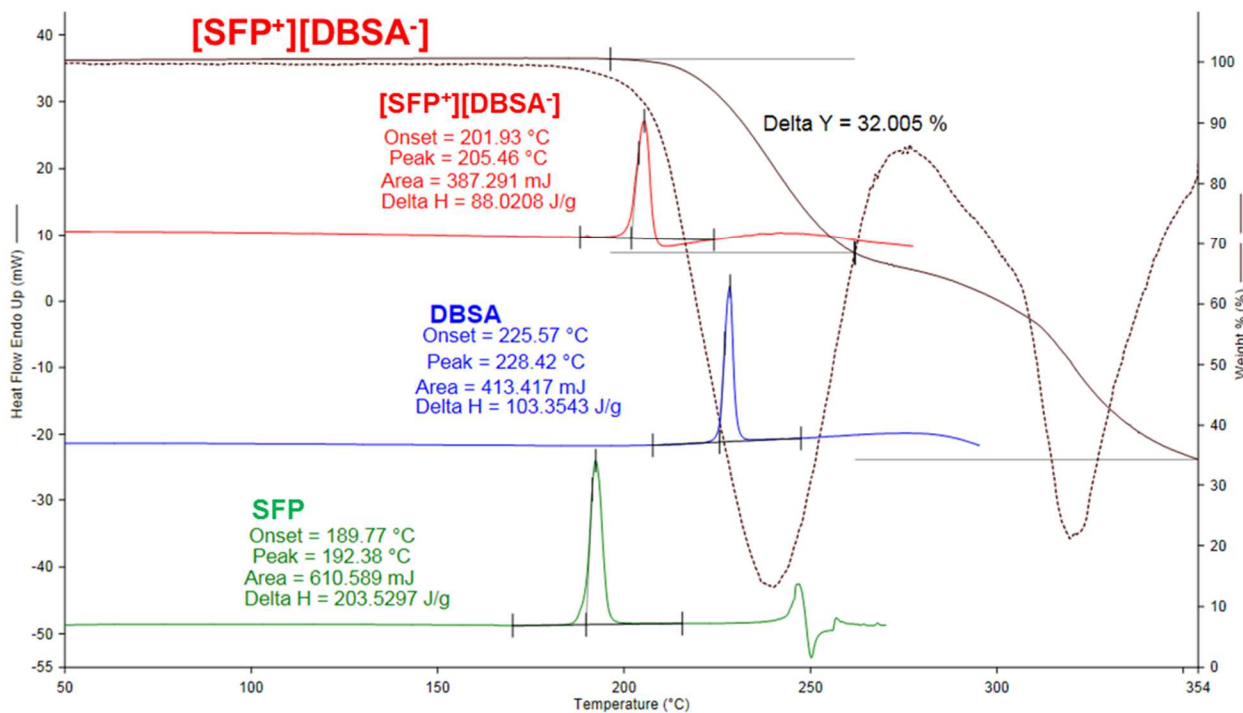
Figure B.4 DSC curve of [SFP⁺][DBSA⁻].
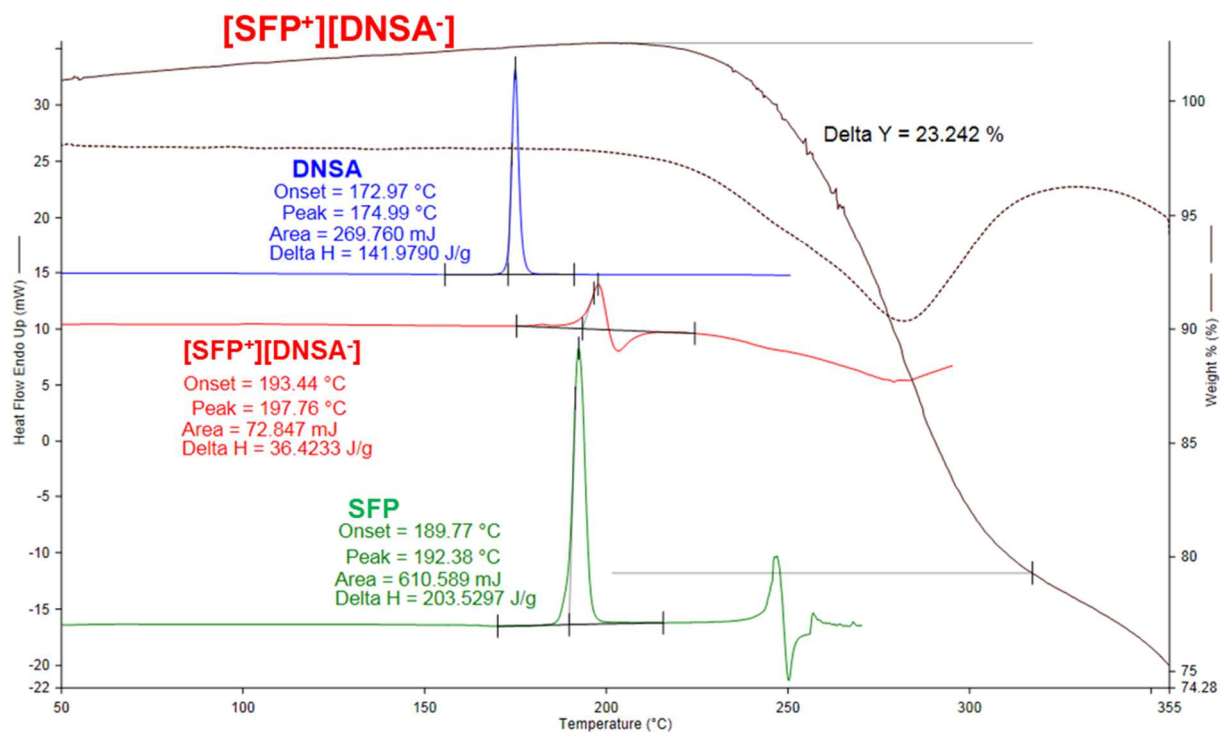
Figure B.5 DSC curve of [SFP+][DNSA-].
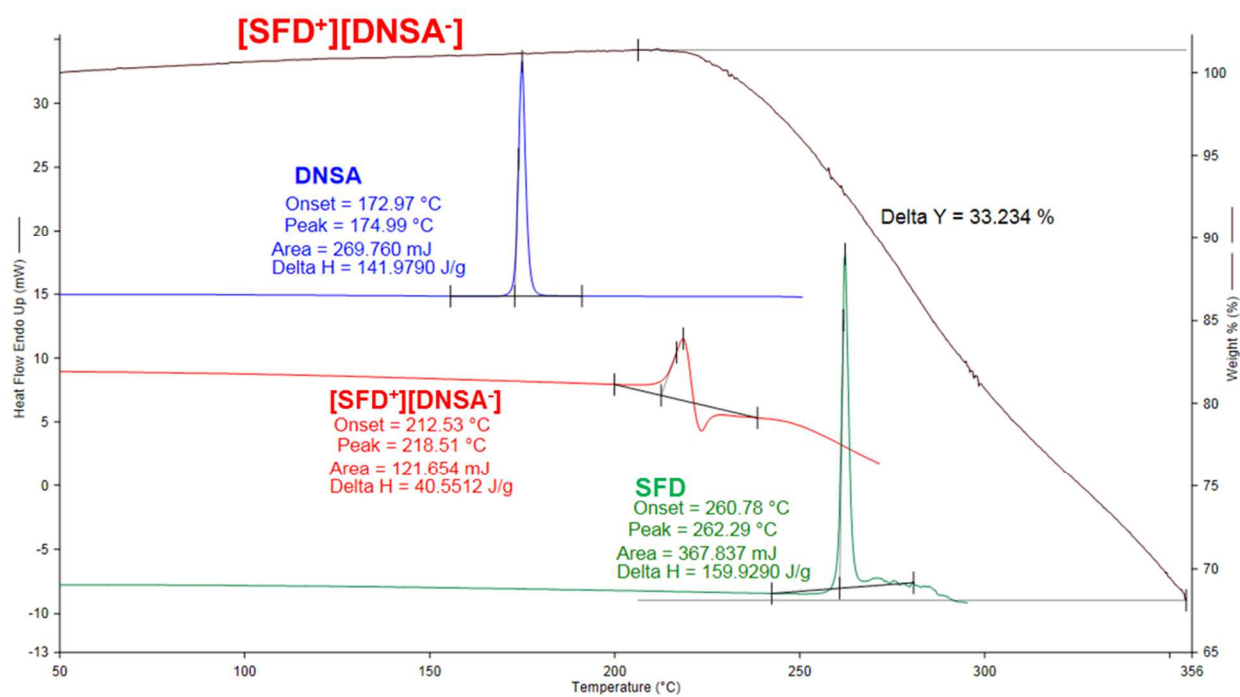
Figure B.6 DSC curve of [SFD+][DNSA-].
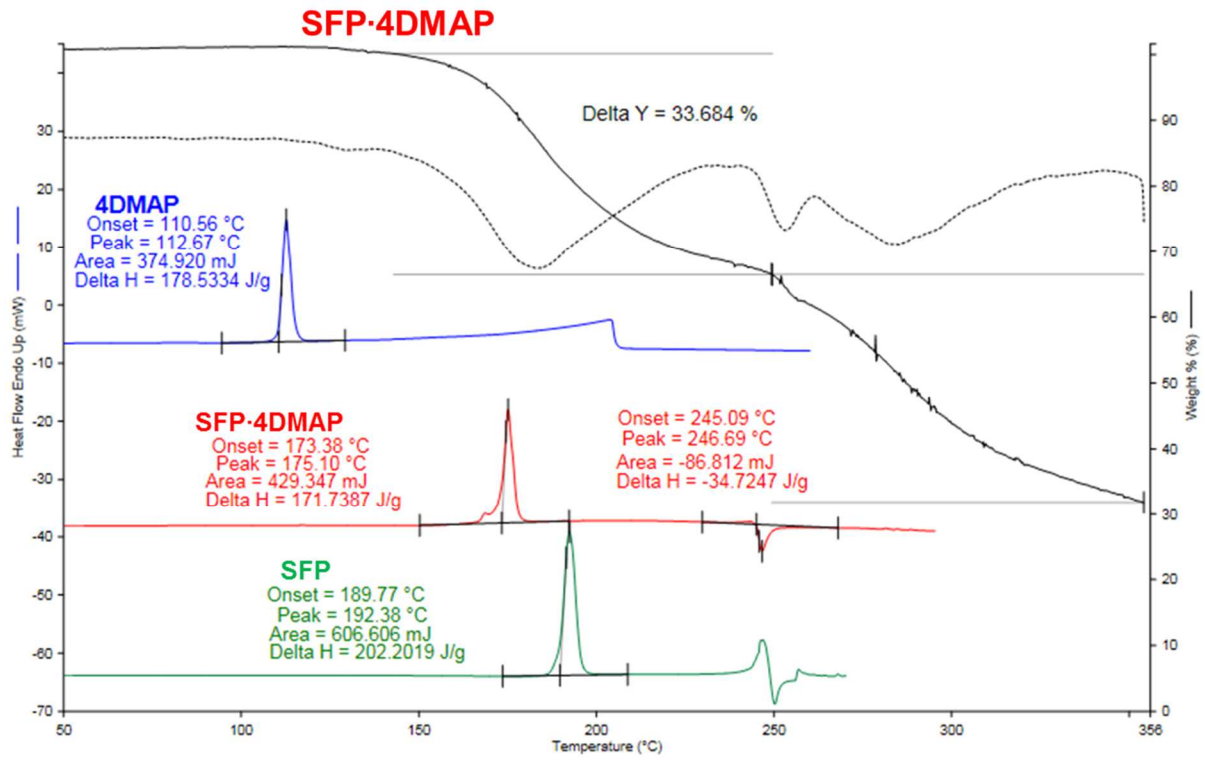
Figure B.7 DSC curve of SFP·4DMAP.

Appendix C
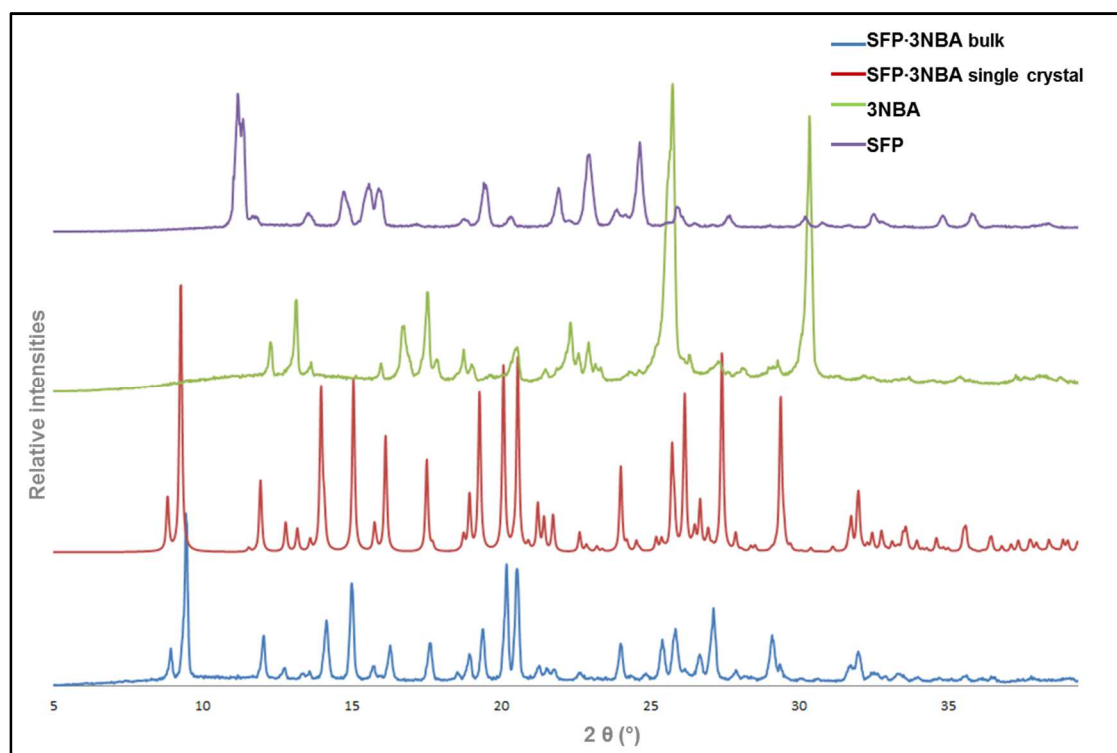
Figure C.1 Powder X-ray pattern of SFP·3NBA.
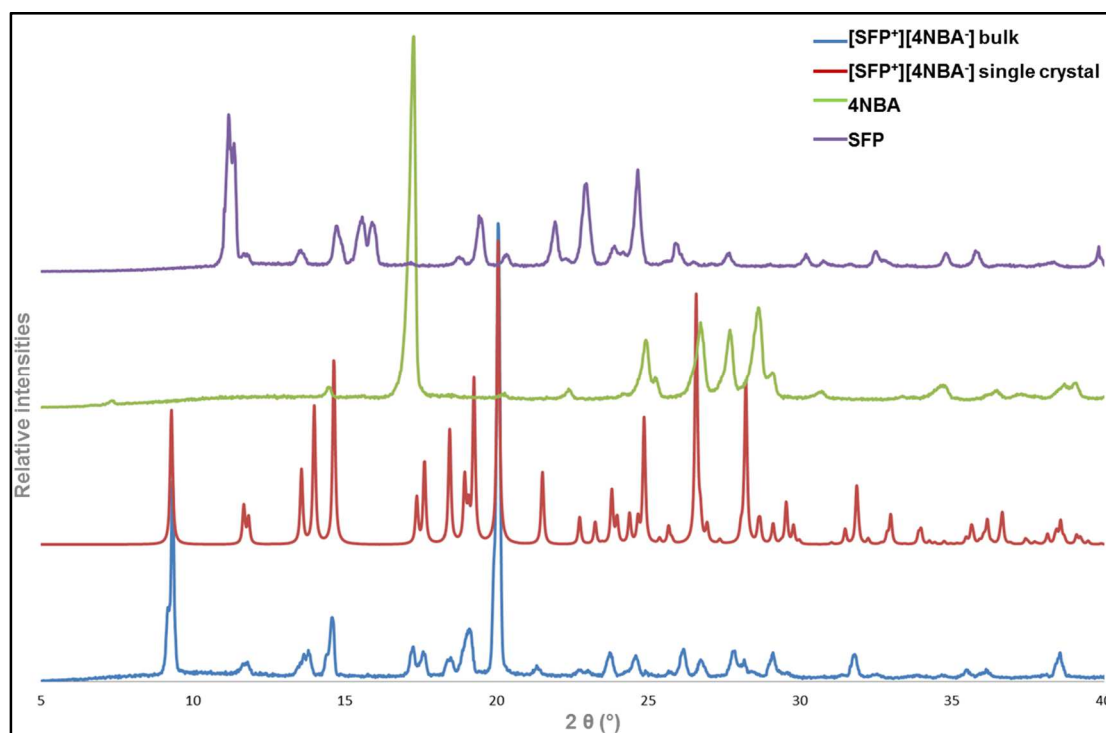
Figure C.2 Powder X-ray pattern of [SFP⁺][4NBA⁻].
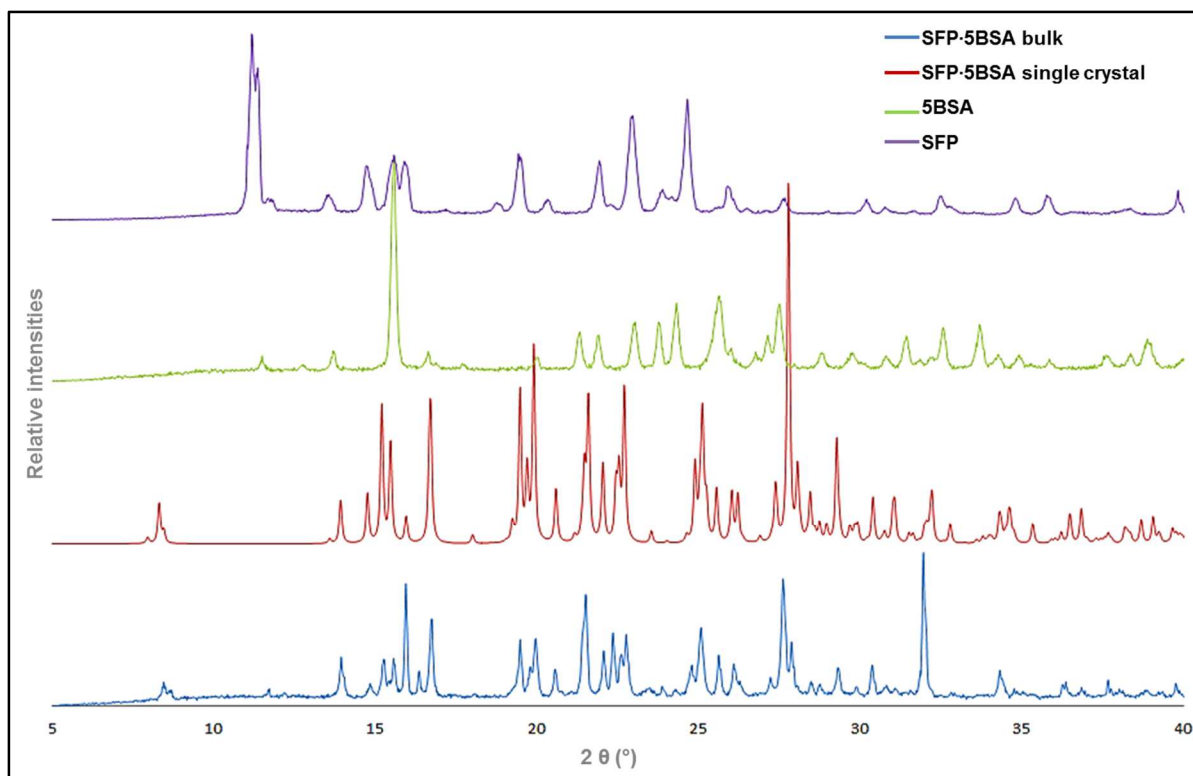
Figure C.3 Powder X-ray diffraction pattern of SFP·5BSA.
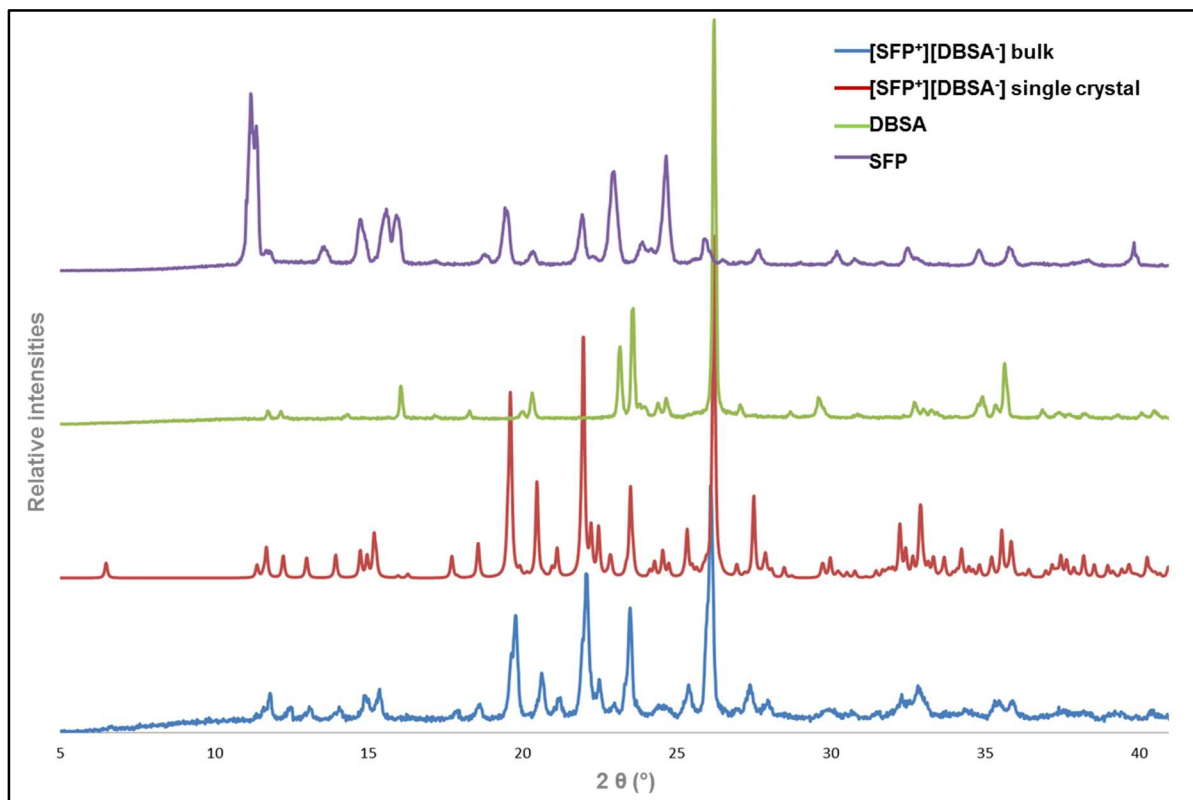
Figure C.4 Powder X-ray diffraction pattern of [SFP+][DBSA-].
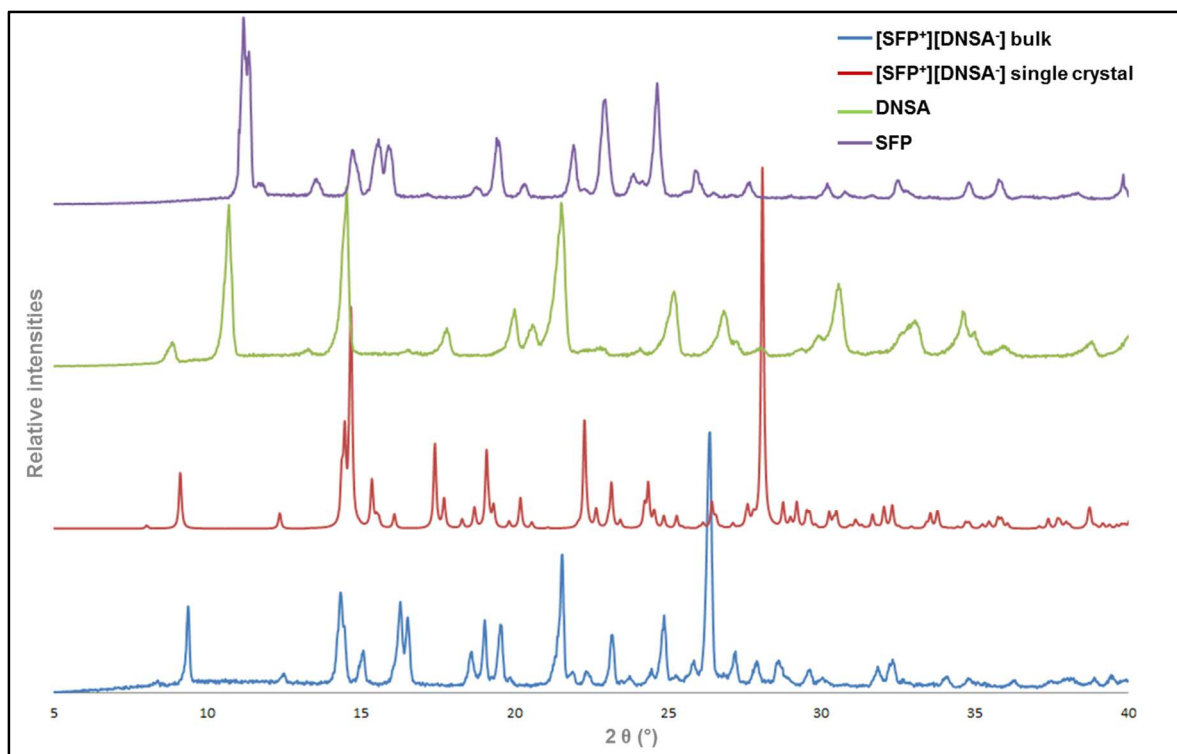
Figure C.5 Powder X-ray diffraction pattern of [SFP+][DNSA-].
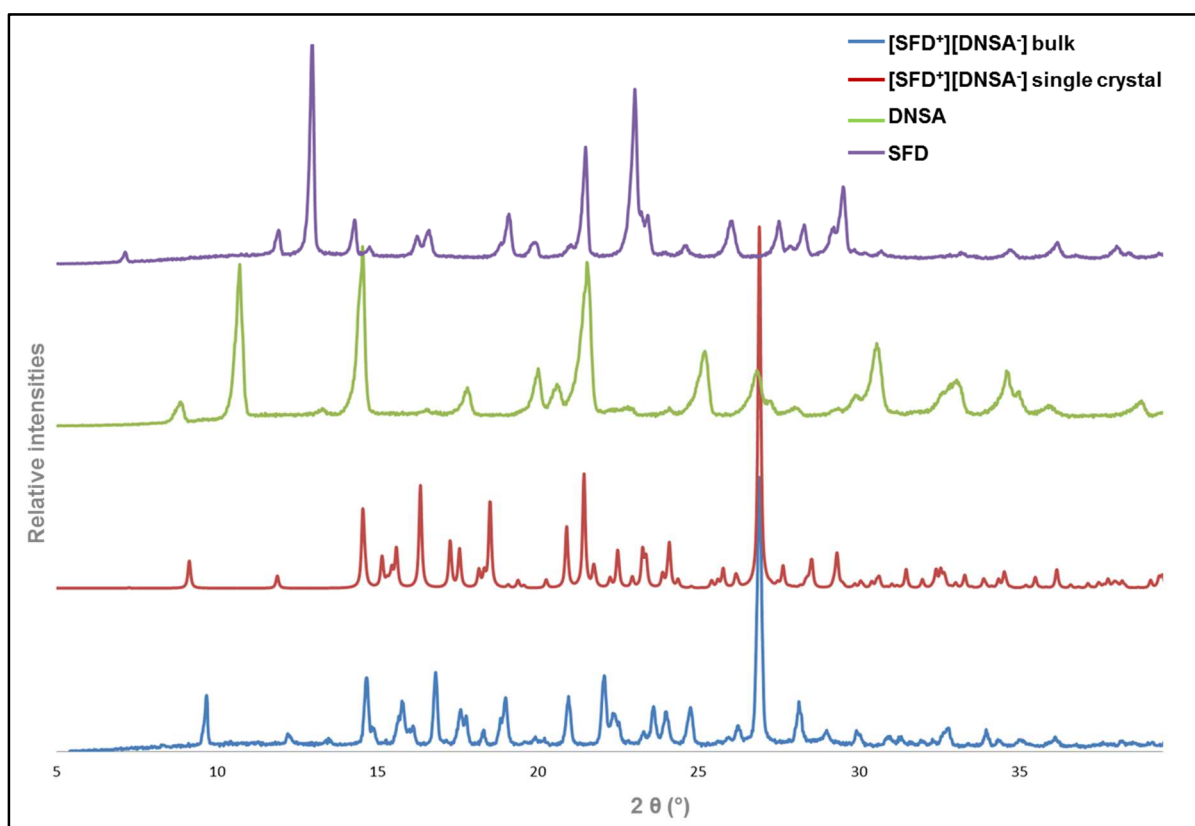
Figure C.6 Powder X-ray diffraction pattern of [SFD+][DNSA-].
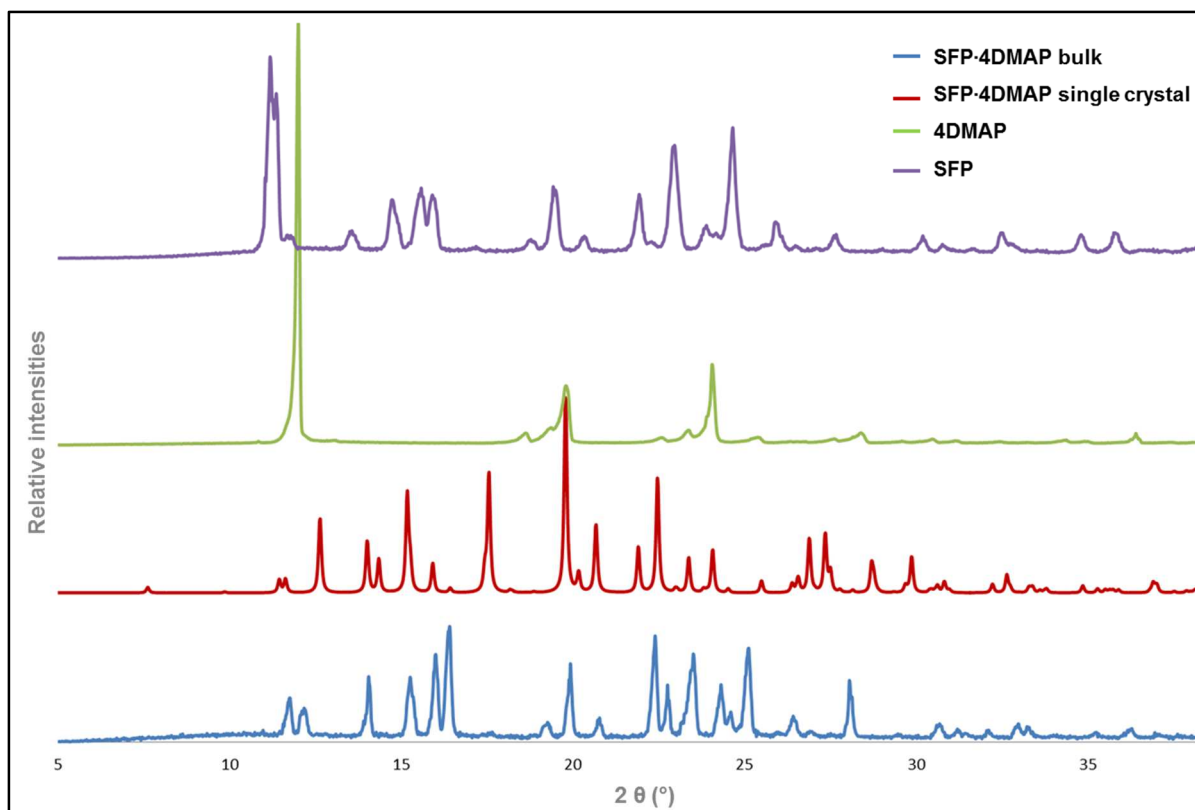
Figure C.7 Powder X-ray diffraction pattern of SFP·4DMAP.

Appendix D
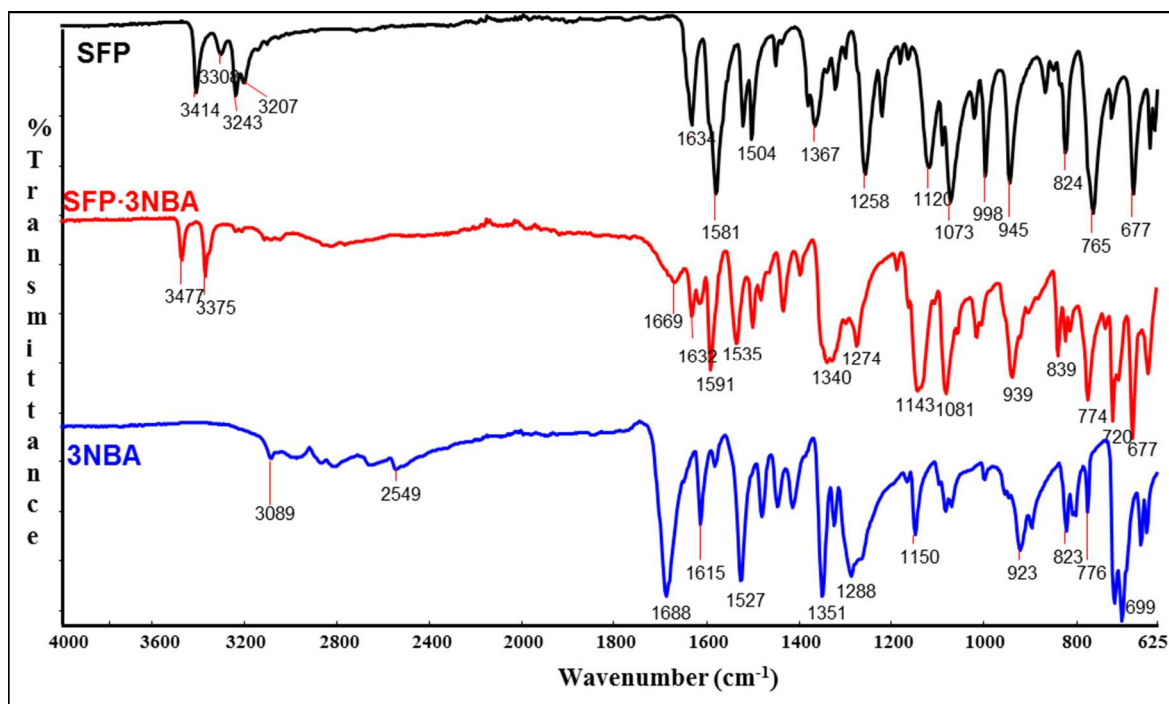
Figure D.1 FTIR spectra of SFP, SFP·3NBA and 3NBA.
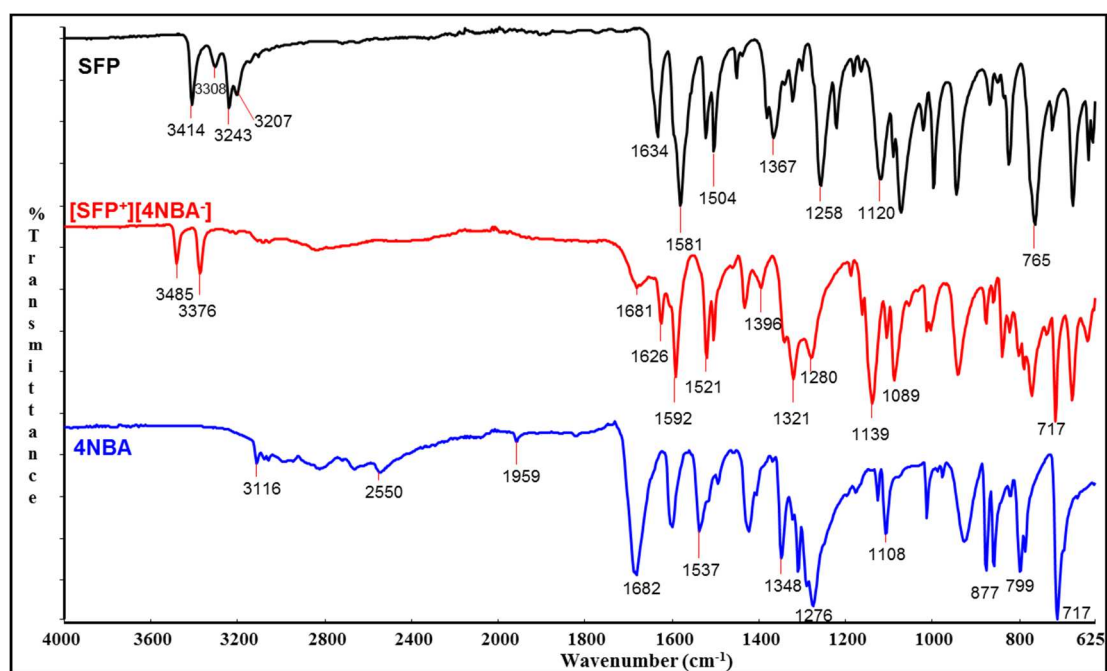
Figure D.2 FTIR spectra of [SFP+][4NBA-], SFP and 4NBA.
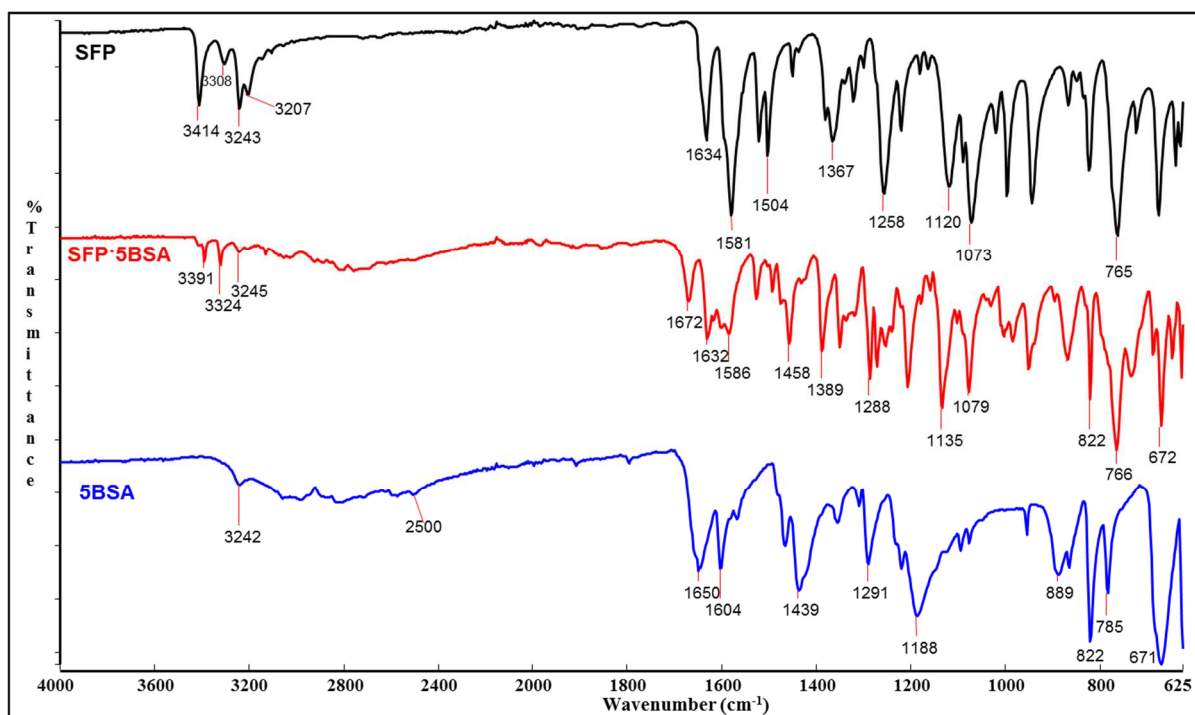
Figure D.3 FTIR spectra of SFP·5BSA, SFP and 5BSA.
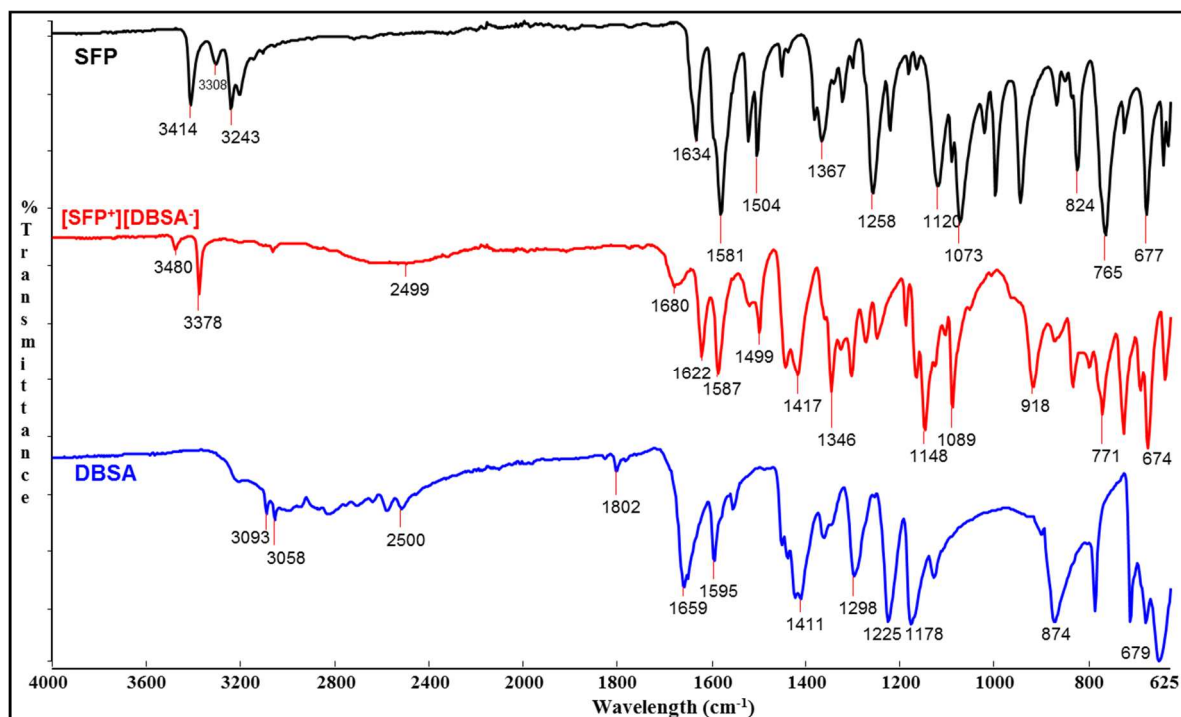
Figure D.4 FTIR spectra of [SFP+][DBSA-], SFP and DBSA.
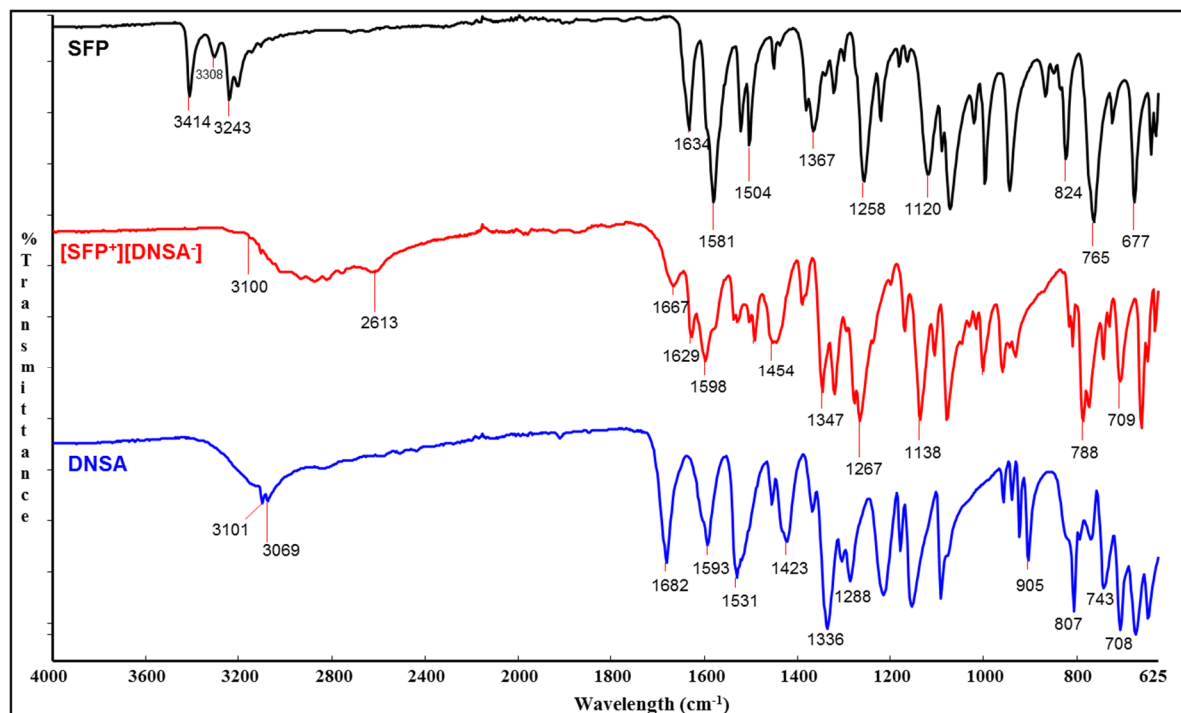
Figure D.5 FTIR spectra of [SFP⁺][DNSA⁻], SFP and DNSA.
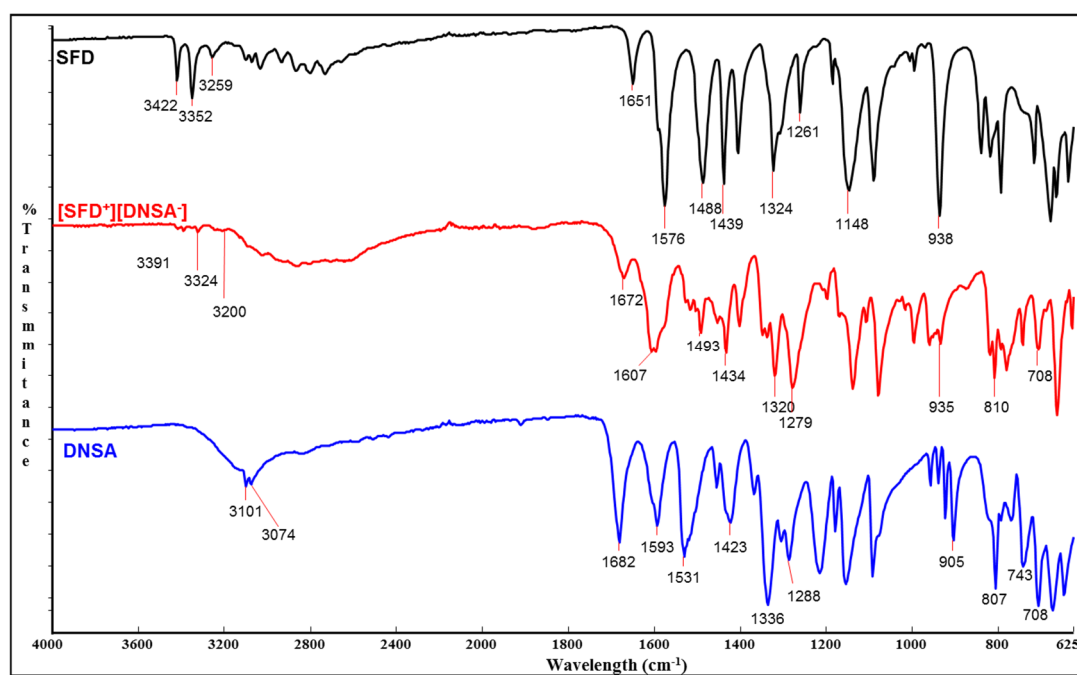
Figure D.6 FTIR spectra of [SFD⁺][DNSA⁻], SFD and DNSA.
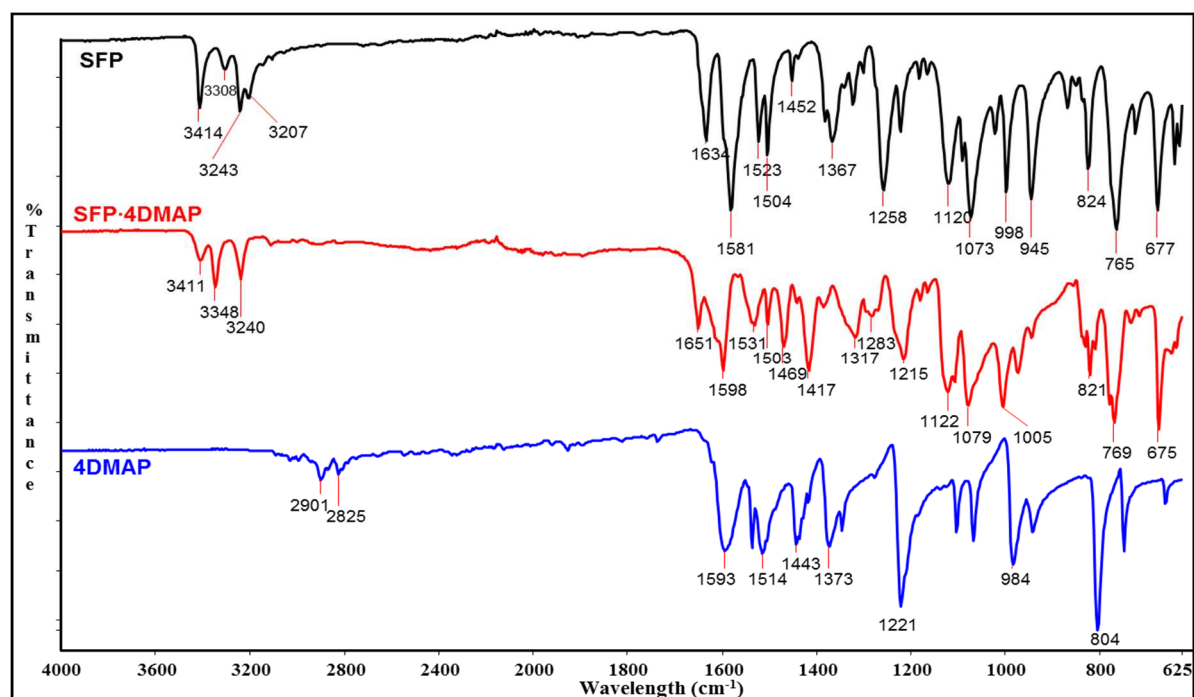
Figure D.7 FTIR spectra of SFP·4DMAP, SFP and 4DMAP.

Table D.1 FTIR absorption bands for the coformers and APIs.

Compound	Experimental frequency bands (cm⁻¹)	Standard frequency bands (cm⁻¹)	Associated functional group(s)	ref
3-nitrobenzoic acid	1688	1820-1695	ν (C=O)	[23]
	3089-2549	3400-2400	ν OH	
	1288	1320-1210	ν (C-O)	
	1150	1170-1140	ν (C-N)	
	699,776,923	880,780,690	γ (CH) meta oops	
	1527	1550-1490	$\nu_{as}NO_2$	
	1351	1355-1315	$\nu_{s}NO_2$	
	823	910-825	$\beta_{s}NO_2(\delta_{s})$	
	719	726-723	$\gamma_{as}NO_2(\omega)$	
4-nitrobenzoic acid	1682	1815-1695	ν (C=O)	[23]
	3116-2550	3400-2400	ν OH	
	1276	1320-1210	ν (C-O)	
	1108	1180-1125	ν (C-N)	
	799 (para oop)	850-800	γ (CH) meta oops	
	1959 (para sub)	2000-1950	para substitution	
	1537	1550-1490	$\nu_{as}NO_2$	
	1348	1355-1315	$\nu_{s}NO_2$	
	877	885-880	$\beta_{s}NO_2(\delta_{s})$	
	717	720-717	$\gamma_{as}NO_2(\omega)$	

Table D.1 continued.

5-bromosalicylic acid	1291 1650 3245-2500 1439 1188 671 626	1295-1205 1690-1660 3300-2500 1440-1395 1195-1185 700-670 625	ν (C-O)c ν (C=O) bonded vOH β OHh γ COc ν (C-Br) β (C-Br)	[24]
3,5-dibromosalicylic acid	1299 1178 1659 3310-2500 1411 1225 787 679	1320-1210 1260-1000 1690-1655 3300-2400 1440-1400 1420-1260 780-760 700-670	ν (C-O)c ν (C-O)h ν (C=O) bonded ν OH β OHh γ COc γ COh, γ OH ν (C-Br)	[25]
3,5-dinitrosalicylic acid	3325-2950 3101 940 1682 1336 1288 1423 1336 1531 905, 807 743, 708	3400-2400 3110-3095 940-930 1695-1670 1320-1210 1265-1250 1455-1415 1350-1315 1550-1500 790-910 760-710	bonded ν OH ν CH ν (C-N) ν (C=O) ν (C-O)c ν (C-O)h β OHh ν sNO2 ν asNO2 β NO2(δ) γ NO2(ω)	[26]
4-dimethylamino pyridine	- 1373, 1221 804 1537, 1514 1593 2901 2825 1345	3100-3015 1390-1245 920-782 1540-1470 1590-1570 2935-2860 2870-2825 1382-1266	ν CH β CH γ CH ν (C=C) ν (C=C) semi-circle stretch ν as(CH) in CH3 ν s(CH) in CH3 + N–(CH3)2 ν CN	[27]
Sulfadiazine	3422 3352 3259 1324 1148 938 1651,1576 1261	3425 3360 3200-2700 1325 1155-1140 945 1652 ,1580 1382-1266	ν asNH2 ν sNH2 ν NH ν asSO2 ν sSO2 ν (S-N) β NH2(δ as), β NH2(δ s) ν CN	[28] [29]
Sulfapyridine	3414 3308 3243, 3207 1634 1581 1367 1120 765 1258	3500 3300 3245-3200 1652 1550 1360-1310 1160-1135 775 1382-1266	ν asNH2 ν sNH2 ν NH β NH2(δ as) β NH2(δ s) ν asSO2 ν sSO2 ν (S-N) ν CN	[30] [30b]

(vs) very strong; (s) strong; (m) medium; (sh) shoulder; (br) broad; (w) weak; (vw) very weak.
(v) stretching; (v$_s$) sym. stretching; (v$_{as}$) asym. stretching;(β) in-plane bending;(γ) out-of-plane bending;(δ) scissoring; (ω) wagging;
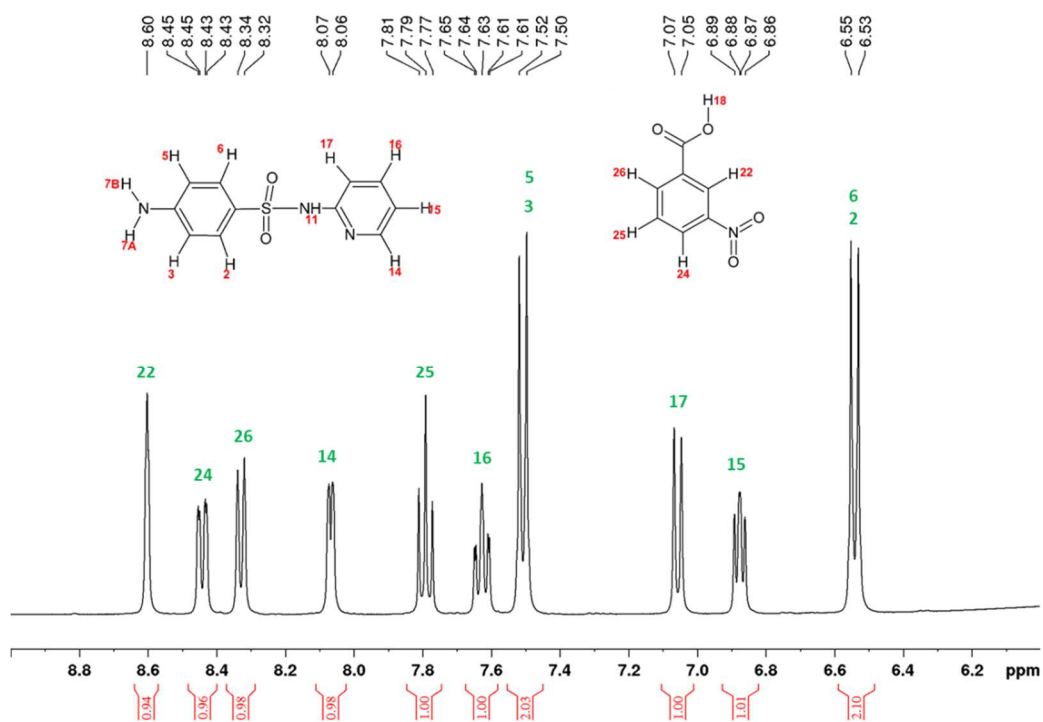
Appendix E

Figure E.1 Proton NMR spectrum (400MHz) of SFP·3NBA showing that both starting materials are present in the product. Peaks are referenced to the DMSO peak at 2.5 ppm (not shown).
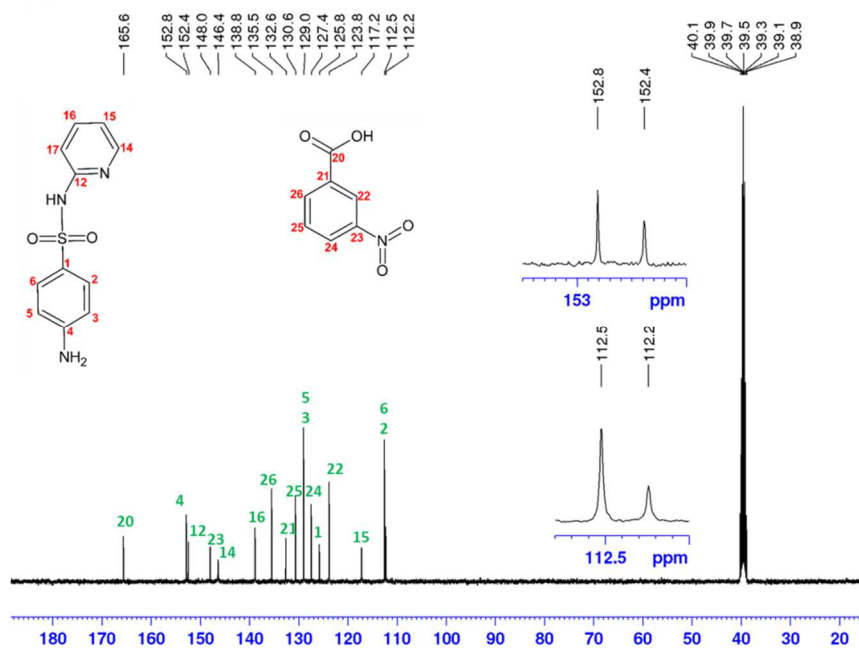

Figure E.2 Carbon NMR spectrum of SFP·3NBA showing that both starting materials are present in the product. Peaks are referenced to the DMSO peak at 40 ppm
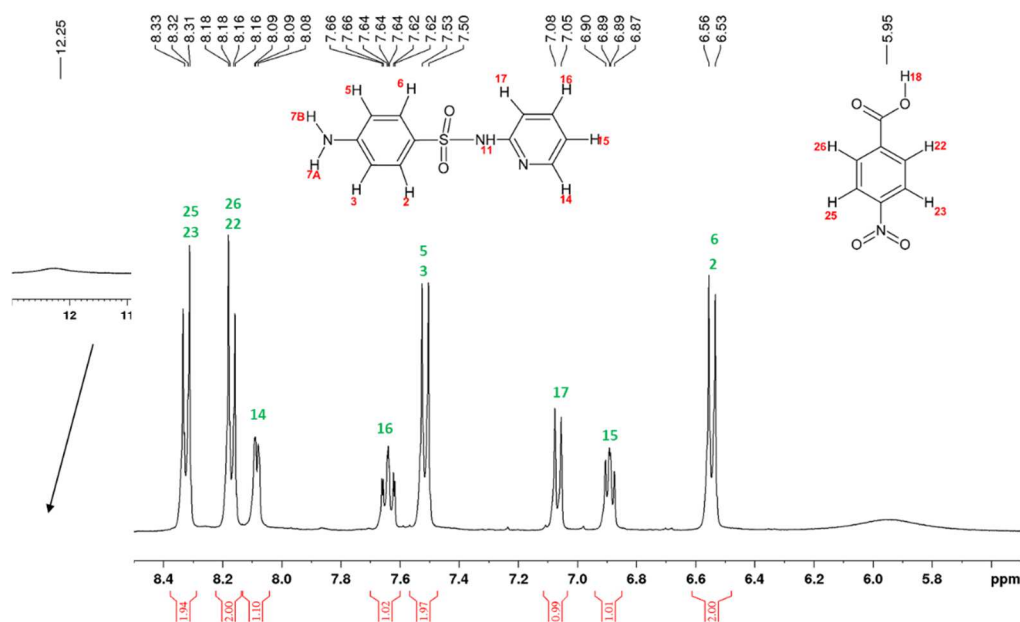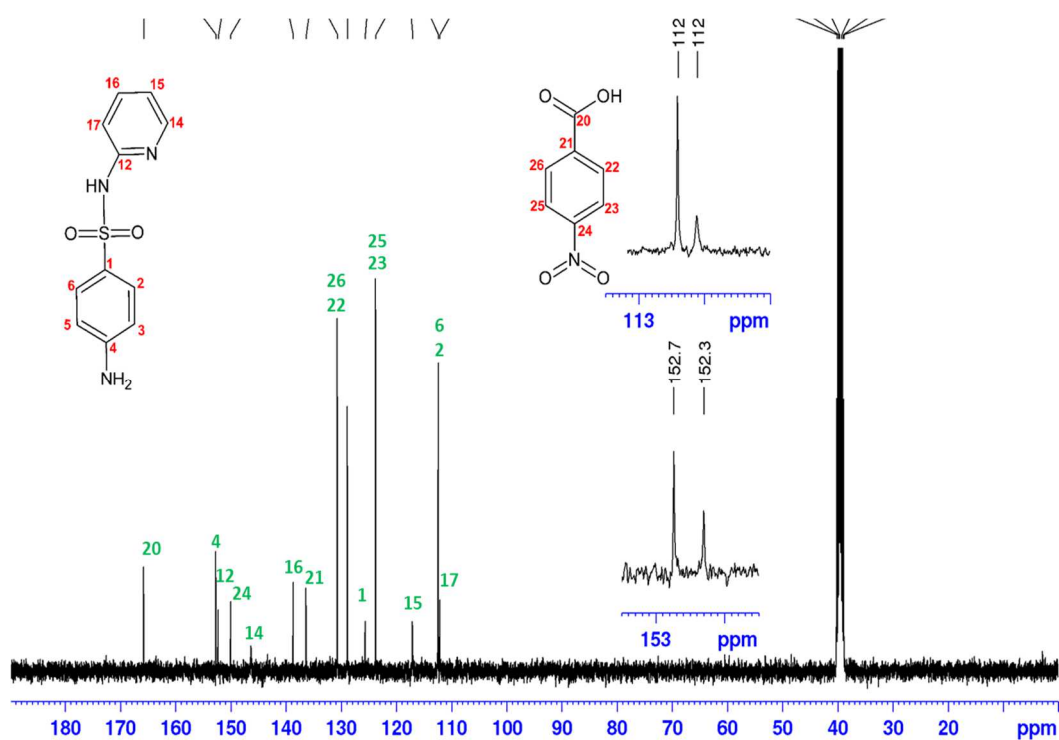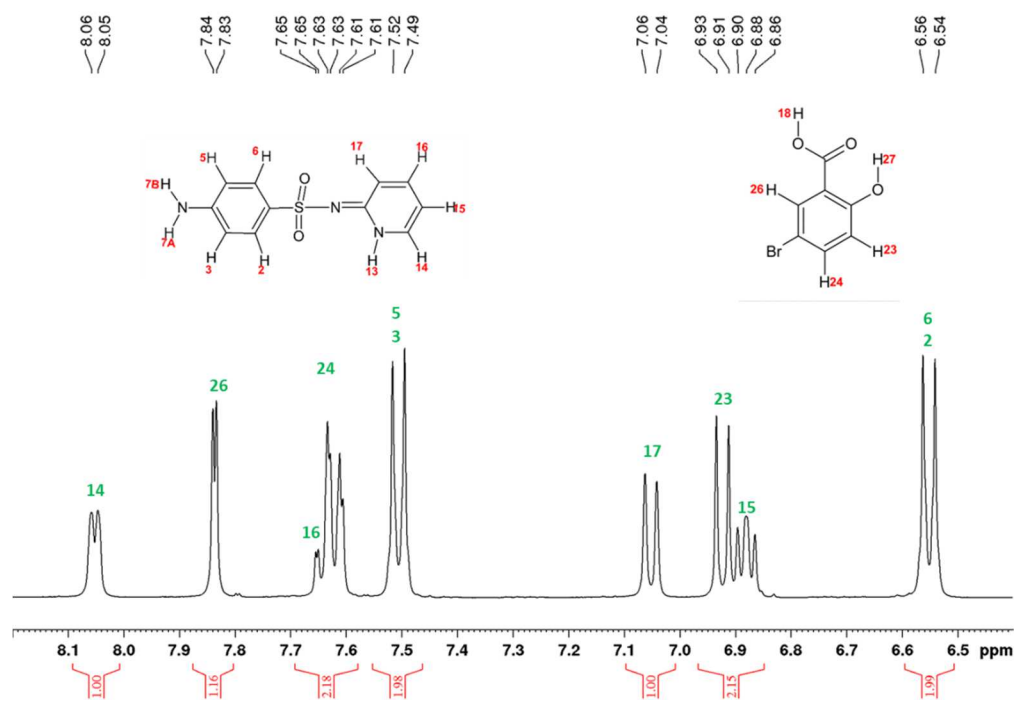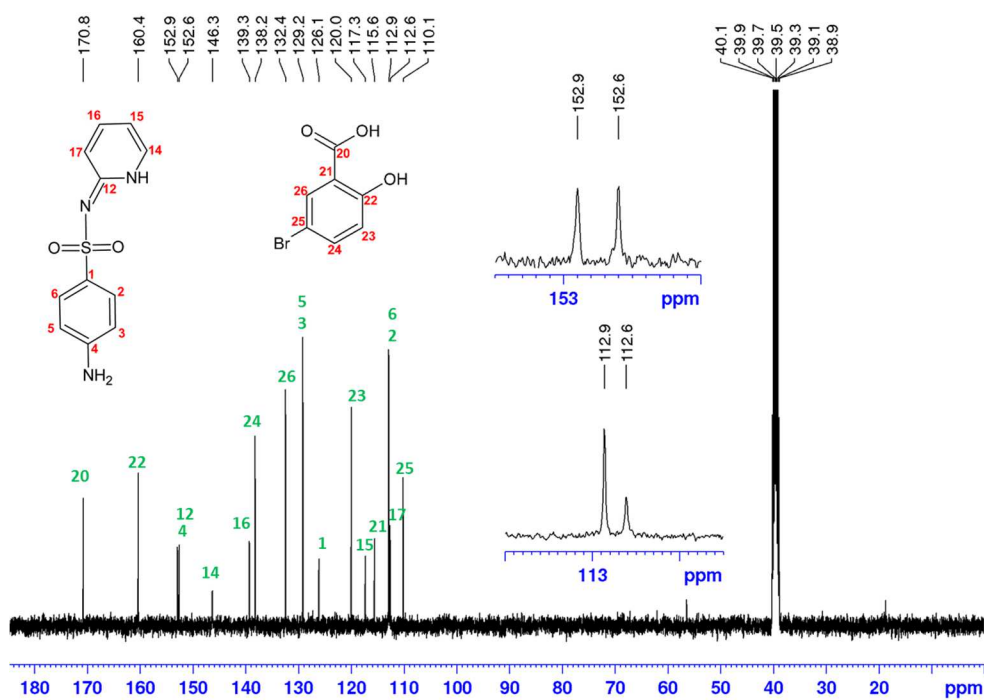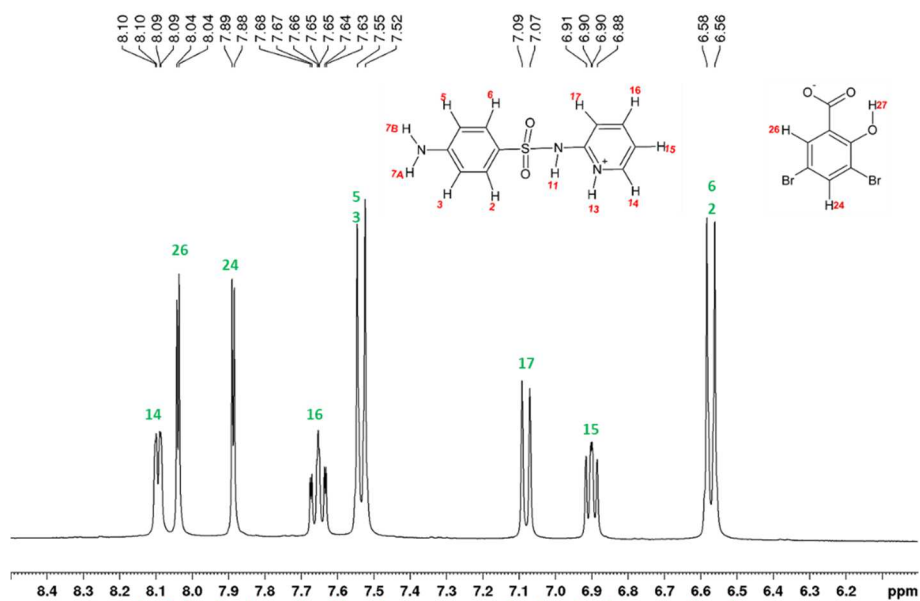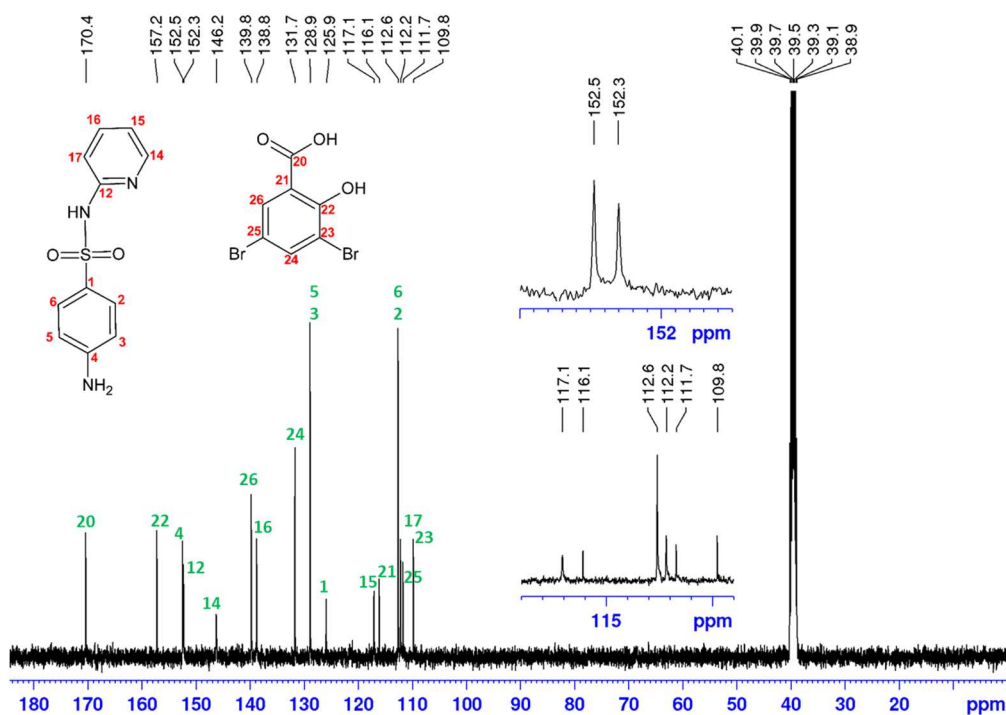
Figure E.3 Proton NMR spectrum (400MHz) of [SFP⁺][4NBA⁻] showing that both starting materials are present in the product. Peaks are referenced to the DMSO peak at 2.5 ppm (not shown).

Figure E.4 Carbon NMR spectrum of [SFP⁺][4NBA⁻] showing that both starting materials are present in the product. Peaks are referenced to the DMSO peak at 40 ppm.
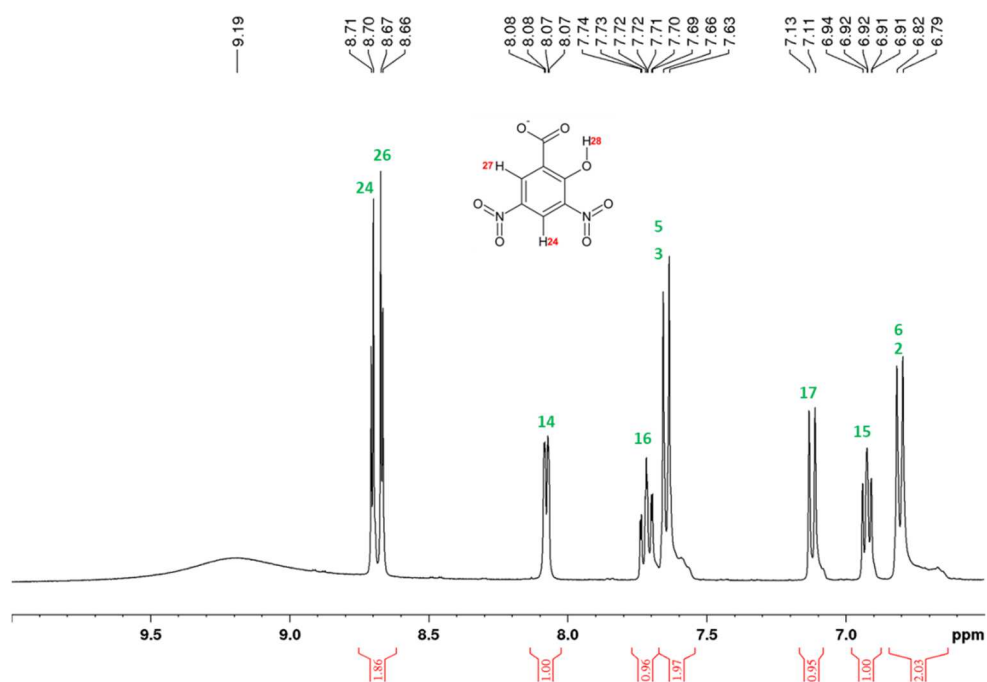
Figure E.5 Proton NMR spectrum (400MHz) of SFP·5BSA showing that both starting materials are present in the product. Peaks are referenced to the DMSO peak at 2.5 ppm (not shown).
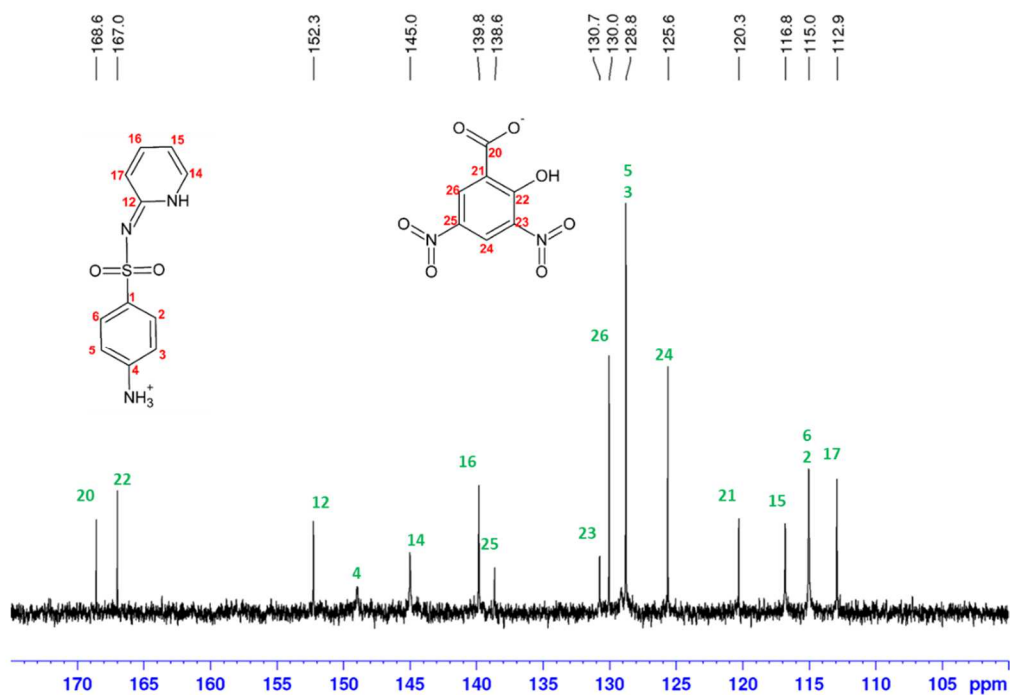

Figure E.6 Carbon NMR spectrum of SFP·5BSA showing that both starting materials are present in the product. Peaks are referenced to the DMSO peak at 40 ppm.

Figure E.7 Proton NMR spectrum (400MHz) of [SFP⁺][DBSA⁻] showing that both starting materials are present in the product. Peaks are referenced to the DMSO peak at 2.5 ppm (not shown).
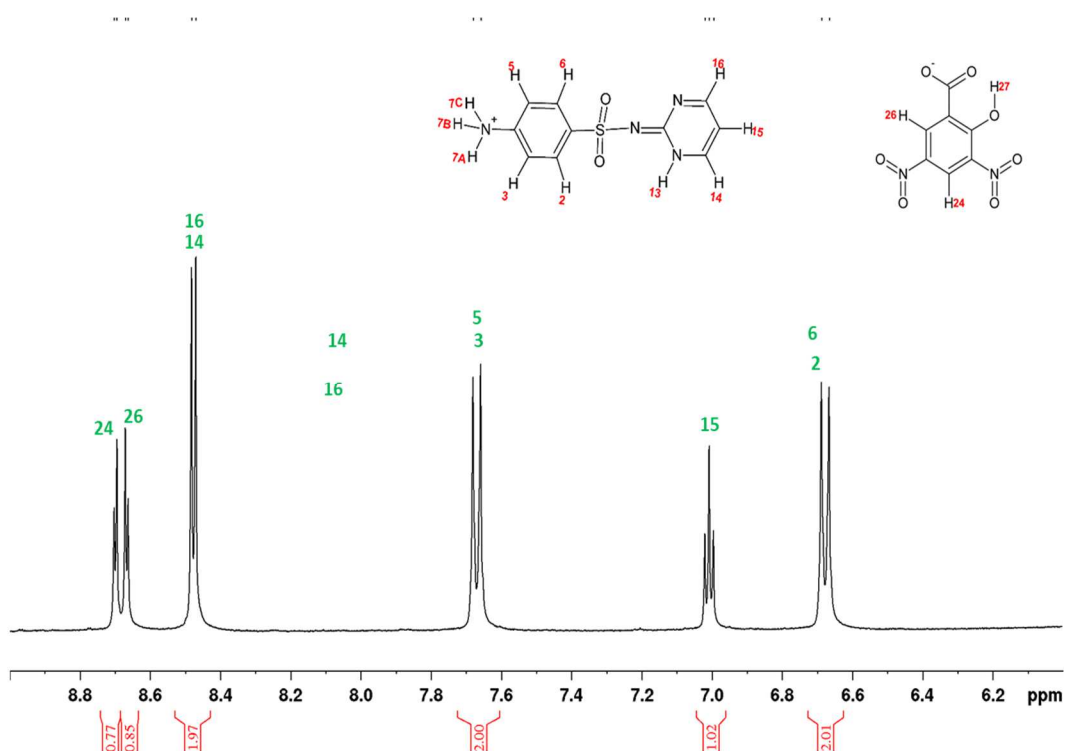

Figure E.8 Carbon NMR spectrum of [SFP⁺][DBSA⁻] showing that both starting materials are present in the product. Peaks are referenced to the DMSO peak at 40 ppm

Figure E.9 Proton NMR spectrum (400MHz) of [SFP+][DNSA-] showing that both starting materials are present in the product. Peaks are referenced to the DMSO peak at 2.5 ppm (not shown).
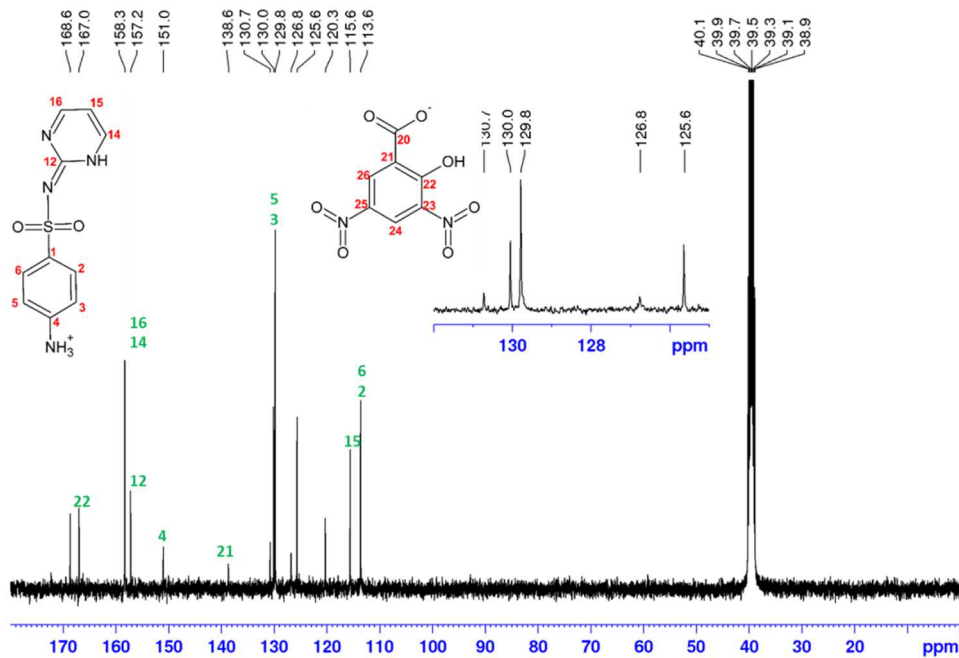

Figure E.10 Carbon NMR spectrum (400MHz) of [SFP+][DNSA-] showing that both starting materials are present in the product. Peaks are referenced to the DMSO peak at 40 ppm.
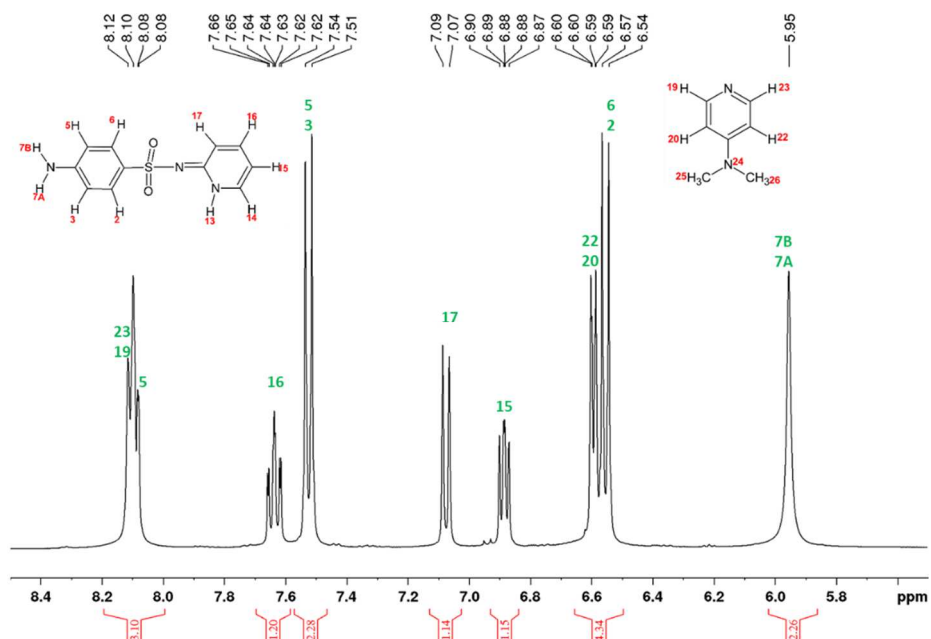
Figure E.11 NMR spectrum (400MHz) of [SFD⁺][DNSA⁻] showing that both starting materials are present in the product. Peaks are referenced to the DMSO peak at 2.5 ppm (not shown).

Figure E.12 Carbon NMR spectrum (400MHz) of [SFD⁺][DNSA⁻] showing that both starting materials are present in the product. Peaks are referenced to the DMSO peak at 40 ppm

Figure E.13 NMR spectrum (400MHz) of SFP·4MAP showing that both starting materials are present in the product. Peaks are referenced to the DMSO peak at 2.5 ppm (not shown).
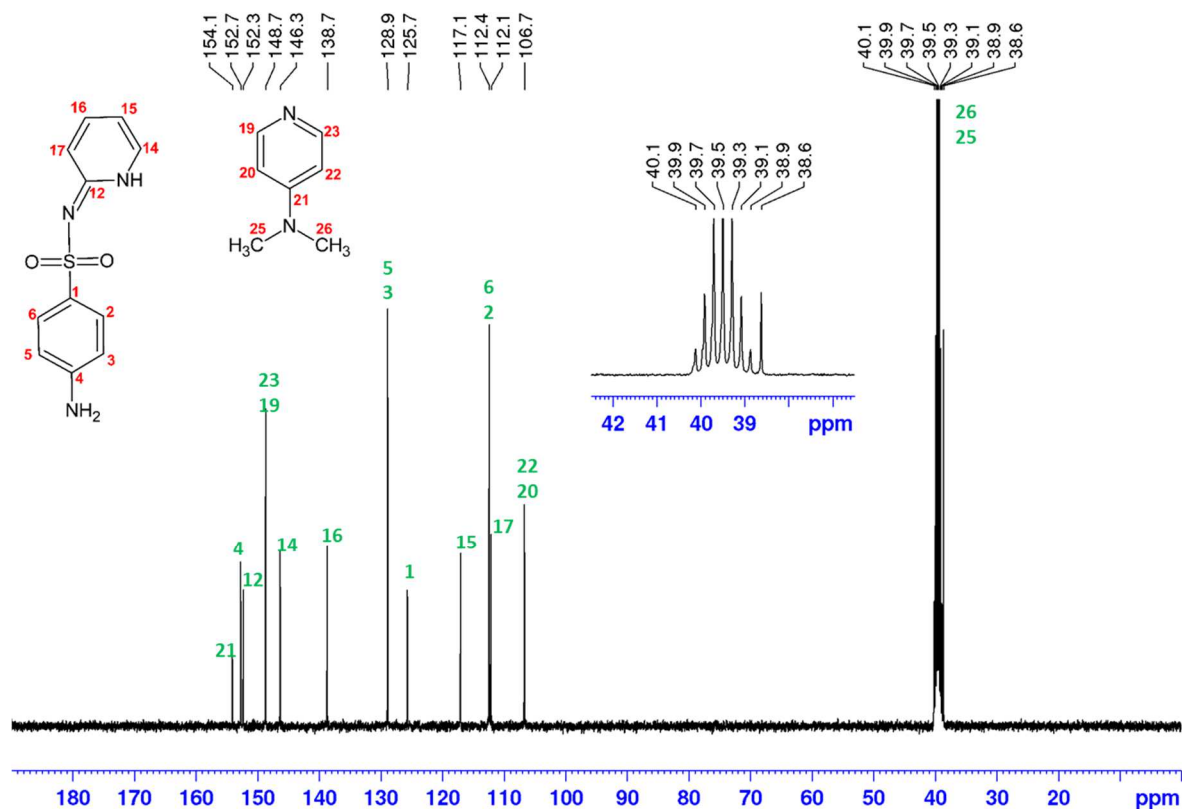

Figure E.14 Carbon NMR spectrum (400MHz) of SFP·4MAP showing that both starting materials are present in the product. Peaks are referenced to the DMSO peak at 40 ppm.
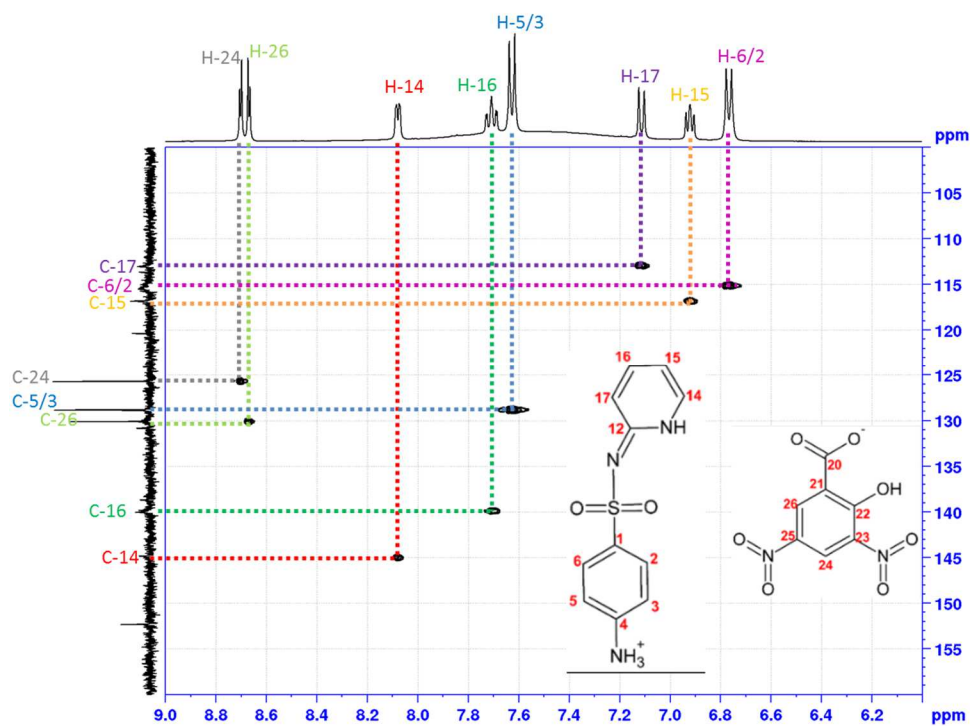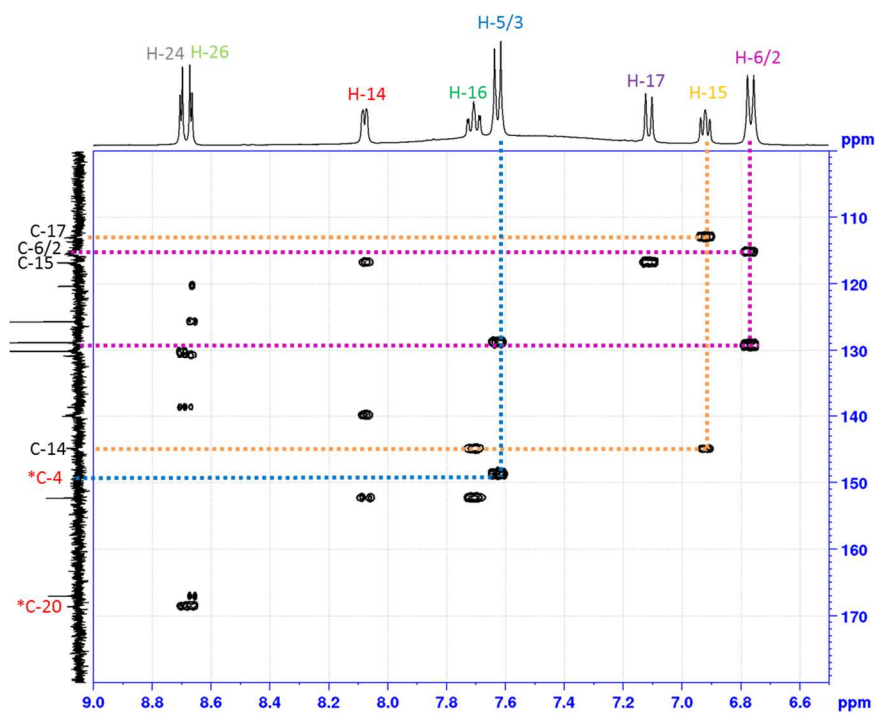
Figure E.15 2D HSQC spectrum of [SFP+][DNSA-].

Figure E.16 2D HMBC spectrum of [SFP+][DNSA-], quaternary carbons are also observed e.g C4, C20 indicated with an asterisk.